Master Thesis Report

The Dynamic Behavior of High-rise Building with Soil-Structure Interaction and the Application of Tuned Mass Damper

Y. Djapara

Technische Universiteit Delft

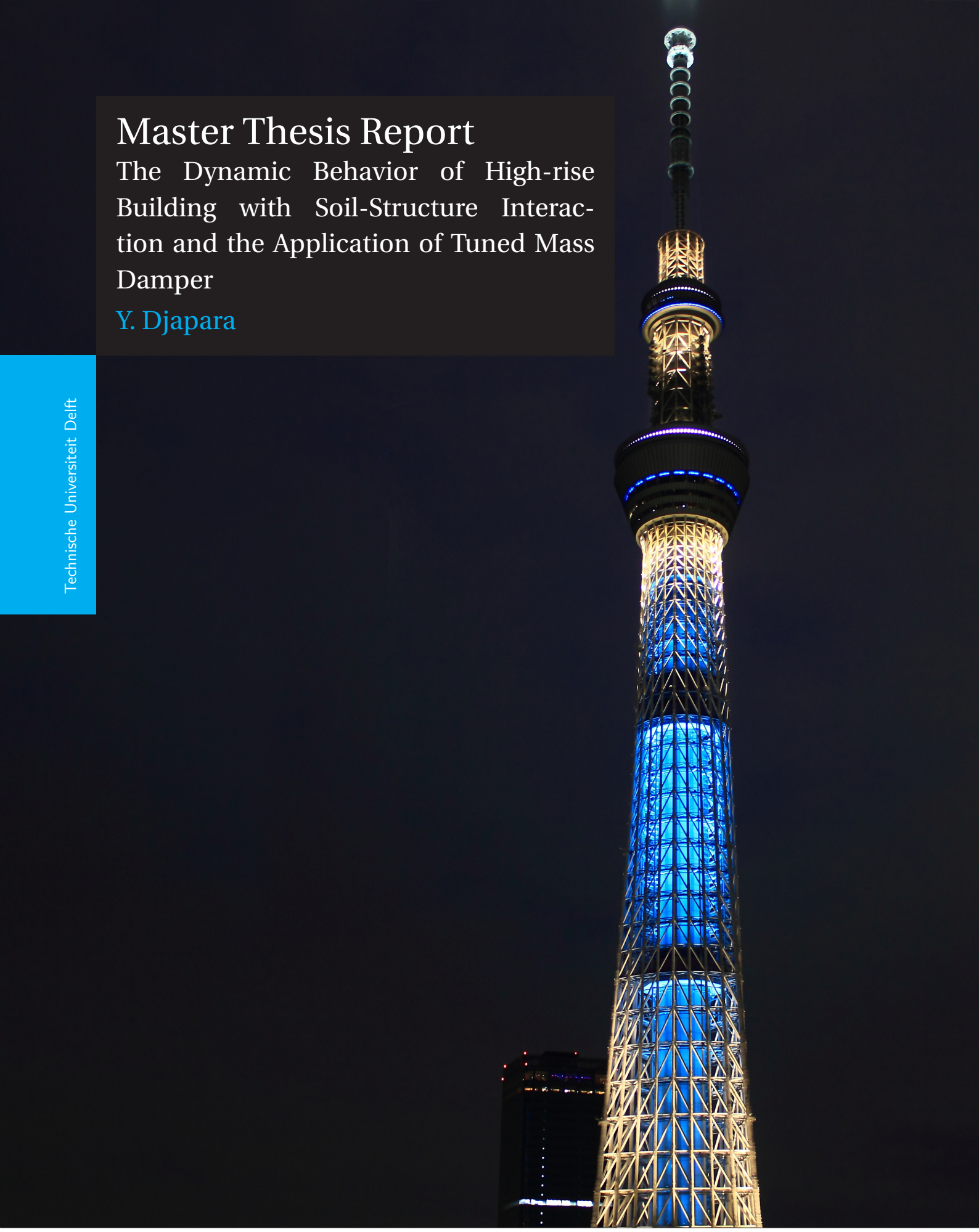

TU Delft Delft University of Technology

Challenge the future

***Cover immage**: Tokyo Sky-Tree*

Master Thesis Report

The Dynamic Behavior of High-rise Building with Soil-Structure Interaction and the Application of Tuned Mass Damper

by

Y. Djapara

in partial fulfillment of the requirements for the degree of

Master of Science
in Civil Engineering

at the Delft University of Technology,
to be defended publicly on Monday November 27, 2017 at 14:00 AM.

Thesis committee:

Prof. Dr. A. V. Metrikine,	Delft University of Technology	, Chairman
Ir. S. Sanchez Gomez,	Delft University of Technology	, Daily Supervisor
Prof. Ir. R. Nijsse	Delft University of Technology	, Supervisor
Ir. A. Robbemont	Zonneveld Ingenierus	, Supervisor
Dr. Ir. K. C. Terwel	Delft University of Technology	, Graduation Coordinator

An electronic version of this thesis is available at http://repository.tudelft.nl/.

TU Delft Delft University of Technology

zonneveld ingenieurs®

PREFACE

I am proud to present my eleven months of work on this master thesis on the Tuned Mass Damper as a fulfillment of the degree of Master of Science in Civil Engineering at the Delft University of Technology. This project was carried out in cooperation with a company, Zonneveld Ingenieurs. It is a gratifying experience to have, and I am very grateful that I am allowed to work on this thesis in Delft.

The accomplishment of this thesis is influenced by a lot of support which I am thankful to God and all of the people involved in this project. First of all, I would like to give thanks to Jesus Christ my God to whom my life is dedicated to and the source of my joy and hope. I would like to express my gratitude to my parents and my girlfriend Khairina Anindya, who always supports me in every condition.

The idea which has a significant influence on this thesis is generated by the discussion with the thesis committee and the meeting we have together. Therefore I would like to be thankful to the chairman, Prof. Andrei Metrikine who has allowed me to be under his supervisor and for his advice and also his teaching in the Structural Dynamic Course. To my daily supervisor Ir. Sergio Sanchez who has given a tremendous amount of time to guide me through this process, also who has connected me to the company. To Ir. Arnold Robbemont for the opportunity to work in the company and even a discussion time which he spares. To Prof. Rob Nijsse who is inspiring during the course in Delft University especially MEGA course, and also for the discussion and guidance. To Ir. Karel Terwel who has to help me in my study time in Delft until my graduation.

I would like thanks to the Indonesian government who has to give me the scholarship that I may study in the Netherlands. I hope that my knowledge may provide benefits to Indonesia, for the goods to all of the people. Also to all of my friends in Delft University who have warmly welcomed me and also has the experience to do project together and even activity outside the University.

Soli Deo Gloria

Yosua Djapara
Delft, November 2017

ABSTRACT

The trend of the slender and high-rise building has made the structure prone to dynamic loading. This thesis is focused on the dynamic behavior of the high-rise building subjected to wind action. The acceleration becomes a limiting criterion in designing such structure which can be categorized as the comfort criteria of the building. Nausea and motion sickness from the acceleration of the building has been studied by human experience, and numerous building code has included this in the design criteria [6]. The tuned mass damper (TMD) comes from the basic vibration absorber theory by Frahm in 1909; then the studied continued and applied in a building. At present, the TMD is a well-known technology to mitigate vibration, but it is not always applicable in every building case. Therefore a study of the interaction between the building properties also the soil structure interaction (SSI) is made in the application of the TMD.

This thesis aims to study the dynamic behavior of a high rise building with the implementation of TMD and to take into account the SSI, also to indicate which type of building is preferable to apply a TMD. The model for the high-rise building is an analytical one-dimensional model which is validated by the finite element program (FEP). The analytical model can give a good fit for the building response but due to the model of the wind load is a random load, it is challenging to match precisely the TMD performance due to the comparison of different load phase. The physical characteristic and tendency of the TMD performance to different building parameter still can be studied in this analytical model.

It is shown in this study that the damping plays an important role not only to reduce the acceleration of the building but also influence the effectiveness of TMD. The acceleration is drastically reduced in the lower damping ratio area, which makes the TMD more effective if the building has lower damping ratio contributed from the material, structural joints, and SSI. The reducement of the acceleration by increasing stiffness and mass is very limited compared to the application of TMD.

There are two building data for the base of the analysis; the first is the European Patent Office EPO building which is designed by Zonneveld Ingenieurs and the new proposal of slender high rise building in Rotterdam. The EPO building has a unique geometry which the contribution of torsional vibration is high. The slender high rise building shows that the TMD is more effective in reducing the acceleration in this case. The reason is the slender high rise has higher acceleration compare to EPO building when the required building stiffness for the deformation limit is applied.

CONTENTS

NOMENCLATURE

ω	Frequency
ω_n	Natural Frequency
ρA	Mass per unit height
ρ	Density
τ	Torque
$\theta_{(z,t)}$	Torsional deformation in time domain
$\theta_{t_{(t)}}$	TMD torsional deformation in time domain
$\tilde{\theta}_{(z,\omega)}$	Bending deformation in frequency domain
$\tilde{\theta}_{t_{(\omega)}}$	TMD torsional deformation in frequency domain
$\tilde{u}_{(z,\omega)}$	Torsional deformation in frequency domain
$\tilde{u}_{t_{(\omega)}}$	TMD translational deformation in frequency domain
c	Viscous Damping
C_q	SSI torsional dashpot
C_r	SSI rotational dashpot
C_s	SSI translational dashpot
C_t	TMD translational damping value
C_θ	TMD torsional damping
EI	Stiffness of the beam model
$f_{(\omega)}$	Wind load in frequency domain
$f_{(z)}$	Wind load shape function
G	Shear stiffness
J	Polar moment of inertia
k	Spring Stiffness
K_D	Dynamic stiffness matrix
K_q	SSI torsional stiffness
K_r	SSI rotational stiffness
K_s	SSI translational stiffness
K_t	TMD translational spring stiffness
K_θ	TMD torsional stiffness
L	Length

m	Mass
m_t	TMD mass
$q_{(z,t)}$	Wind load as a function of time and space
t	Time
$u_{(z,t)}$	Bending deformation in time domain
u_θ	TMD torsional deformation
$u_{t_{(t)}}$	TMD translational deformation in time domain
z	Coordinate along the building height
AMD	Active Mass Damper
BC	Boundary Conditions
DOF	Degrees of Freedom
DRMD	Distributed Rotational Mass Damper
DTMD	Distributed Tuned Mass Damper
EOM	Equation of Motion
IC	Interface Conditions
RTMD	Rotational Tuned Mass Damper
SSI	Soil Structure Interaction
TMD	Tuned Mass Damper

1

INTRODUCTION

The trend of slender and lighter high rise building has made the structure is prone to dynamic loading. Therefore the human comfort in term of building's acceleration becomes a crucial limiting factor in designing a high rise building. Since then, many damping devices and structural systems are made to make the structure achieve an admissible acceleration.

1.1. GENERAL

Early in the 19th century, a high rise structure is to describe a building about 100m height for office or residential uses. With a growing of technology and knowledge, a high rise structure now can reach much taller to 800m height. Therefore, to build a high rise structure is more complex and challenging. Firstly, the purpose of building high rise is not only as a place for people to live or work, but lately, a high rise building is also built for a landmark. It makes the aesthetic value of the structure becomes more important which influence the geometry of the structure and its dynamic behavior. Secondly, human factor in designing high rise plays an important role and has significant effect. The quality of the building inside has to be maintain regarding the air, light quality and also comfort criteria regarding building movement. As example in the Netherlands, strict daylight penetration limits the width of the building and therefore has effect on the slenderness of the structure. Also, the safety of the people in case of emergency such as fire and extreme cases also crucial in high rise structure. This human factor affects the strength and stiffness of the structural elements and total stability of the structure. Thirdly, economic and environmental demand in high rise structure has significant influence in the strength and stability of the structure. To reduce the transportation cost of the material and reducing the cost to build the foundation, light material is preferred. Sustainability issues also made the engineers think about future use of the high rise or demolishing process, which aim for the element to be easily removed or reused. All of these factors influence the slenderness and lightness of the high rise which can make it sensitive to the dynamic behavior.
In this research of high rise structure, the design is to be located in the Netherlands. This geographical context has an influence of the structure in two major ways. Firstly, the strong wind condition which gives not only large internal forces in the structure, but also vibration. Secondly, the soft soil condition in the Netherlands. Looking at the perspective of structural vibration, soft soil condition has a contribution to the structural damping of the high rise.

1.2. PROBLEM STATEMENT

In the lighter and slender high rise structure, dynamic response due to wind loading has the major problem. To improve the dynamic behavior of the building, mass and stiffness can be designed to some extent. It can be improved by redistributing the stiffness to have lower value in the bottom, stronger in the middle and using outrigger structure at the top [3]. But in higher and slender high rise, damping plays more important role in reducing the dynamic responds. In modern high rise building, natural damping is not sufficient and additional or external damping is needed to reduce dynamic responses [24].

The tuned mass damper (TMD) is a well-known technology to mitigate vibrations in structures but it has also limitation and not always gives benefits in every case. Previous studies of dynamic behavior of high-rise

buildings have suggested that the soil structure interaction (SSI) plays an important role in the overall energy dissipation due to characteristics of the soils. But in these cases of soft soils, the effectiveness of TMD's might be reduced drastically [14].

1.3. AIMS OF THE PROJECT

Though the TMD in SSI with high damping condition is not effective. It can be seen in the model from the literature [14] (Figure 1.1) that a conventional mass connected to a translational spring and dashpot model is used. Therefore the aim of the project is:

1. To study the dynamic behavior of a high rise building with the application of TMD in SSI. This include the effect of each parameter of the building and the soil structure interaction which describe in the boundary condition.
2. To study the performance of different types of TMD model in the high rise building.
3. Study the TMD's influence in the total cost of the structure. TMD is not cost efficient solution for all the building, so introducing the limitation and the situation in which the TMD has a good role in reducing the total cost is desired.

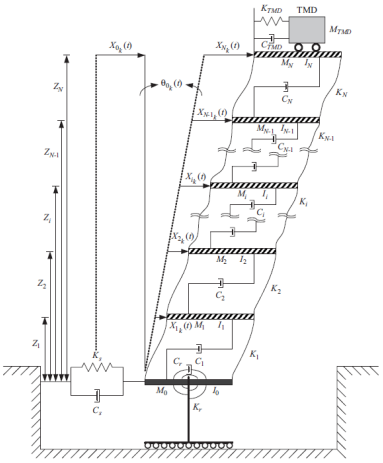

Figure 1.1: Discrete Model of High Rise with TMD

1.4. METHODOLOGICAL APPROACH

Currently there is no high-rise building in the Netherlands that uses this technology (TMD), therefore, experimental evidences cannot be extracted. However, it is necessary to explore the possibilities of TMD usage in future buildings. In order to do so, theoretical models that study the effectiveness of use of TMD's as a solution should be developed. The theoretical models can be derived from the simple system of a lumped mass or 1 degree of freedom system, many degrees of freedom system, and infinitely many degrees of freedom or continuous system.

1.5. RESEARCH QUESTIONS

Some research questions which correlated with the aims and the background of the thesis are:

1. What is the influence of mass, stiffness, and damping on the performance of TMD?
2. Under what condition the application of TMD is beneficial to the total cost of the building?
3. What is the effect of different types of TMD in term of reducing the building acceleration?
4. What is the effect of SSI on the effectiveness of the TMD?
5. How does the dynamic behavior of the high rise building on different SSI condition?

1.6. REPORTING STRUCTURE

I **Literature Study**
The literature study provide existing theory and application related with the topics. The literature study includes he general overview of high rise structure and its dynamic behavior. In this chapter the background theory of dynamic systems and the solution are discussed. The next chapter discussed the theory and application of tuned mass damper. The last chapter is about the relation of both systems and the soil characteristics.

II **Modeling**
Parametric modeling of the system is done with the mathematical programming such as Maple and Matlab based on the vibration theory. First, the physical meaning of the mathematical variable are discussed and elaborate with the solution method. To validate the output, discrete and continuous system are compared.

III **Analysis**
The parameters and the output of the models are further analyzed in this chapter. The parameters can be grouped in three types which are: the characteristics of the structure, TMD, and soil. Analyzing the trend of each characteristics can leads to obtain the solution of this project. The main interest are the parameter of the TMD which can be the quantity, types and position of the TMD.

IV **Conclusion and Recommendation**
The important and significant points of the resulting analysis is written down in this chapter. The criticism to this report and method is also given by the author to improve the future research of this topics.

I

LITERATURE STUDY

2

DYNAMICS OF HIGH-RISE BUILDING

In this chapter, the characteristics, limitation, and modelling of high rise structure are discussed. The model in this literature are the mathematical model to analyze the dynamic behavior of the structure. There are three system which will be discussed those are 1DOF, NDOFs, and 1 Dimensional model of continuous system.

2.1. HIGH RISE BUILDING

One of the definition of high rise structure can be derived from the internal forces. A building can be defined as a high rise if the stresses due to horizontal loading are larger than due to vertical loading [11]. This horizontal loading can be caused by various source such as earthquake, machinery, and the wind load on the façade of the building. In this thesis, the loading is limited to the wind loading only which varies from the height of the building and the time.
Wind induced vibration in high rise structure can be differentiated in thee response component according to the direction of the excitation. The first direction is along the wind excitation when the excitation is parallel to the wind direction, the second is when the excitation is perpendicular to the wind direction which is across wind excitation, and the third is the torsional if the structure is asymmetric [15]. The across wind excitation caused by the negative pressure acts on the side façade of the building caused by wind. This excitation are induced by wake flow field and vortex shedding. The wake region is the vortices caused by the wind Figure2.1(left). The vortex shedding is a phenomena when a fluid flows around a bluff body creating an oscillation Figure2.1(right).

Figure 2.1: Wake Excitation (left) [ntl.bts.gov] and Vortex Shedding (right) [projectggroupf.wordpress.com]

The vibration can also classified by the aeroelastic effects which are: lateral vibration by vortex, lateral vibration by galloping instability, and buffering vibration by gust wind [13]. The first is the vortex induced vibration (VIV) which is occur when the frequency of the vortex shedding is close to the natural frequency of the structure. The second is the galloping instability when the frequency of the structure is below those of vortex induced vibration. The third is buffering when the velocity fluctuations in an oncoming flow causing unsteady loading around a structure.
There are two types of criteria which should be satisfied in designing a high rise which are ultimate limit and serviceability limit. Ultimate limit is related to the internal forces and buckling of the structural element while serviceability limit is related to the deflection and acceleration which disturb the comfort level of the user. The wind induced vibration gives a dynamic response in the building in term of a displacement and an acceleration which also affect the internal force of the structural elements. In this thesis, the attention is more to the serviceability limit which in many case is the main limiting factor when designing a high rise structure. In the Netherlands, the acceleration limits are regulated from the Netherlands building code NEN6702 (2.2).

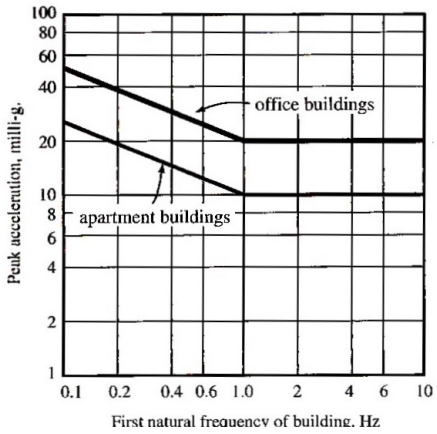

Figure 2.2: Dutch Comfort Criteria for Buildings [11]

The displacement limit of a high rise building can be obtained by: H (height of the building) divided by 750 if the base rotation is not taking into account and by 500 if it does.
To improve the structural response to vibration, mass, stiffness and damping are the three parameters which contributes to dynamics of structure. The total damping comprises internal material damping, damping due to the energy loss in the structural joints and the energy dissipation by soil-structure interaction.

2.2. SINGLE DEGREE OF FREEDOM

The simplest system to model a structure is a single degree of freedom (DOF) system. Degree of freedom is defined as the number of possible direction for the system to move. One of the example of the single degree of freedom system is a mass connected to a spring or and dashpot. The system can be undamped or damped, but due to the interest of this thesis is on the damping, damped system is discussed in this explanation. The vibration of a dynamic system can be separated into two condition related to time. Transient vibration is defined as a temporary vibration of a mechanical system which consist of free and forced vibration. Steady-state vibration is defined as a vibration of a mechanical system after sufficiently long time which means the effect of the initial conditions are no longer applied.
To obtain the response of the dynamic system, three steps should be done which are: write the equation of motion, solve the free vibration, and solve the force vibration. These three steps will be discussed in detailed.

2.2.1. EQUATION OF MOTION (EOM)

The equation of motion is derived from the Newton's second law which is

$$F = m * \ddot{x} \tag{2.1}$$

In case of mass spring dashpot system Figure2.3, the equation of motion becomes:

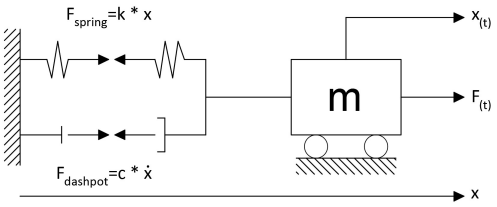

Figure 2.3: Mass-spring-dashpot system

2.2.2. FREE VIBRATION

There are two mechanism that drive the dynamic behavior of dynamic system. The first mechanism is a motion due to initial condition which called free vibration. In mathematical term, this is the solution of the

homogeneous equation. So the equation of free vibration can be written as:

$$\begin{aligned} m\ddot{x} + c\dot{x} + kx &= 0 \\ \ddot{x} + 2nx + \omega_n^2 x &= 0 \end{aligned} \tag{2.2}$$

Where $\omega_n = \sqrt{k/m}$ later known as the natural frequencies of the vibrating system with the given initial condition, and n is just a replacement from c/2m which contain the information about the damping of the system. One of the output in solving the free vibration is the characteristic value, in this case is the natural frequency or eigenvalue of the system. The presence of natural frequency means that the system may vibrate with a certain amplitude without the presence of the external force.

The free vibration for the damped system can be distinguished in two cases. The so called critically damped free vibration is the case when the system does not oscillate and go to the equilibrium position (Figure 2.5). This is the case when the damping is larger than the natural frequency ($n > \omega_n$). The other case is the damped free vibration when the system is oscillating but gradually decays to the equilibrium position (Figure 2.4). This happen when the damping is smaller than the natural frequency ($n < \omega_n$).

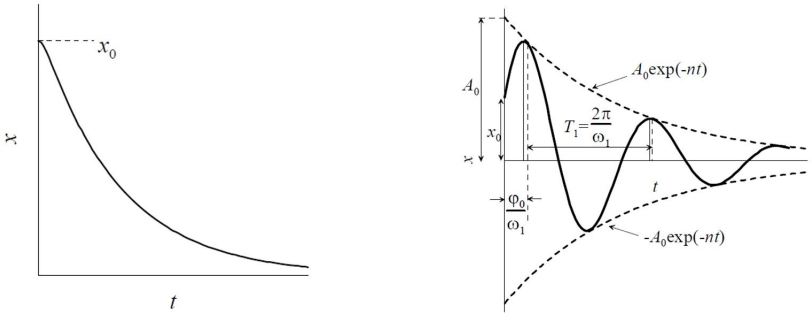

Figure 2.4: Critically damped free vibration (left) Damped free vibration (right)

2.2.3. FORCED VIBRATION

The second mechanism is the forced vibration which is the motion due to the external force. In mathematical term, this linked to one of the particular solutions. While in undamped system the particular solution is in the same type as the load, there must be a phase shift in damped system. Which means that the response and the force are never in phase (pointing at the same direction). There can be more than one form of particular solution in damped system. For harmonic force, the particular solution can be: $x_{part} = X_c \cos(\omega t) + X_s \sin(\omega t)$ or $x_part = Re(Xe^{i\omega t})$ if it is a cosine load or $Im(Xe^{\omega t})$ if sinusoidal.

Under general disturbing force when the load is irregular and non-periodic, there are 2 ways to find the force vibration. The first is based on the assumption that the force is a superposition of a sequence of short impulse which used Duhamel's Integral. The second is based on the application of Fourier series which assume that the force is a continuous superposition of its harmonic component.

Then the total response of the equation of motion is the sum of the free vibration response and forced vibration.

2.2.4. STEADY-STATE VIBRATION

The steady-state vibration will occur in undamped system because the damping decays the free vibration gradually, leaving only the force vibration. The steady-state response of the damped system can be found:

$$\begin{aligned} x_{steady} &= |X| \cos(\omega t - \phi) \\ x_{static} &= \frac{F_o}{k} \\ |X| &= \frac{F_o}{k} \frac{1}{\sqrt{\left(1 - \frac{\omega^2}{\omega_n^2}\right)^2 + \left(\frac{2n}{\omega_n}\right)^2 \frac{\omega^2}{\omega_n^2}}} \\ \frac{|X|}{x_{static}} &= \frac{1}{\sqrt{\left(1 - \frac{\omega^2}{\omega_n^2}\right)^2 + \left(\frac{2n}{\omega_n}\right)^2 \frac{\omega^2}{\omega_n^2}}} \end{aligned} \tag{2.3}$$

The (2.6) is known as the dynamic magnification factor which means that the dynamic response of a system can be obtain by multiplying the static response with this dynamic magnification factor.

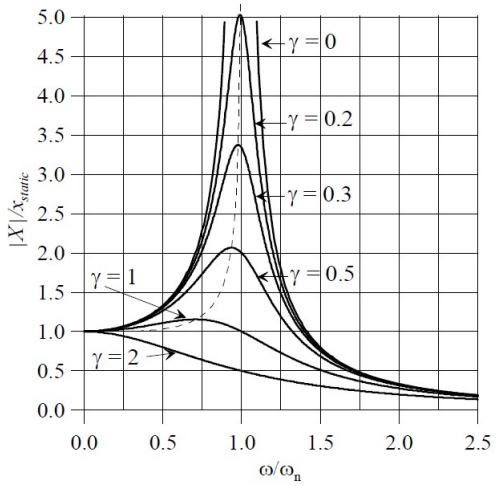

Figure 2.5: Magnification Factor

If this equation is plotted vs frequency (Figure 2.6), it can be seen (also from (2.6)) that if the damping is zero ($\gamma = 0$) and the natural frequency of the system is equal to the frequency of the load ($\omega/\omega_n = 1$), the response goes to infinity. This is known as the beating or resonance phenomena.

2.3. MULTI DEGREES OF FREEDOM STRUCTURE

The example of N-DOFs (N is a certain number >1) system can be seen in Figure 1.1 which each of the floors is the mass and each mass consist of 1DOF (translation) except the base floor which also can rotate. The principle of N-DOFs system is the same with the 1DOF system, but the equation is more convenient to write in the matrix form since it has many EOMs. The three steps of solving the 1DOF system still can be applicable in N-DOFs system. One of the method to form the EOMs is through the displacement method when each of the DOFs are moved to a certain displacement and obtain the reaction force contributes to the particular DOF. Then the matrix form of the EOMs can be written as:

$$[M]\ddot{x} + [C]\dot{x} + [K]x = [F] \tag{2.4}$$

Where [M], [C], and [K] are respectively mass, damping, and stiffness matrix of the system. One way to check the EOM is to look at these matrixes. The mass matrix should have a positive value on the diagonal (meaning: a stable system) and should be diagonal matrix if there is no rigid constrained between masses. The stiffness matrix should be symmetric and have positive value in the diagonal. Because the criteria for a stable system is having a pure imaginary of the characteristic value $s^2 = -k/m$, and it cannot be the case if one of the k or m has negative value. Because the system has many masses, it has also many natural frequencies depend on the number of the mass. There is additional characteristic value which is the eigenvector. It tells the information of the displacement relation in one modes to the others. Three methods will be introduced to solve the N-DOFs system which are the model analysis, Fourier analysis, and direct numerical integration. The modal analysis is the fastest method since it used the orthogonality property which can decouple the matrix EOMs to its components. But this method cannot handle system with high damping value since the damping matrix cannot be decoupled. The direct numerical integration can handle any case but slow processing time. Therefore the one will be used in this thesis is the Fourier analysis which can handle damping but only limited to a linear system.

2.4. CONTINUOUS SYSTEM

A continuous system can be define as a system which is discretized to an infinitely many masses to have a continuous properties along the system. Which means that a continuous system can also be describe as a

system with infinitely many degree of freedom. In this thesis the continuous system has only one dimensional structures. Which means that the mechanical behavior (stress) of the structure is varies only on one coordinate regardless the number of the direction of the movement.
A high rise building is often modeled as a beam. There are three types of beam theory which are: Euler-Bernoulli Beam, Timoshenko Beam, and Rayleigh Beam. The simplest model is an Euler-Bernoulli beam, the theory neglect the influence of rotational inertia and also assumed that the cross section of the beam remain planar to the central axis. The Rayleigh beam take into account the influence of rotational inertia but neglect the rotational of the cross section. The most advance model is Timoshenko beam model which takes into account both of the phenomena. In this case, the Euler-Bernoulli Beam is enough as a representation of a high rise building because a building has small rotational inertia and also has a high slenderness. While the effect of the cross section rotation is high on a thick beam. A Euler-Bernoulli beam has two degree of freedom for each discretized mass namely deflection and rotation. The rotation defined as the first derivative of the deflection. The derivation of the equation of motion can be seen on the Appendix (A.8), the final equation can be seen below:

$$\rho A \frac{\partial^2 u}{\partial t^2} + \frac{d^2}{\partial x^2}\left(EI\frac{\partial^2 u}{\partial x^2}\right) = q_{(x,t)} \tag{2.5}$$

To obtain the response, this equation can be solve by many methods. Two well-known methods are the method of separation of variables and Fourier transform. The method of separation of variables assumes that the solution or the response of the vibration can be defined as two separate functions of time and coordinate ($(u(x,t) = W(x)\Phi(t))$). But this method cannot work if one of the boundary condition contains time derivation which in the case in this thesis with TMD. Therefore another method with an application of Fourier Transform can be used. This method also known as a solution in the frequency domain because the Fourier Transform change the function from a time domain to the frequency domain.

2.5. MODEL OF DAMPING

Every conservative structure in the world can dissipate energy which means that if we vibrate a structure by an impulse, the conservative structure will be on its original position after a period of time. This energy dissipation through time is defined as a damping. In high rise building, the source of damping can be categorized as follow:

1. Damping from the Material This damping is come from the internal friction in the material itself. The physical mechanism which produce damping in the material differs from each specific material. Some of the physical mechanism are thermoelasticity, eddy-current effect, stress induced, and electronic effect.

2. Damping from Structural Joints The energy dissipation from the structural joints comes from the local frictional effect in the joint. The cause can be also through air pumping which is trapped in the structural joints.

3. Damping from Soil Structure Interaction Vibration on the building that propagating to the soil is dissipated through the radiation to the deeper layer and histeretic loss in soil due to its imperfect elasticity (material damping).

4. Aerodynamic Damping When a flow of air interacts with an object, there is a restoring moment which is opposite to the movement of the object create by the airflow. This restoring moment is known as aerodynamic damping which is dependent on the dynamic pressure create by air speed.

5. Added Damping To overcome acceleration problems in building, engineers build many types of artificial dampers. One of the example is discussed in this thesis which is a tuned mass damper.

6. Radiation Damping A vibrating object have a vibrating energy of electrons. Radiation damping occurs when the electron is converted to electromagnetic energy and emitted in from of radio wave, infrared, or light.

In previous research, it is state that the observation of damping turn to be non-linear. A method to linearized damping has been introduced by Rayleigh (1877) which is well known now as a viscous damping. Viscous damping is an energy loss caused by liquid lubricant in which its force is proportional to its relative velocity. These damping then modeled as a mathematical expression for the equation of motion. Some types of the damping model which has been studied are discussed in the next section below.

2.5.1. MATERIAL DAMPING

To model the material damping [5], there are two categories which has been made in the literature which are the frequency dependent model and the frequency independent model.

1. Kelvin-Voigt Model Kelvin-Voigt model is consist of a spring which is paralel with a dashpot as it can be seen in the figure. The spring and dashpot model the behavior of a viscoelastic solid. By definition, viscoelasticity is the viscous and elastic characteristic of a material. The equation of motion of a single degree of freedom system of the Kelvin-Voigt model can be seen in the equation below:

$$m\ddot{u} + c\dot{u} + ku = 0 \tag{2.6}$$

2. Collar Model
   Another model of damping is the Collar model which model a damping of a system depend on the frequency. This model is also called a frequency dependent damping as it can be seen in the equation below:

$$m\ddot{u} + (b/\omega)\,\dot{u} + ku = 0 \tag{2.7}$$

3. Kimball-Lovell Model
   Kimball and Lovell ovserved that material damping in engineering material is not dependent on the frequency. Therefore they build a damping model which is independent of the frequency as can be seen in the equation below:

$$m\ddot{u} + (k + ib)u \tag{2.8}$$

4. Myklestad Model
   Myklestad model is an alternative of the Kimball-Lovell model in which the spring constants is replace by an exponential term as it can be seen in the equation below:

$$m\ddot{u}C_1 e^{im}u \tag{2.9}$$

5. Reid Model
   Reid model is build to handle multiple frequency forced vibration and also free vibration. The damping term of the Reid model can be seen in the equation below:

$$m\ddot{u} + b|u/\dot{u}|\dot{u} + ku = 0 \tag{2.10}$$

Kelvin-Voigt model is the well known model for the damping which is chosen also in this thesis. The advantage of this model is the simplicity that the damping is linear while it can modeled the behavior of a viscoelastic solid.

2.5.2. VISCO-ELASTIC BODY

To apply the Kelvin-Voigt model in the continuos system, a model called visco-elastic body is applied in the Euler-Bernoulli beam. The definition of visco-elastic bodies is when the mechanical properties of system is varies through time. This is the combination of elastic theory from Hooke's Law and the viscous phenomena from Newton's Law.
The assumption in this theory is the system is linear: which taking into account the small deformation, and follows Boltzmann's superposition theory. The theory state that if a stress cycle $\sigma_1(t)$ gives a strain $\varepsilon_1(t)$ and stress $\sigma_2(t)$ gives a strain $\varepsilon_2(t)$, then the sum of the cycle $\sigma_1(t) + \sigma_2(t)$ gives a strain $\varepsilon_1(t) + \varepsilon_2(t)$.
The stress can be expressed as the summation of Hooke's and Newton's Law as falling:

$$\begin{aligned} \sigma &= \sigma_o + \sigma_s \\ \sigma_o &= E\varepsilon \\ \sigma_s &= \eta\dot{\varepsilon} = \eta\frac{\partial}{\partial t}\varepsilon \\ c^* &= \eta/E \\ \sigma_{(t)} &= E\left(1 + c^*\frac{\partial}{\partial t}\right)\varepsilon_{(t)} \end{aligned} \tag{2.11}$$

The major advantage is: The model is the simplest model which can represent damping which is increases with the increase of the natural frequency of the system as it can be seen in the later chapter.

3

TUNED MASS DAMPER

This chapter discusses the theory and application of tuned mass damper (TMD) on a high-rise building. The introduction explains about the initial idea of TMD, the model which is applied in this thesis is also discussed.

3.1. INTRODUCTION

Tuned mass damper in principal is a vibration absorber which is first introduced by Hermann Frahm in 1909. This is used to improve high vibration in resonance phenomena. The vibration absorber can be damped or undamped, the magnification factor of both can be seen in Figure3.1.

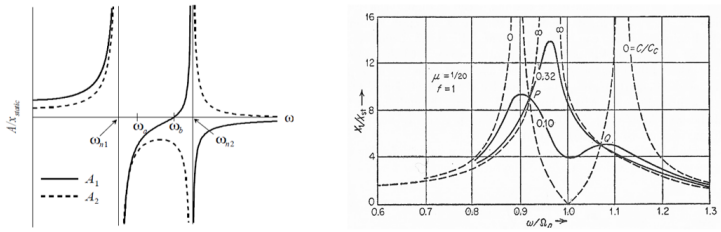

Figure 3.1: Magnification Factor of undamped vibration absorber (left) [15] and Magnification factor of damped vibration abserober (right) [10]

Those figures are obtained from two degrees of freedom system which consist of the primary system (1st mass) and the auxiliary system (2nd mass) which is the absorber. It can be seen on the Figure3.1 that as the frequency of the load (ω) reach ω_b, the primary system has 0 amplitude. The positive value of amplitude means that the system is in phase with the load. The natural frequency of the auxiliary system is tuned to the natural frequency of the primary system to get high effectiveness. So that when the first resonance takes place, the main system absorbs the energy from the load, then the second resonance can occur when the auxiliary system absorbs the energy from the primary system. But in case of moderately stiff soil and stiff rock, the mass damper should be tuned to the natural frequency of the soil structure system rather than the structure with clamped base [24].

For the undamped vibration absorber, the plot only gives the information about the primary system. The work done by the damping is given by the force times the relative displacement of the two masses. When the damping is 0 (damping force is zero), and when the damping is infinite (the two masses are locked together) the relative displacement is zero, there is no energy dissipation, and the amplitude is maximum. But in between those values, there is an optimum damping which the auxiliary system absorb the vibration the most [10].

The tuning for the damped vibration absorber can be obtained by the equation below:

$$\begin{aligned} f &= \frac{1}{1+\mu} \\ \mu &= \frac{\text{absorber mass}}{\text{main mass}} \\ f &= \frac{\omega_2}{\omega_1} \end{aligned} \tag{3.1}$$

The maximum damping capacity that can be obtained from TMD is roughly equal to the mass ratio (m/M) but this required fine-tuning. It is desirable to use a damper with a mass ratio at least twice that required added damping to avoid the need of fine tuning [21].
In the relation of the vibration of high-rise structure, the previous study shows that the TMD has low effectiveness in reducing structural response in along wind excitation as also mentioned in previous chapter that this is not the critical vibration. The TMD is more effective in reducing the vibration caused by lock-in excitation than crosswind wake excitation and along wind turbulence [24]. The performance of TMD is expected to reduce 50-60% vibration [13].

3.2. UNDAMPED VIBRATION ABSORBER

The system of the undamped vibration absorber consisting of one primary mass and one absorber mass which is connected only by spring stiffness can be seen in the Figure3.2.

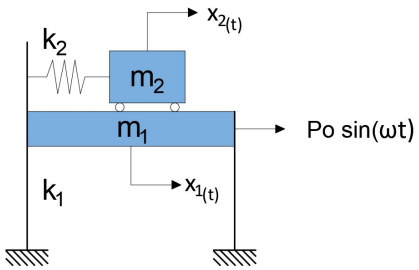

Figure 3.2: Undamped Vibration Absorber System

The equation of motions for the 2 masses can be seen in the equation below:

$$\begin{aligned} m_1\ddot{x}_1 + k_1x_1 + k_2x_1 - k_2x_2 &= P_o \sin(\omega t) \\ m_2\ddot{x}_2 - k_2x_1 + k_2x_2 &= 0 \end{aligned} \tag{3.2}$$

In this case, the main focus is to study the excitation of the system by the harmonic force. Therefore to plot the dynamic magnification factor in steady-state regime, the solution can be found in the form of:

$$\begin{aligned} x_1 &= A_1 \sin\omega t \\ x_2 &= A_2 \sin\omega t \end{aligned} \tag{3.3}$$

The next step is to substitute this steady-state solution to the EOM. From the substitution, it is obtained that:

$$\begin{aligned} \frac{A_1}{x_{st}} &= \frac{1-\frac{\omega^2}{\omega_2^2}}{\left(1-\frac{\omega^2}{\omega_2^2}\right)\left(1-\frac{k_2}{k_1}-\frac{\omega^2}{\omega_1^2}\right)-\frac{k_2}{k_1}} \\ \frac{A_2}{x_{st}} &= \frac{1}{\left(1-\frac{\omega^2}{\omega_2^2}\right)\left(1-\frac{k_2}{k_1}-\frac{\omega^2}{\omega_1^2}\right)-\frac{k_2}{k_1}} \end{aligned} \tag{3.4}$$

In which some terms of the ratio between the properties are introduced as:

Static response:

$$x_{st} = \frac{P_o}{k_2}$$

Natural frequency:

$$\begin{aligned} \omega_2 &= \sqrt{\frac{k_2}{m_2}} \\ \omega_1 &= \sqrt{\frac{k_1}{m_1}} \end{aligned} \tag{3.5}$$

Mass ratio:

$$\mu = \frac{m_2}{m_1}$$

It can be seen from the equation 3.4 that the denominator is the same on both of the system. This explains the resonance phenomena that if the main system has an infinitely large amplitude, then it induce also an infinitely large force to the other system which also resulting infinitely large amplitude. As when the denominator is zero, both of the system has infinitely large amplitude, and this can happen when $\omega = \omega_2 = \omega_1$ which is the requirement of resonance.
It can also be seen the main system can have a zero amplitude if the frequency of the load is the same as the frequency of the absorber system ($\omega = \omega_2$). Using this condition to the absorber's equation resulting $A_2 = -P_o/k_2$ and then $x_2 = -P_o \sin\omega t/k_2$. It can be concluded that the force resulting from this absorber motion is equal to $F_2 = x_2 k_2 = -P_o \sin\omega t$ which is the same as the external force but in the opposite direction and this is why the main system has no vibration at all.
Now the system becomes a 2 DOFs system. To find the natural frequency of this 2DOFs system, we should find the root of the denominator equal to zero. The absorber system is tuned to have the same frequency as the main system because it is not relevant to apply a vibration absorber unless there is a resonance in the SDOF system of the main system only. Therefore the denominator can be written as:

$$\begin{gathered} \left(1-\frac{\omega^2}{\omega_2^2}\right)\left(1-\mu-\frac{\omega^2}{\omega_2^2}\right)-\mu \\ \left(\frac{\omega}{\omega_2}\right)^4-\left(\frac{\omega}{\omega_2}\right)^2(2+\mu)+1=0 \\ \left(\frac{\omega}{\omega_2}\right)^2=\left(1+\frac{\mu}{2}\right)\pm\sqrt{\frac{\mu+\mu^2}{4}} \end{gathered} \tag{3.6}$$

It can be seen that the equation has two real roots which are true because 2 DOFs system also has two natural frequencies. By tuning the frequency of the vibration absorber to the primary system, from the equation 3.4 the frequency response of the system can be written as:

$$\begin{aligned} \left|\frac{X_1}{x_{st}}\right| &= \frac{1-\frac{\omega^2}{\omega_2^2}}{\left(1-\frac{\omega^2}{\omega_2^2}\right)\left(1-\frac{k_2}{k_1}-\frac{\omega^2}{(\omega_2^2)}\right)-\frac{k_2}{k_1}} \\ \left|\frac{X_2}{x_{st}}\right| &= \frac{1}{\left(1-\frac{\omega^2}{\omega_2^2}\right)\left(1-\frac{k_2}{k_1}-\frac{\omega^2}{(\omega_2^2)}\right)-\frac{k_2}{k_1}} \end{aligned} \tag{3.7}$$

To plot the frequency response of the primary mass, we choose the mass ratio:

$$\mu = \frac{1}{20} = 0.05$$

Plotting the equation 3.7 with the frequency ratio $g = \frac{\omega}{\omega_2}$ as x axis and $\left|\frac{X_{1,2}}{x_{st}}\right|$ as y axis resulting in the Figure3.3:

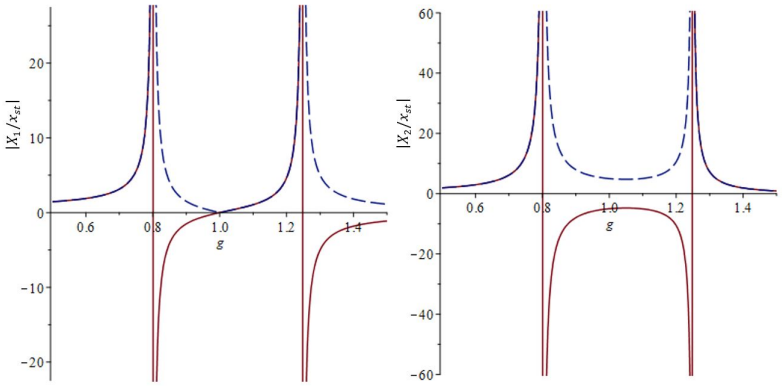

Figure 3.3: Dynamic Magnification Factor in Undamped Vibration Absorber System

It can be seen that when the resonance phenomena occur in a SDOF system, that the amplitude goes to infinity when the frequency of the load is the same as the natural frequency of the main system. Placing a mass attached to the primary system with a spring may absorb all the response. So the vibration absorber will be the one that oscillates instead of the main mass (which now has zero amplitude).

3.3. DAMPED VIBRATION ABSORBER (DVA)

DVA (Figure3.4) was introduced by J.P.Den Hartog and J.Ormondroyd and published in 1928. They observed that by placing a damper in a vibration absorber, there is a method to find the optimum ratio of the main system's frequency and absorber's frequency. It is known by tuning ratio.

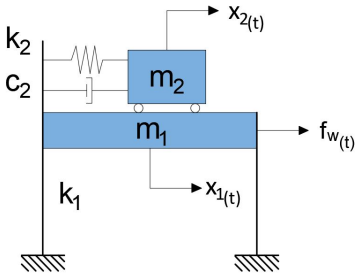

Figure 3.4: Damped Vibration Absorber System

3.3.1. FREQUENCY RESPONSE

The magnification factor should be derived first with the same procedure as the undamped vibration absorber to obtain this tuning ratio.
Equations of Motion:

$$\begin{aligned} m_1\ddot{x}_1 + k_1x_1 + k_2(x_1 - x_2) + c_2(\dot{x}_1 - \dot{x}_2) &= P_o \sin\omega t \\ m_2\ddot{x}_2 + k_2(x_2 - x_1) + c_2(\dot{x}_2 - \dot{x}_1) &= 0 \end{aligned} \tag{3.8}$$

Steady State Solution:

$$x_1 = Im(X_1 e^{i\omega t}); \quad x_2 = Im(X_2 e^{i\omega t}) \tag{3.9}$$

By substituting the steady-state solution to the equations of motion:

$$\begin{aligned} [-m_1\omega^2 + k_1 + k_2 + i\omega c]X_1 - [k_2 + i\omega c_2]X_2 &= P_o \\ -[k + i\omega c]X_1 + [-m\omega^2 + k + i\omega c]X_2 &= 0 \end{aligned} \tag{3.10}$$

Now take a closer look at the main system by expressing the X_2 in X_1 from the equation 3.10:

$$X_1 = P_o \frac{(k_2 - m_2\omega^2) + i\omega c_2}{(-m_1\omega^2 + k_1)(-m_2\omega^2 + k_2) - m_2\omega^2 k_2 + i\omega c_2(-m_1\omega^2 + k_1 - m_2\omega^2)} \tag{3.11}$$

Due to the damping in the system, the equation is now in complex value form. To obtain the amplitude, we need to take the absolute value of equation 3.11 and by doing this, we can eliminate the imaginary part also. At first, separate the imaginary part by multiplying with its complex conjugate.

$$X_1 = \frac{(A+iB)}{(C+iD)} * \frac{(C-iD)}{(C-iD)} = \frac{((AC+BD)+i(BC-AD))}{(C^2+D^2)} \tag{3.12}$$

After separating the imaginary part, the absolute value can be obtain through this equation:

$$\begin{gathered} \text{amplitude} = |X_1| = |E+iF| = \sqrt{(E^2+F^2)} \\ |X_1| = \sqrt{\frac{(A^2C^2+B^2D^2+B^2C^2+A^2D^2)}{(C^2+D^2)^2}} = \sqrt{\frac{(A^2+B^2)(C^2+D^2)}{(C^2+D^2)^2}} = \sqrt{\frac{(A^2+B^2)}{(C^2+D^2)}} \\ \frac{|X_1|}{P_o} = \sqrt{\frac{((k_2-m_2\omega^2)^2+\omega^2c_2^2)}{[(-m_1\omega^2+k_1)(-m_2\omega^2+k_2)-m_2\omega^2k_2]^2+\omega^2c_2^2(-m_1\omega^2+k_1-m_2\omega^2)^2}} \end{gathered} \tag{3.13}$$

Introducing some terms of the ratio between the properties which introduced as:

$$\begin{gathered} \mu = \frac{m_2}{m_1}; \omega_2 = \sqrt{\frac{k_2}{m_2}}; \omega_1 = \sqrt{\frac{k_1}{m_1}}; f = \frac{\omega_2}{\omega_1}; g = \frac{\omega}{\omega_1}; x_s t = \frac{P_o}{k_1}; c_c = 2m_2\omega_1 \\ \frac{|X_1|}{x_s t} = \sqrt{\frac{\left(2\frac{c_2}{c_c}g\right)^2+\left(g^2-f^2\right)^2}{\left(2\frac{c_2}{c_c}g\right)^2\left(g^2-1+\mu g^2\right)^2+\left[\mu f^2g^2-\left(g^2-1\right)\left(g^2-f^2\right)\right]^2}} \end{gathered} \tag{3.14}$$

In which g is the frequency ratio and c_c is the critical damping. We set the natural frequency of the absorber to be the same as the main system (f=1). Using the same mass ratio as the undamped vibration absorber

$$\mu = \frac{1}{20} = 0.05$$

plot with a different value of the damping (Figure3.5)

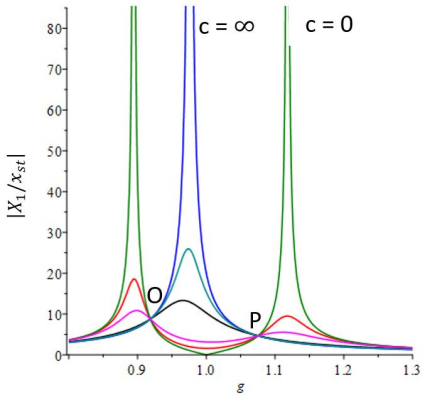

Figure 3.5: Frequency Response Function (DVA)

3.3.2. TUNING RATIO

There are two extreme cases which result in the infinitely large value of the amplitude of the main system. The first is when the $c_2 = 0$ (green plot) which means the same case as the undamped vibration absorber. It can also be seen through mathematical expression below.

$$\begin{aligned} & f = 1; c_2 = 0; \\ \frac{|X_1|}{x_s t} &= \sqrt{\frac{\left(g^2-1\right)^2}{\left[\mu g^2 - \left(g^2-1\right)^2\right]^2}} \\ & \mu g^2 - \left(g^2-1\right)^2 = 0 \\ & g^4 - (2+\mu)g^2 - 1 = 0 \\ g^2 &= \frac{(2+\mu) \pm \sqrt{(2+\mu)^2 - 4}}{2} \end{aligned} \tag{3.15}$$

The equation 3.15 is the same as the equation 3.6 from the undamped system. Now consider the second case which is $c_2 = \infty$ (blue plot). This means the system is the same case as a SDOF system with a combined mass of both main's and absorber's.

$$\begin{aligned} & f = 1; c_2 = \infty \\ \frac{|X_1|}{x_s t} &= \sqrt{\frac{(2g)^2}{(2g)^2\left(g^2 - 1 + \mu g^2\right)^2}} \\ & g^2 - 1 + \mu g^2 = 0 \\ & (1+\mu)g^2 = 1 \\ g^2 &= \frac{1}{(1+\mu)} \end{aligned} \tag{3.16}$$

Through this mathematical expression, it can be seen that the system with infinitely large damping value has only one natural frequency which is a SDOF system.
It is very interesting that in Figure3.5, in the different value of c between 0 and infinity, there are 2 points which all the line intersect and undisturbed by the damping value (points O and P) which is also called the locked points. Then the optimum value of c can be found if these 2 points is the maximum peak throughout the frequencies and if these 2 points are the same height.
While the first criteria can be easily found by decreasing/increasing the value of c, the key to the second criteria is the ratio of the natural frequency of the main system and the absorber. Den Hartog define this as the tuning ratio, the derivation of the tuning ratio is explained in the procedure below.

1. These 2 locked points are undisturbed by the damping value

The mathematical expression below describes a condition how the magnification factor is not disturbed by the damping value.

$$\frac{|X_1|}{x_s t} = \sqrt{\frac{A\left(\frac{c_2}{c_c}\right)^2 + B}{C\left(\frac{c_2}{c_c}\right)^2 + D}} \quad ; \quad \frac{A}{C} = \frac{B}{D} \tag{3.17}$$

Using the complete equation from 3.13 to 3.17, the equation for this condition becomes:

$$\begin{aligned} \left(\frac{1}{g^2 - 1 + \mu g^2}\right)^2 &= \left(\frac{g^2 - f^2}{\mu f^2 g^2 - (g^2-1)(g^2-f^2)}\right)^2 \\ \mu f^2 g^2 - \left(g^2-1\right)\left(g^2-f^2\right) &= \pm\left(g^2-f^2\right)\left(g^2-1+\mu g^2\right) \end{aligned} \tag{3.18}$$

The equation 3.18 has two forms of the equation. The equation with a negative sign on the right-hand side gives a trivial solution (the root of g=0) which leads to 0 response. So taking into account the positive sign on

the right-hand side resulting:

$$\begin{aligned}\mu f^2 g^2 - (g^2-1)(g^2-f^2) &= (g^2-f^2)(g^2-1+\mu g^2)\\ \mu f^2 g^2 - g^4 + g^2 f^2 + g^2 - f^2 &= g^4 - g^2 + \mu g^4 - g^2 f^2 + f^2 - \mu g^2 f^2\\ (2+\mu)g^4 - 2(1+f^2+\mu f^2)g^2 + f^2 &= 0\\ g^4 - \frac{2(1+f^2+\mu f^2)}{2+\mu}g^2 + \frac{f^2}{2+\mu} &= 0\end{aligned} \tag{3.19}$$

2. These 2 locked points should be in the same height

Take a look at the equation 3.13, due to the presence of the first condition, any number of c/c_c can be applied. To simplified the equation, choose $c/c_c = \infty$

$$\begin{aligned}\frac{|X_1|}{x_s t} &= \sqrt{\frac{\left(2\frac{c_2}{c_c}g\right)^2 + \left(g^2-f^2\right)^2}{\left(2\frac{c_2}{c_c}g\right)^2\left(g^2-1+\mu g^2\right)^2 + \left[\mu f^2 g^2 - \left(g^2-1\right)\left(g^2-f^2\right)\right]^2}} * \frac{c_c/c_2}{c_c/c_2}\\ &= \sqrt{\frac{(2g)^2}{(2g)^2(g^2-1+\mu g^2)^2}}\end{aligned} \tag{3.20}$$

Then from this point, take into account the second condition which means that point O which is located at g1 is at the same height or have the same $|X_1|/x_s t$ with point P which is located at g2. This condition can be described mathematically using equation 3.20:

$$\begin{aligned}\frac{-1}{g_1^2-1+\mu g_1^2} &= \frac{1}{g_2^2-1+\mu g_2^2}\\ (g_1^2+g_2^2)(1+\mu) &= 2\\ (g_1^2+g_2^2) &= \frac{2}{1+\mu}\end{aligned} \tag{3.21}$$

Now we can finalize the derivation of the tuning ratio by using the characteristics of a quadratic equation for the equation 3.19 that:

$$\begin{aligned}x^2 + ax + b = 0 \quad ; \quad x_1 + x_2 &= -a\\ g_1^2 + g_2^2 &= \frac{2(1+f^2+\mu f^2)}{2+\mu}\end{aligned} \tag{3.22}$$

Therefore, the expression of $f = (\omega_2/\omega_1)$ which is the ratio between absorber's natural frequency and natural frequency of the main system can be obtained by substituting equation 3.22 to 3.21:

$$\begin{aligned}\frac{2}{1+\mu} &= \frac{2(1+f^2+\mu f^2)}{2+\mu}\\ \frac{2(2+\mu)}{1+\mu} &= 2+2(1+\mu)f^2\\ f^2 &= \frac{4+2\mu-2-2\mu}{2(1+\mu)(1+\mu)} = \frac{1}{(1+\mu)^2}\\ f &= \frac{1}{(1+\mu)}\end{aligned} \tag{3.23}$$

The natural frequency of the absorber can be determined using this tuning ratio(f):

$$\omega_2 = \frac{\omega_1}{\left(1+\frac{m_2}{m_1}\right)} \tag{3.24}$$

With this tuning, the Figure3.5 can be plot again with the different natural frequency of the absorber system. It is expected that the point O and P now is at the same height which is the optimum effectiveness of the absorber (Figure3.6). Although the point O and P is now at the same height, a proper value of damping (c) should be determined so that the peak or maximum value is located at the point O and P. Usually, the

optimum value of c can be seen if the plotting line is a approach a straight line between O and P points (this situation can be viewed in the magenta colored line in Figure3.6). In the case when the damping value is too small can be seen in the red colored line, and the case when the damping value is too high can be viewed in the black colored line. These two lines have a peak/peaks, not in the point O and P which means the damping value is not yet at an optimum value.

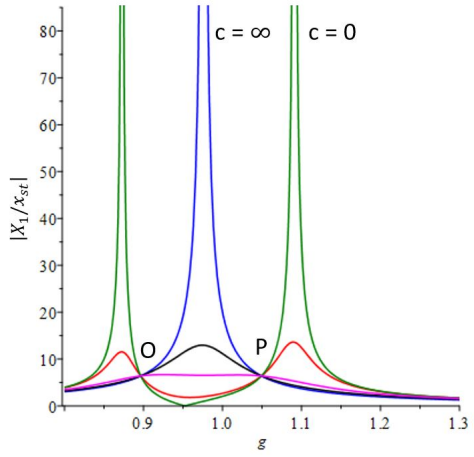

Figure 3.6: Frequency Response Function (Optimum)

3.4. DAMPED VIBRATION ABSORBER IN DAMPED SYSTEM

The soft soil condition also affects the damping of the building. Therefore to study this effect, a two degree of freedom system with a damper in the primary system is modeled.

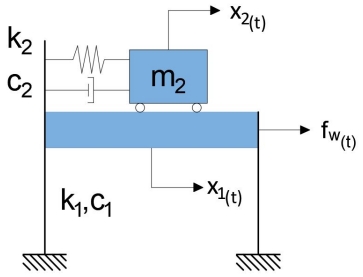

Figure 3.7: DVA in Damped System

Equation of Motions (EOM):

$$\begin{aligned} m_1(\ddot{x}_1) + k_1 x_1 + c_1(\dot{x}_1) + k_2(\dot{x}_1 - \dot{x}_2) + c_2(\dot{x}_1 - \dot{x}_2) &= P_o \sin \omega t \\ m_2(\ddot{x}_2) + k_2(x_2 - x_1) + c_2(\dot{x}_2 - \dot{x}_2) &= 0 \end{aligned} \tag{3.25}$$

Steady State Solution:

$$x_1 = \Im X_1 e^{i\omega t} \quad ; \quad x_2 = \Im X_2 e^{i\omega t} \tag{3.26}$$

Substituting the steady state solution to the EOM resulting:

$$\begin{aligned} (-\omega^2 m_1 + k_1 + i\omega c_1 + k_2 + i\omega c_2)X_1 - (k_2 + i\omega c_2)X_2 - P_o &= 0 \\ (-\omega^2 m_2 + k_2 + i\omega c_2)X_2 - (k_2 - i\omega c_2)X_1 &= 0 \end{aligned} \tag{3.27}$$

The expression for X2 in the equation 3.27 top can be expressed with X1 obtained from the equation 3.27 bottom, by doing this, the expression for X1 after this substitution can be written as:

$$\begin{aligned} X1 = &-(P_o(-m_2\omega^2 + k_2 + i\omega c_2))/ \\ &(\omega^2 c_1 c_2 + i\omega^3 c_1 m_2 + i\omega^3 c_2 m_1 + i\omega^3 c_2 m_2 - \omega^4 m_1 m_2 \\ &- i\omega c_1 k_2 - i\omega c_2 k_1 + \omega^2 k_1 m_2 + \omega^2 k_2 m_1 + \omega^2 k_2 m_2 - k_1 k_2) \end{aligned} \tag{3.28}$$

Using the same method as in the equation 3.11 to 3.13, the dynamic magnification factor for DVA in the damped system as shown below:

$$\frac{|X_1|}{x_s t} = \sqrt{\frac{(-\omega^2 k_1 m_2 + k_1 k_2)^2 + \omega^2 c_2^2 k_1^2}{\omega^2 A^2 + B^2}} \tag{3.29}$$

in which:

$$\begin{aligned} A &= ((-m_1 - m_2)c_2 - c_1 m_2)\omega^2 + c_1 * k_2 + c_2 k_1 \\ B &= -\omega^4 m_1 m_2 + ((m_1 + m_2)k_2 + c_2 c_1 + m_2 k_1)\omega^2 - k_1 k_2 \end{aligned} \tag{3.30}$$

To compare this equation to the DVA system, input the c1 equal to zero, the mass ratio

$$\mu = \frac{m2}{m1} = 0.05 \tag{3.31}$$

and the tuning ratio $\omega_2/\omega_1 = 1/(1+\mu)$. It can be seen that the plotting result (Figure3.8(left)) is the same as in Figure3.6.

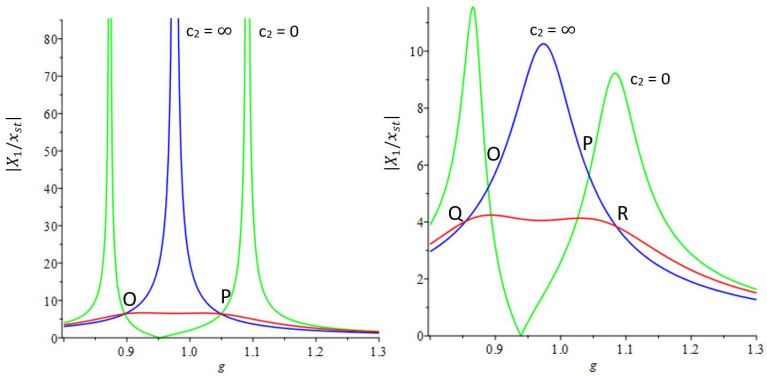

Figure 3.8: FRF DVA Validation (left) DVA with Damped Structure (right)

Figure3.8 FRF DVA Validation (left) DVA with Damped Structure (right) Now with the same equation, plot with the presence of damping value c1 = 0.1 which can be seen in Figure3.8(right). Some difference which occurs due to the presence of damping are:

1. The peak is reduced
2. The point O and P is no longer the optimum points (Q and R)
3. The effectiveness of TMD is reduced

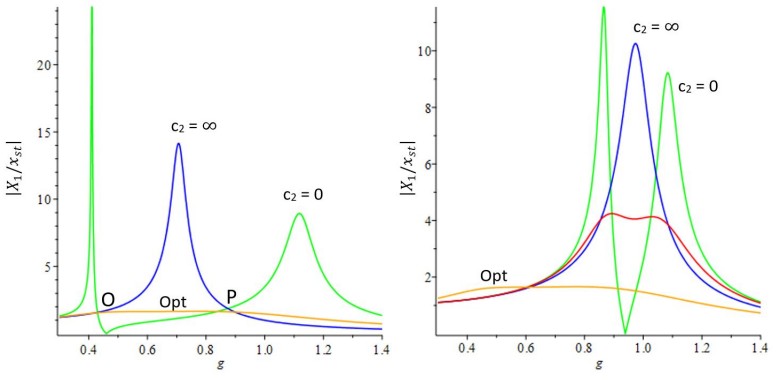

Figure 3.9: Comparison FRF with Higher Absorber Mass

The solution to gain high effectiveness in here can be to increase the peak again by reducing the mass and stiffness of the main mass. But it can also be looked at the different way, to increase the TMD effectiveness is

to lower the intersection points between the blue and green line which means reducing the value of the point (O, P, Q, and R). Therefore it can be done with moving the two peaks of the undamped absorber mass (green line) further away. The two peaks are displaced further away when the mass of the absorber is increased which can be seen in Figure3.9.

The point O and P in Figure3.9 (left) still not the optimum points but because of the scaling, we couldn't see this. But it is true that the optimum point also reduced as the two peaks of the green line are move further. The tuning ratio is no longer the same as DVA but the stiffness of the absorber (k2) still have to be tuned until the optimum points (Q and R) is at the same height. The damping of the absorber (c2) also has to be tuned until the maximum peak is at the optimum points (Q and R).

3.5. ACTIVE MASS DAMPER

Although the concept of a passive mass damper for vibration absorber [16] is proofed to reduce the response of the primary system, there are still weak points of a passive mass damper. Some of the negative points which can be observed through previous chapter are:

1. The effectiveness of passive mass damper can be increased only by increasing the ratio of TMD mass and primary mass which is small in the case of a high-rise building.

2. Due to small mass ratio, damping ratio is also small. Therefore it is practically difficult to tune the TMD. Also, the time for mass absorber to reach steady state is longer due to small damping ratio [24].

Therefore the active mass damper is introduced to optimize the vibration absorber system. The model for the AMD can be seen in the Figure3.10.

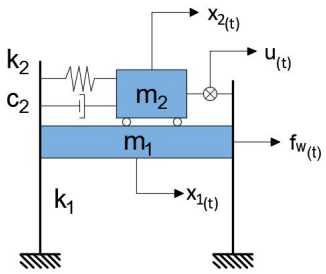

Figure 3.10: Active Mass Damper

The main idea of the AMD is to be able to set the actuator or control force $u_{(t)}$ to the desired response of the primary mass.

3.5.1. FREQUENCY RESPONSE

For stufy purpose of the AMD system, the term relative motion and different type of loading is introduced by [3] in the following equation:

$$\begin{aligned} y_{(t)} &= x_{2\,(t)} - x_{1\,(t)} \\ f_{w\,(t)} &= m_1 \omega_1^2 F e^{i\omega t} \end{aligned} \tag{3.32}$$

The $u_{(t)}$ is the control force which can be described through many algorithm, the convensional algorithm for the control force is the full-state feedback law:

$$u_{(t)} = -Q\ddot{x}_1 = -m_1 q \ddot{x}_1 \tag{3.33}$$

In which Q is the feedback gain and q is normalized feedback gain. The equation of motion for the mass absorber in the AMD system is:

$$\begin{aligned} m_2\ddot{x}_2 + c_2\dot{x}_2 + k_2 x_2 - c_2\dot{x}_1 - k_2 x_1 &= u_{(t)} \\ m_2(\ddot{y} + \ddot{x}_1) + c_2\dot{y} + k_2 y &= u_{(t)} \\ m_2\ddot{y} + c_2\dot{y} + k_2 y &= u_{(t)} - m_2\ddot{x}_1 \end{aligned} \tag{3.34}$$

and the equation of motion of the primary system can be written as:

$$m_1\ddot{x}_1 + k_1 x_1 - c_2\dot{y} - k_2 y = -u_{(t)} + f_{w(t)} \tag{3.35}$$

Through elimination of equation 3.34 and 3.5.1, we can obtain the equation which is indipendent from the control force $u_{(t)}$ which is:

$$(m_1 + m_2)\ddot{x}_1 + k_1 x_1 = f_{w(t)} - m_2\ddot{y} \tag{3.36}$$

Because there are two unknown responses (x_1, x_2) we should use two equations to obtain the responses. The first equation which is used is the equation 3.36, and the second equation is obtained from the substitution of the control force (3.33) to equation 3.34 resulting:

$$m_2\ddot{y} + (m_2 + m_1 q)\ddot{x}_1 + k_2 y + c_2\dot{y} = 0 \tag{3.37}$$

The response of the system can be obtained in the form of:

$$x_{(t)} = Xe^{i\omega t} \quad ; \quad y_{(t)} = Ye^{i\omega t} \tag{3.38}$$

By substituting the solution to the equation 3.36 and 3.37, the equations become:

$$\begin{aligned} -\omega^2 m_2 Y + \left[-\omega^2(m_1 + m_2) + k_1\right] X_1 &= m_1\omega_1^2 F \\ \left[-\omega^2 m_2 + i\omega c_2 + k_2\right] Y - \omega^2(m_1 q + m_2) X_1 &= 0 \end{aligned} \tag{3.39}$$

The expression of Y is obtained from the equation 3.39 bottom equation which can be written as:

$$Y = \frac{\omega^2(m_1 q + m_2)}{-\omega^2 m_2 + i\omega c_2 + k_2} X_1 \tag{3.40}$$

We can obtain the frequency response by substituting the equation 3.40 to the 3.39 top equation.

$$X_1 = \frac{m_1 {\omega_1}^2 \left(-\omega^2 m_2 + i\omega c_2 + k_2\right)}{-m_1 m_2 \left(q-1\right)\omega^4 - i\left(m_1 + m_2\right) c_2 \omega^3 + \left(\left(-k_1 - k_2\right) m_2 - k_2 m_1\right)\omega^2 + i c_2 k_1 \omega + k_1 k_2} \tag{3.41}$$

To simplify the equation, some ratio between the parameter is introduced (similar with the previous mass damper system)

$$\mu = \frac{m_2}{m_1} \; ; \; \omega_2 = \sqrt{\frac{k_2}{m_2}} \; ; \; \omega_1 = \sqrt{\frac{k_1}{m_1}} \; ; \; f = \frac{\omega_2}{\omega_1} \; ; \; g = \frac{\omega}{\omega_1} \; ; \; x_s t = \frac{P_o}{k_1} \; ; \; \eta = \frac{c_2}{c_c} = \frac{c_2}{2m_2\omega_2} \tag{3.42}$$

We can obtain the frequency response by separating the real and imaginary part of the equation 3.41 and taking the absolute value from it just like the procedure in section 3.3 from equation 3.12. The frequency response can be written as:

$$\left|\frac{X_1}{F}\right| = \sqrt{\frac{\left(f^2 - g^2\right)^2 + 4\eta^2 f^2 g^2}{\left(\left(1-q\right)g^4 - \left(\mu f^2 + f^2 + 1\right)g^2 + f^2\right)^2 + 4\eta^2 f^2 g^2 \left(-\mu g^2 - g^2 + 1\right)^2}} \tag{3.43}$$

3.5.2. TUNING RATIO

Due to the presence of the control force $u_{(t)}$, the optimum damping should be depend on it. The optimum damping ratio can be derived with the similar concept of locked points as the DVA by Den Hartog in the section 3.3.

1. These 2 locked points are the intersection between 2 functions

These 2 functions are the response function with zero damping and the response function with infinite damping. By substituting damping ratio equal to zero and infinite to the frequency response function (3.43), the equation becomes:

$$\begin{aligned} \left(\frac{1}{1-(1+\mu)g^2}\right) &= \left(\frac{\left(f^2 - g^2\right)}{(1-q)g^4 - \left(\mu f^2 + f^2 + 1\right)g^2 + f^2}\right) \\ g^4 - \frac{2\left(\mu f^2 + f^2 + 1\right)}{2 + \mu - q} g^2 + \frac{2f^2}{2 + \mu - q} &= 0 \end{aligned} \tag{3.44}$$

Using the characteristic of a quadratic equation to the equation 3.44:

$$\begin{gathered} x^2 + ax + b = 0 \quad ; \quad x_1 + x_2 = -a \\ g_1^2 + g_2^2 = \frac{2\left(\mu f^2 + f^2 + 1\right)}{2 + \mu - q} \end{gathered} \tag{3.45}$$

2. These 2 locked points should be in the same height

This statement can be written in the equation form such as:

$$\left|\frac{X_1}{F}\right|_{(g_1)} = \left|\frac{X_1}{F}\right|_{(g_2)} = \alpha \tag{3.46}$$

The symbol α is the maximum response of the primary mass. From the previous section of DVA, we know that the optimum situation is when the maximum response (α) is placed on the two locked points.
Since the locked points is not influenced by the damping, we can use the infinite damping value to simplify the frequency response equation (3.43) which can be written as:

$$\begin{gathered} \left|\frac{X_1}{F}\right| = \sqrt{\frac{1}{(1 - g^2(1+\mu))^2}} = \pm\frac{1}{(1 - g_{1,2}^2(1+\mu))} \\ \frac{1}{1 - g_1^2(1+\mu)} = \frac{-1}{1 - g_2^2(1+\mu)} \\ g_1^2 + g_2^2 = \frac{1}{1+\mu} \end{gathered} \tag{3.47}$$

From these two conditions, by substituting equation 3.45 to 3.47, the tuning ratio can be obtained such as:

$$f = \sqrt{\frac{1-q}{(\mu+1)^2}} \tag{3.48}$$

3.5.3. NORMALIZED CONTROL FORCE

The value of the normalized control force (q) must be derived from the desired maximum response (α). This condition can be obtained through equation 3.47 (first equation):

$$\frac{1}{1 - g^2(1+\mu)} = \alpha \tag{3.49}$$

The expression of g can be obtained by substituting the tuning ratio (f) to the equation 3.44. The root for the quadratic equation can be obtained trhough:

$$\begin{gathered} ax^2 + bx + c = 0 \quad ; \quad x = \frac{-b \pm \sqrt{b^2 - 4ac}}{2a} \\ g_{1,2}^2 = \frac{1}{1+\mu}\left(1 \pm \sqrt{\frac{\mu+q}{2+\mu-q}}\right) \end{gathered} \tag{3.50}$$

Finally the expression of normalized control force is obtained through substitution of equation 3.50 to 3.49:

$$q = \frac{2 + \mu - \mu\alpha^2}{\alpha^2 + 1} \tag{3.51}$$

Nishimura derived also the optimum damping ratio for active damped vibration absorber in undamped primary system which can be seen in the equation below:

$$\eta = \sqrt{\frac{3(\mu+q)}{8(1+\mu)}} \tag{3.52}$$

3.5.4. FREQUENCY RESPONSE PLOT

The mass ratio is chosen as the same value as the DVA in section 3.3. To plot the frequency response, first we determine the maximum response we would like to achieve. Then the other parameters can be derived from the α.

$$\begin{aligned} \mu &= \frac{1}{20} = 0.05 \\ \alpha &= 3 \\ q &= \frac{2+0.05-0.05*3^2}{3^2+1} = 0.16 \\ f &= \sqrt{\frac{1-0.16}{(0.05+1)^2}} = 0.873 \end{aligned} \tag{3.53}$$

Optimum Damping:

$$\eta = \sqrt{\frac{3(0.05+0.16)}{8(1+0.05)}} = 0.274$$

Now we can plot the frequency response for the main system which depicted in Figure3.11

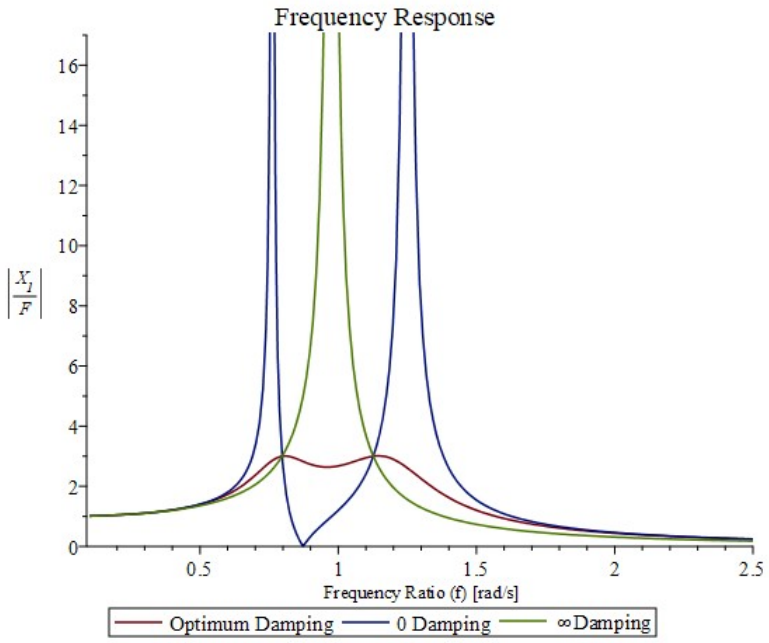

Figure 3.11: AMD Frequency Response for the Primary Mass

It is true that the DVA (section 3.3) and AMD (section 3.5) has different loading case,

$$m_1\omega_1^2 F e^{i\omega t} \quad ; \quad P_o \sin\omega t$$

but because we applied

$$m_1 = 1 \quad ; \quad \omega_1 = 1$$

and since the response is observed in the frequency domain and the harmonic time form of the loading is canceled, therefore we can compare the result for the DVA and AMD which is depicted in the Figure3.12.

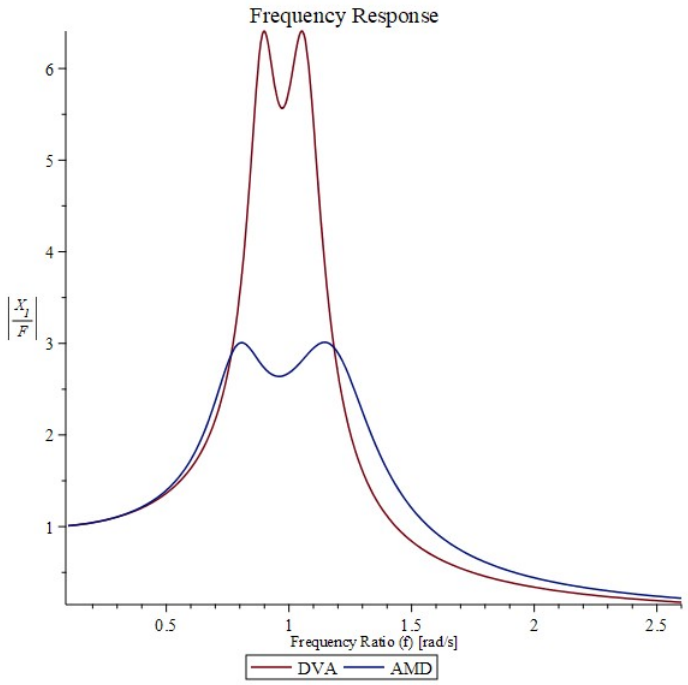

Figure 3.12: Comparison of Frequency Response AMD and DVA

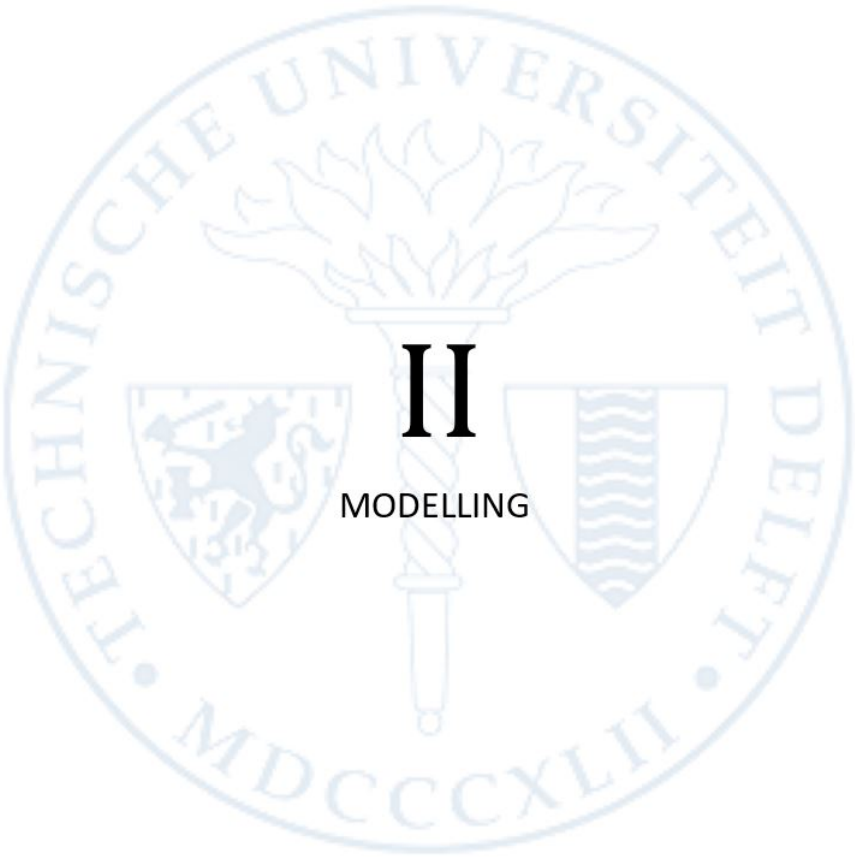

II

MODELLING

4

BUILDING CASE

This chapter discusses the data for the case study which is the European Patent Office (EPO). EPO building is designed by Zonneveld; the building has a slenderness of 1:5 and the ratio between its length and width are 1:8. It's quite a slender and wide building. This building can be categorized as one of the tall buildings in The Netherlands.

4.1. BUILDING DESCRIPTION

To build the analytic model of the high rise building, structural mechanism and flow of forces on the building need to understand carefully. In this thesis, the wind loading is considered to be the main horizontal loading on the building. The first element which interacts with the wind load is the facade of the building, then it transfers the force to the floor or the perimeter beam, then from the floor to the main load-bearing structure. The main load-bearing structure or called the stability system is the main element which resists the horizontal load. Then the force is transferred by this stability system to the base of the building which is the foundation and to the soil.

The dynamic of European Patent Office is analyzed by Zonneveld in collaboration with TNO. A wind tunnel test is performed to the building model, and then the dynamic wind pressure is inputted to the finite element program, TNO Diana. Static analysis is performed with finite element program SCIA Engineer. The dimension of the building is:

Building Parameter		
Building Height	105	m
Building Width	156	m
Building Thickness	18	m

Table 4.1: EPO building data

4.1.1. SCOPE AND ASSUMPTION

This thesis is focused on the influence of the TMD in reducing the dynamic response of a building. The TMD is mainly used to reduce the response of the building on the serviceability limit especially acceleration. The vibration of a building due to horizontal wind loading is mainly on the horizontal axis. Therefore we neglect the vertical vibration of the building. Then we can determine the building properties which contribute to the horizontal vibration which can be categorized in three main components:

- Superstructure : Building mass, stiffness and damping
- SSI Component : Translation and rotation of the base due to interaction between the building foundation and soil
- TMD Component : TMD mass, spring, and dashpot

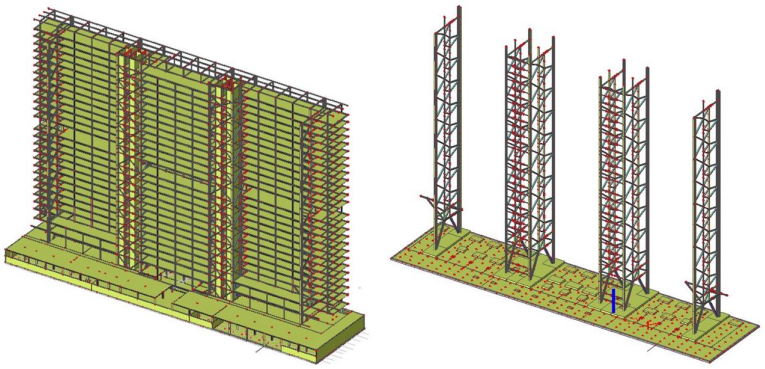

Figure 4.1: European Patent Office Building

The European Patent Office (EPO) building use a steel frame as the main load bearing structure. There are four main steel frame in the building, and each of them are supported by a concrete block of 20x2m at the base as it can be seen in the Figure4.1.

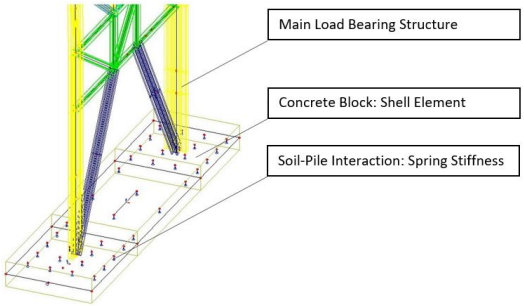

Figure 4.2: Group Piles Model in SCIA Engineer (Zonneveld)

The concrete block is then supported by a group of piles. The piles are modeled as a vertical and horizontal spring-dashpot elements on the finite element program.The large proportion of the piles is located under the tip of the steel frame as it can be seen in the Figure4.2.

To understand the behavior of the concrete plate on the base, the deformation of the plate is observed. The deformation of the concrete plate due to horizontal wind load on the building (static analysis) is shown in Figure4.3. The static analysis means that the fluctuating component of the wind is taken into account by a constant load factor. It can be seen that the plate on the base of the building does not act as a rigid plate, the large deformation is concentrated on the thick concrete plate below the steel frame especially the location which has direct contact with the steel profile. The rest of the concrete plate has hardly resisted any deformation.

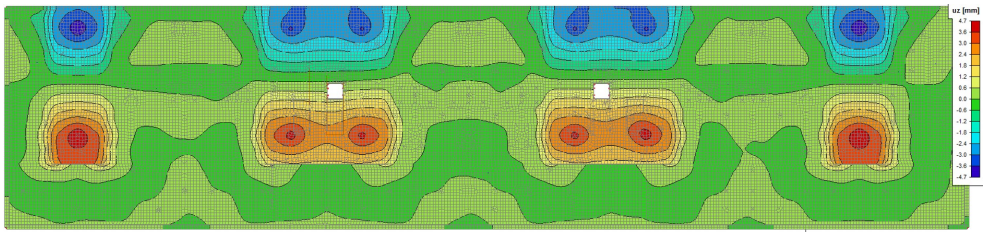

Figure 4.3: Deformation of The Base Concrete Plate due to Horizontal Wind Load

The one dimensional model for the building can be seen in the Figure4.4. The torsional vibration (Figure4.4 (right)) has a significant influence because the width of the EPO Building is larger than the height. A torsional load can be derived from a horizontal load with a certain eccentricity along the building width. This torque

can also be seen as a bending moment in the plane on the floor. Then the floor transferred the force to the steel frame which in principal receives a horizontal force the same as the bending beam case. Therefore both stiffness of the beam (EI) and the torsional rod (GJ) comes from the four steel frames as the main load-bearing structure in the building.

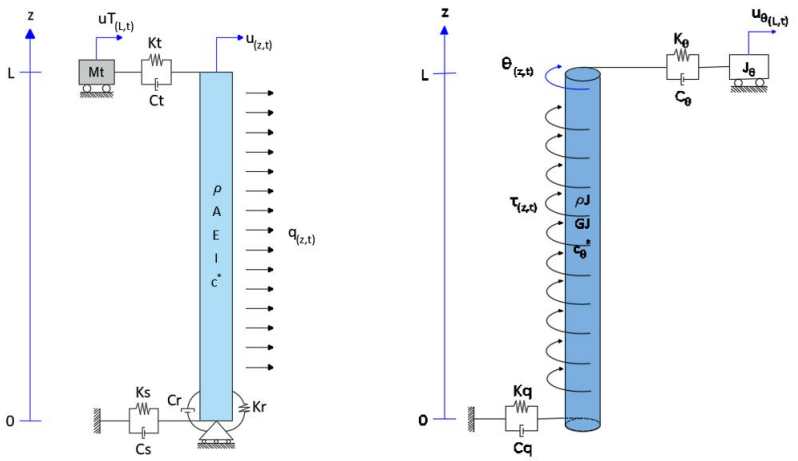

Figure 4.4: Continuous System: High Rise Building with TMD Model

The base resistance to the rotational on the beam is majority taken by the vertical group piles under the steel frame Figure4.2. This rotational resistance is modeled as a rotational spring and dashpot at z = 0. The horizontal resistance of the group piles is modeled as a translation spring-dashpot for the beam and as a torsional spring-dasphot for the torsional rod.

The derivation of equation of motion of the Euler-Bernoulli beam and torsional rod can be seen in the appendix A, the equation can be written as:

$$\begin{aligned} \rho A \frac{\partial^2}{\partial t^2} u_{(z,t)} + \frac{\partial^2}{\partial z^2}\left(EI\left(1 + c^* \frac{\partial}{\partial t}\right)\frac{\partial^2}{\partial z^2} u_{(z,t)}\right) &= q_{(z,t)} \\ \rho J \frac{\partial^2}{\partial t^2}\theta_{(z,t)} + \frac{\partial}{\partial z}\left(GJ\left(1 + c_\theta^* \frac{\partial}{\partial t}\right)\frac{\partial}{\partial z}\theta_{(z,t)}\right) &= \tau_{(z,t)} \end{aligned} \tag{4.1}$$

The ρA is the distributed mass, EI is the stiffness and c^* is the damping properties of the beam. While for the torsional bar, J is the polar moment of inertia and GJ is the torsional stiffness of the bar.

4.1.2. ANALYTICAL MODEL

The model which is used in this thesis to analyzed the EPO building is the continuous system of a Euler-Bernoulli Beam as it can be seen in Figure4.4. The method of analysis in this thesis is the frequency domain analysis using Fourier Transform. The reason for the chosen model and method are:

- Euler-Bernoulli is the most simple model compare to the Rayleigh and Timoshenko beam theory. This model is sufficient to model the high rise building because the effect of rotational inertia and the shear deformation is not significant in this case.
- A high rise building's main stability system (core) resist the load through bending stiffness which is the major component of the building compared to the shear stiffness of the building frame.
- Wind load is the only horizontal loading which is considered therefore zero initial condition can be taken into account, and Fourier Transform can be applied.
- Wind loading is a continuous loading on the building which has no time duration such as Earthquake loading. Therefore analysis in the frequency domain is the only method to identify the damping of the building.
- The wind load spectrum is well known tools to take wind loading into account. This spectrum contains various data of the wind load which is used in the building code to design a building.

- Fourier transform can handle boundary condition with time components such as dashpot which is considered in this thesis for the SSI and TMD.

In every model and theory, there is some assumption which has to be satisfied to perform the analysis. The assumptions which are made due to the Euler-Bernoulli beam model and Fourier Transform method are:

- The cross-section of the beam remain planar to the central axis which neglects the rotational of the cross-section.
- The system has a small vibration or small deformation theory is applied. The theory can be applied if the beam slope squared is smaller than 1.
- Fourier Transform uses the principle of superposition which states that a periodic function can be expanded to a summation of sines and a cosines function. This method can be applied only in the linear system.
- The torsional behavior is assumed constant along the width, in later chapter it can be seen through the finite element model that this is not the case.

The derivation of the dynamic of a Euler-Bernoulli beam can be seen on the Appendix A. It is shown that the dynamic stiffness matrix from the equation A.23 is:

$$\begin{bmatrix} Ks+i\omega Cs & \beta^3 EI^* & Ks+i\omega Cs & -\beta^3 EI^* \\ EI^*\beta^2 & -(Kr+i\omega Cr)\beta & -EI^*\beta^2 & -(Kr+i\omega Cr)\beta \\ \gamma\cosh(\beta L)+EI^*\beta^3\sinh(\beta L) & \gamma\sinh(\beta L)+EI^*\beta^3\cosh(\beta L) & \gamma\cos(\beta L)+EI^*\beta^3\sin(\beta L) & \gamma\sin(\beta L)-EI^*\beta^3\cos(\beta L) \\ EI^*\beta^2\cosh(\beta L) & EI^*\beta^2\sinh(\beta L) & -EI^*\beta^2\cos(\beta L) & -EI^*\beta^2\sin(\beta L) \end{bmatrix} \tag{4.2}$$

A condition of the linear homogeneous algebraic equation of

$$\underline{\underline{K_D}} * \underline{C} = 0 \tag{4.3}$$

is the determinant of the matrix $\underline{\underline{K_D}}$ is equal to zero. By doing so, we can obtain the frequency equation which the roots of this equation are the natural frequency of the system. The frequency equation which is obtained through Determinant$|K_D|$ can be written as:

$$\begin{aligned} \text{Frequency Equation} = & |2EI^*\beta^3((EI^*\beta^3(-\beta^4 EI^{*2} - CrCs\omega^2 + (iCrKs + \\ & 2iCr\gamma + iKrCs)\omega + Kr(Ks+2\gamma))\cos(\beta L) + (-\beta^4((Kr+i\omega Cr)\beta^2 + \\ & i\omega Cs + Ks + \gamma)EI^{*2} + (-CrCs\omega^2 + (iCrKs + iKrCs)\omega + \\ & KrKs)\gamma)\sin(\beta L))\cosh(\beta L) - (\beta^4((Kr+i\omega Cr)\beta^2 - i\omega Cs - Ks - \gamma) \\ & EI^{*2} + (-CrCs\omega^2 + (iCrKs + iKrCs)\omega + KrKs)\gamma)\sinh(\beta L) \\ & \cos(\beta L) + 2EI^*\beta((Ks+i\omega Cs)\sin(\beta L)\gamma\sinh(\beta L) + 1/2\beta^2(\beta^4 \\ & EI^{*2} - CrCs\omega^2 + (iCrKs + irCs)\omega + KrKs)))| \end{aligned} \tag{4.4}$$

4.2. BUILDING PROPERTIES

This section discusses how to obtain all the properties needed for the one dimensional model from the model in finite element program. The building properties are categorized into two groups: superstructure and soil-structure interaction. The TMD properties is set to zero when searching the building properties.

4.2.1. SUPERSTRUCTURE

There are three properties which are needed from the superstructure namely: building mass, building stiffness, and building damping.

BUILDING MASS

The total mass of the building comes from two sources: self-weight and the vertical load of the building. The data from Zonneveld which is from the SCIA Engineer shows that the total mass of the building is: 1,004,143 kN. This total mass needs to be converted to a distributed mass over the height for the one-dimensional model. Then the total mass divided by the building height is $9.5x10^5 kg/m$.

BUILDING STIFFNESS

The stiffness of the building can be obtained through a static equation. Since Zonneveld has designed the dimension of the structure in the SCIA Engineer software, we can obtain the static loading of the building which is shown in the Figure4.5. There are two types of the load, the number in green color represents the point load on the perimeter of the building due to the wind pressure on the building side and building roof. The number in magenta color is the distributed load along the floor which represents the wind pressure on the building facade. The total building height is 110 m, but the 5 m on top is a roof structure which also received a wind load but directly transfers it to the the steel frame.

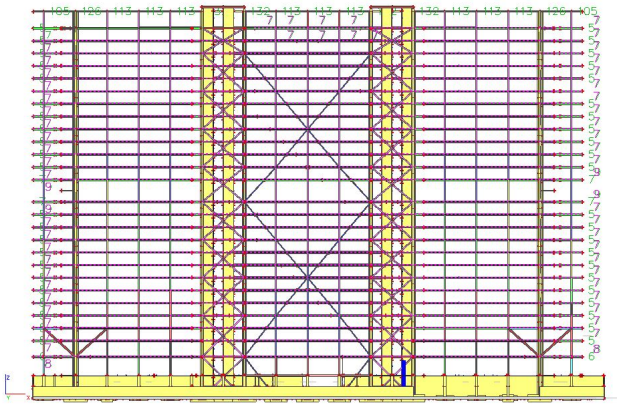

Figure 4.5: Wind Load on the Building

Then in this case, the building can also be modeled as an Euler-Bernoulli beam model which resist a distributed horizontal load and a point load on the top due to the load which is transfered from the roof (Figure4.6).

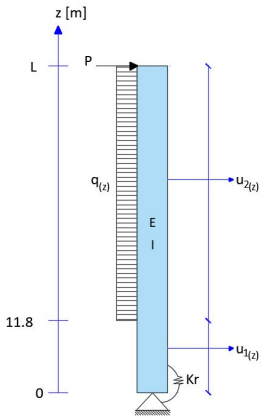

Figure 4.6: Building Model for Static Analysis

The building height is 105 m. To obtain the distributed load over the z coordinate on the beam ($q_{(z)}$), the distributed load on the floor (q_{floor}) and the point load (p_{floor}) should be transform through the equation below:

$$q_{(z)} = \frac{\sum_{i=1}^{26} q_{floor(i)} * B_{width} + p_{floor(i)}}{105 - 11.8} = 314.44 kN/m \tag{4.5}$$

$$P = 2007 kN$$

The number 26 comes from the number of floor in which the distributed and point load acts on the floor, it can be seen in the Figure4.5 that the wind load start from the height of 11.8 m to the 105 m in which 26 floors are present. The point load P is just a summation of a point loads present at the top of the building. The

deformation on the top of the building which is obtain from the finite element program can be seen in the Figure4.7:

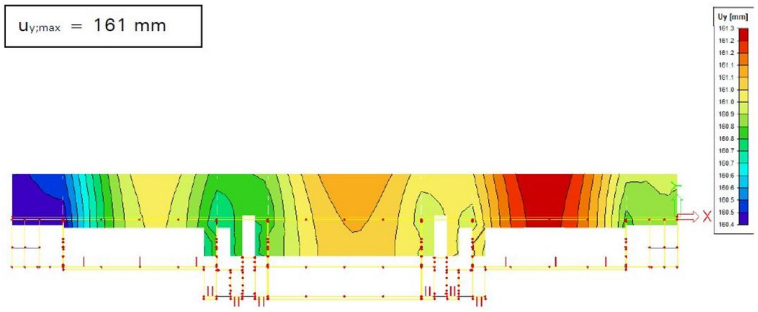

Figure 4.7: Building Top Deformation

The derivation of the static analysis of an Euler-Bernoulli beam can be seen in the appendix B. The final equation for the deformation on the top of the building is:

$$u_{2_{(z)}} = \frac{1}{EI}\Big(\frac{1}{24}qz^4 + \frac{1}{6}(-Lq-P)z^3 + \frac{1}{4}L(Lq+2P)z^2 + \frac{1}{6} \\ \frac{(-KrL1^3q+3EIL^2q-3EIL1^2q+6EILP)z}{Kr} + \frac{1}{24}qL1^4\Big) \tag{4.6}$$

To complete the equation 4.6, the value of rotational stiffness K_r should be obtained first. This value can be obtained by observing the botom rotation of the building which is shown in the Figure4.3. There is two maximum deformation which is a: 4.7 mm and b:-4.7 mm. The rotation on the bottom can be obtain through the equation below:

$$\theta_{(0)} = \frac{\partial u_{1_{(0)}}}{\partial z} = \tan^{-1}\left(\frac{a-b}{l_{distance}}\right) = \tan^{-1}\left(\frac{(4.7+4.7)/1000}{18.1}\right) = 0.0005rad \tag{4.7}$$

The final equation for the rotation on the bottom of the beam can be seen in the B.16. By substituting the properties below, we can obtain the value of the rotational stiffness Kr which is:

$$\frac{\partial u_{1_{(0)}}}{\partial z} = \frac{1}{EI}\left(\frac{1}{2}\frac{\left(qL^2 - qL1^2 + 2LP\right)EI}{K_r}\right) \\ K_r = 3.84 * 10^{12} \tag{4.8}$$

Then with the value of the Kr, the stiffness EI from the equation 4.6 can be obtained as:

$$u_{2_{(L)}} = 0.161 = \frac{1}{EI}\Big(\frac{1}{24}qL^4 + \frac{1}{6}(-Lq-P)L^3 + \frac{1}{4}L(Lq+2P)L^2 + \frac{1}{6} \\ \frac{(-KrL1^3q+3EIL^2q-3EIL1^2q+6EILP)L}{Kr} + \frac{1}{24}qL1^4\Big) \\ EI = 5.1 * 10^{13} \tag{4.9}$$

The building stiffness can also be obtained from the frequency equation in 4.4. But to plot this equation the properties from the soil structure interaction must be obtained. The value of building stiffness and damping will be tuned to the natural frequency obtained by the finite element software after the SSI properties is obtained.

BUILDING DAMPING

The Eurocode determines the value of the building damping which can be used for the high rise design. In this case, the building damping which is used for the dynamic analysis in TNO Diana is 1%. This damping

is derived from the experimental result and is categorized based on building material. This value is an approximation based on the experimental result. Zonneveld also does an experimental result from the existing building which is Montevideo and Kemedy Building in the Netherlands. The result shows that the building damping is 1% for Montevideo and 2% for Kemedy which both of them use steel structure as the main structural material. The influence of this damping uncertainty is discussed in the later chapter.

The damping in the one-dimensional model is defined by the value of c^* We would like to know the value of the c^* to have 1% building damping. The procedure to identify the damping is to apply a hammer test on the structure. In an analytical model such as one dimensional model in this thesis, the hammer test is represented by a point load which has a very high force in a very short time. In the frequency domain, this load is a constant load of 1N over the frequency which also called the white noise spectrum. This model can be seen in the appendix A.2.

Identification of the damping is done in the frequency domain, this method is introduced by Kennedy-Pancu which is called the bandwidth of half-power points. First, the response in the frequency domain should be obtained. The graph of this frequency response can be seen in the figure below:

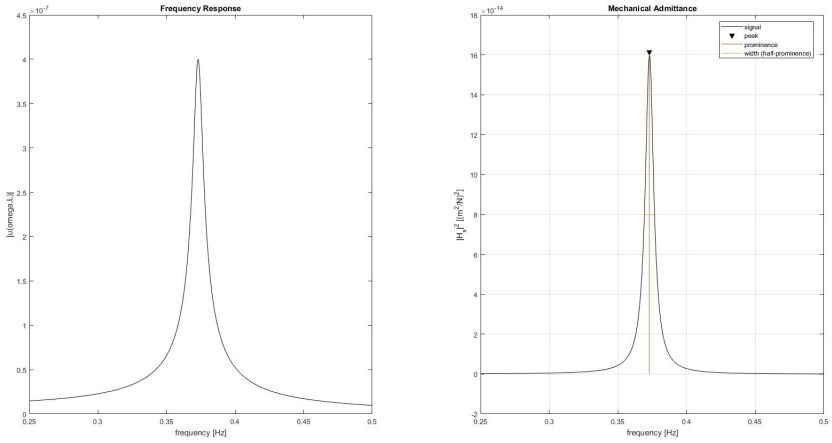

Figure 4.8: Frequency Response

The damping can be identified from the squared of the frequency response is also called the power spectral density. It describe the power (amount of energy transferred per unit time) or rate of work, in the frequency domain. Then the damping ratio can be identified by taking the half of the peak value, then measure the width of the graph which is intersect with this half peak value. In the equation form this can be written as:

$$\zeta = \frac{width}{2\omega_n} = \frac{\tilde{u}^+_{(peak/2)} - \tilde{u}^-_{(peak/2)}}{2\omega_n} = \frac{0.0074}{0.3729} = 0.01 = 1\% \tag{4.10}$$

where ω_n is the frequency where the peak located (natural frequency). This 1% damping is obtain by the value of $C^* = 8.5 * 10^{-3}$.

4.2.2. SOIL STRUCTURE INTERACTION

The pile design use soil data available from the CPT test and calculated to a single spring stiffness. Therefore this single spring stiffness represents the interaction between pile and soil which is modeled in the finite element software Figure4.2.

Due to the load settlement behavior, the stiffness of the single pile on soil subjected to a static load is different than to the dynamic load. According to the SBR-hanboek Fundering en Cement 1998-1-3, the spring stiffness of the dynamic load is higher than the static load due to this settlement behavior. The spring stiffness which is used for the static analysis (SCIA Engineer (Zonneveld)) is shown in the Figure4.9.

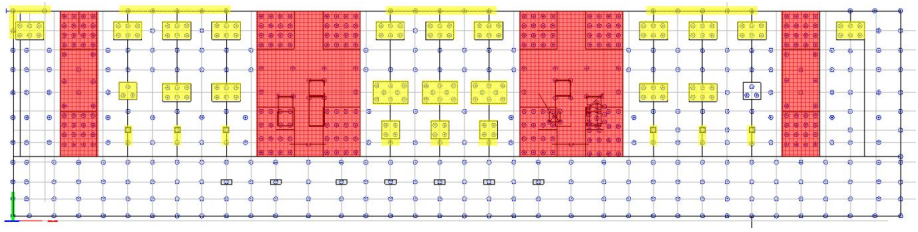

Figure 4.9: Pile-Soil Properties (Zonneveld)

The rectangular shape is the concrete blocks and the circle is the spring stiffness in this model. The vertical stiffness for each single spring is 358 MN/m for the red color area, 181 MN/m for the yellow color area, and 123 MN/m for the rest. The properties of pile and soil interaction in the dynamic analysis (TNO Diana) are shown in the Figure4.10.

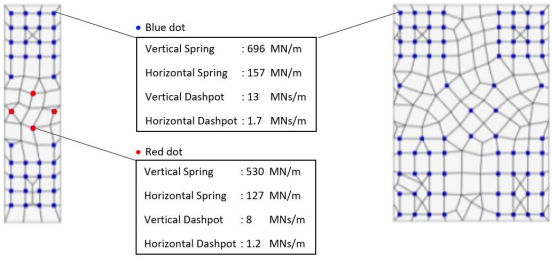

Figure 4.10: Pile-Soil Properties (TNO Diana), Left Figure (Frame 1), Right Figure (Frame 2)

Because the concrete block is not act as a rigid pile as it is shown in Figure4.3 for static case, the behavior of the soil structure interaction is non linear due to the relation between force and the flexibility of the concrete block. Because in the dynamic analysis, the force has a fluctuating value over time. For smaller load, the concrete may behave as a rigid plate and the force is well distributed to the pile. In this case the rotational spring stiffness has a larger value. But there is a limit when the force is high enough that the plate behave as a flexible plate, in this case the rotational spring stiffness has a lower value.

REDUCTION FACTOR

In this thesis, a conservative approach is done by using the largest reduction which is the static analysis case in Figure4.3. This deformation figure is caused by a wind force which resulting a maximum displacement of 161mm (Figure4.7) on top of the building. On the dynamic analysis by TNO Diana, the result of the displacement can be seen in the Figure4.11.

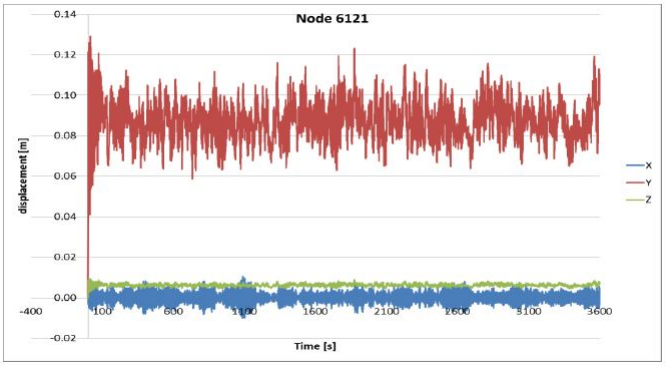

Figure 4.11: Displacement Response on the Top of the Building Height and Middle of the Building Width

It can be seen that the maximum of the displacement from the fluctuating wind force is less than the static analysis. Therefore because the structure still behave in the elastic region, the total force which is transfered to the concrete block is also larger in the static analysis case. Then it can be concluded that the behavior in Figure4.3 is the conservative case although there is still uncertainty that the structure may has a larger response when the non linear analysis is performed. From the finite element program (SCIA Engineer) the reaction force on each vertical spring can be obtained which is shown in the Table 4.2.

no	7	6	5	4	3	2	1	2	3	4	5	6	7
Coordinate [m]	-20.8	-19	-17.3	-15.5	-13.8	-11.3	-9.3	-7.1	-4.4	-2.2	-0.5	1.3	3
Spacing [m]		1.8	1.7	1.8	1.7	2.5	2	2.2	2.7	2.2	1.7	1.8	1.7
Force [kN]	1134	1171	1076	844	580		20		652	930	1093	1093	974
	1233	1367	1270	932		256		306		1034	1313	1264	1077
	1232	1367	1270	934						1306	1318	1268	1081
	1134	1171	1077	844	580		20		654	935	1099	1100	984
Moment Arm [m]	11.5	9.7	8	6.2	4.5	2	0	2.2	4.9	7.1	8.8	10.6	12.3

no	1	2	3	4	5	6	7	8	9	10	11
Coordinate [m]	2.6	0.9	-0.9	-2.6	-6.6	-9.3	-12.3	-14.8	-17.3	-19.8	-22.3
Spacing [m]		1.7	1.8	1.7	4	2.7	3	2.5	2.5	2.5	2.5
Force [kN]	924	948	879	710	193.5		-265.83	-796	-1051	-984	-755.475962
	1044	1135	1053	794				-826	-1182	-1081	-801.475962
	1084	1161	1074	812			-265.83	-812	-1163	-1068	-807.475962
	1053	1041	950	771	193.5		-265.83	-758	-1003	-948	-779.475962
	1058	1049	958	781	193.5		-265.83	-763	-1018	-955	-782.475962
	1093	1175	1088	828				-813	-1204	-1080	-810.475962
	1055	1148	1070	813			-265.83	-812	-1198	-1092	-804.475962
	936	964	898	732	193.5		-265.83	-770	-1049	-987	-754.475962
Moment Arm [m]	11.9	10.2	8.4	6.7	2.7	0	3	5.5	8	10.5	13

Table 4.2: Reaction Force on the Spring Elemen, Top Table (Frame 1), Bottom Table (Frame 2)

Then the bending moment in the group piles can be calculated by multiply the reaction force to the moment arm for each pile, the total bending moment of the group piles for the first and second steel frame are:

$$\begin{aligned} M &= \sum_{i=1}^{n} F_i * e_i \\ M_1 &= 3.49 * 10^8 Nm \\ M_2 &= 5.75 * 10^8 NM \end{aligned} \tag{4.11}$$

It is known from the equation 4.7 that the maximum rotation on the bottom is 0.005. If the rotation of the concrete block in the frame 1 and frame 2 are taken into account separately, the rotation 0.005 is for the frame 1 while 0.000453 is the rotation for the frame 2. Then the rotational stiffness can be obtain as follow:

$$\begin{aligned} Kr_1 &= \frac{M_1}{\theta_1} = \frac{3.49 * 10^8}{0.0005} = 6.98 * 10^{11} Nm/rad \\ Kr_2 &= \frac{M_2}{\theta_2} = \frac{5.75 * 10^8}{0.000453} = 1.27 * 10^{12} Nm/rad \end{aligned} \tag{4.12}$$

Then the total rotational stiffness for the whole building can be calculate. Also the comparison can be made between the method from the static beam (equation 4.8) and from the finite element program. It can be seen

from the equation 4.13 that the error of the static beam method is 2.46% which is small.

$$\begin{aligned} Kr &= 2 * Kr_1 + 2 * Kr_2 = 3.93 * 10^{12} Nm/rad \\ \text{error} &= \left| \frac{Kr_m2 - Kr_m1}{Kr_m2} \right| = \left| \frac{3.84 - 3.93}{3.93} \right| = 2.46\% \end{aligned} \tag{4.13}$$

This is the rotational stiffness when the concrete block is considered as a flexible plate from finite element program. If the concrete bloc is considered as a rigid plate, then the rotational stiffness can be obtain through following equation:

$$\begin{aligned} Kr_1 &= \sum_{i=1}^{n} K_{s_i} * e_i^2 = 1.0663 * 10^{12} Nm \\ Kr_2 &= \sum_{i=1}^{n} K_{s_i} * e_i^2 = 2.133 * 10^{12} Nm \end{aligned} \tag{4.14}$$

It can be concluded that the reduction factor for the rotation stiffness due to the flexibility of the concrete block in the case of the static load (SCIA Engineer Figure4.3) is:

$$\begin{aligned} &\text{Frame 1:} \\ &\text{Reduced Factor}: \frac{0.698}{1.0663} = 65.47\% \\ &\text{Frame 2:} \\ &\text{Reduced Factor}: \frac{1.27}{2.134} = 59.53\% \end{aligned} \tag{4.15}$$

The soil parameter for a single pile from the Figure4.10 should be converted to the rotational and translational spring-dashpot of the beam model in Figure4.4. This section shows the procedure to obtain the value of the translation spring stiffness and damper, also rotational stiffness and damper.

DYNAMIC PARAMETERS OF THE SSI

The dynamic parameter for the SSI is dependent to the frequency of the excitation or the natural frequency of the structure. In the design method for the high rise building, Gazetas create a table which gives a procedure in deriving the dynamic stiffness and dashpot of the pile foundation. In this thesis, the dynamic stiffness and dashpot is shown in the Figure4.10. The rotational stiffness and dashpot for the dynamic analysis of one dimensional model can be obtained by the equation:

$$\begin{aligned} Kr_1 &= \sum_{i=1}^{n} K_i * e_i^2 = 2.07 * 10^{12} Nm \\ Cr_1 &= \sum_{i=1}^{n} C_i * e_i^2 = 3.87 * 10^{10} Nsm \\ Kr_2 &= \sum_{i=1}^{n} K_i * e_i^2 = 4.15 * 10^{12} Nm \\ Cr_2 &= \sum_{i=1}^{n} C_i * e_i^2 = 7.75 * 10^{10} Nsm \end{aligned} \tag{4.16}$$

The flexibility of the concrete block is taken into account by multiplying the value from the equation 4.16 by the reduction factor (equation 4.15). Then the final value of the SSI properties for the one dimensional model can be written as:

$$\begin{aligned} Kr &= 2 * 2.07 * 10^{12} * 0.6547 + 2 * 4.15 * 10^{12} * 0.5953 = 7.65 * 10^{12} \\ Cr &= 2 * 3.87 * 10^{10} * 0.6547 + 2 * 7.75 * 10^{10} * 0.5953 = 1.43 * 10^{12} \end{aligned} \tag{4.17}$$

For the pile soil interaction in the horizontal or translational axis the concrete block is assumed to be rigid. Because the width of the concrete block is 9 times higher than its thickness, then intertia of the concrete in the horizontal direction is 9^3 higher. Therefore the value of the translational spring and dashpot for the one

dimensional model is the number of piles multiplied by its spring stiffness or dashpot properties (Figure4.10).

$$
\begin{aligned}
Ks_1 &= 36piles * 157N/m + 4piles * 127N/m = 6.16 * 10^9 N/m \\
Cs_1 &= 36piles * 1.7Ns/m + 4piles * 1.2N/m = 6.60 * 10^7 Ns/m \\
Ks_2 &= 76piles * 157N/m = 1.19 * 10^{10} Ns/m \\
Cs_2 &= 76piles * 1.7Ns/m = 1.29 * 10^8 Ns/m \\
K_s &= 2 * Ks_1 + 2 * Ks_2 \\
C_s &= 2 * Cs_1 + 2 * Cs_2
\end{aligned}
\tag{4.18}
$$

In summary, the properties for the SSI in the one dimensional model (Figure4.4 (right) bending vibration) can be seen in the Table4.3.

SSI Parameter		
Ks	$3.62 * 10^{10}$	N/m
Kr	$7.65 * 10^{12}$	Nm/rad
Cs	$3.9 * 10^8$	Ns/m
Cr	$1.43 * 10^{11}$	Nms/rad

Table 4.3: EPO SSI Properties for One Dimensional Model

4.2.3. NATURAL FREQUENCY AND MODE

In the case of the wind load, the building is excited on the low frequency because the characteristic of the wind load spectrum has a high value on the low frequency. It is known from the finite element program that the first two natural frequency (Figure4.12) of the building is the torsional mode 0.285 Hz (1.79 rad/s) and the bending mode 0.337 Hz (2.117 rad/s).

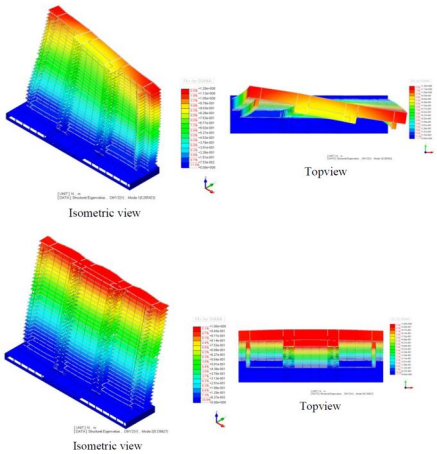

Figure 4.12: Building Natural Frequency; Top: Torsional; Bottom: Bending

For the one dimensional model, the natural frequency can be obtained by plotting the frequency equation in the equation 4.4. To obtain the similar frequency as the finite element program, the building mass and stiffness is changed to:

Building Parameter		
EI	$4.7 * 10^{13}$	Nm^2
ρA	$8.7 * 10^5$	kg/m
C^*	$8.5 * 10^{-3}$	s

Table 4.4: EPO building data

The plot of the frequency equation using the properties from table 4.3 and 4.4 can be seen in theFigure4.13. The natural frequency of the system for bending vibration is the root of the frequency equation. In the graph, it can be seen that the value is 0.3345 Hz which is similar to the value from finite element program.

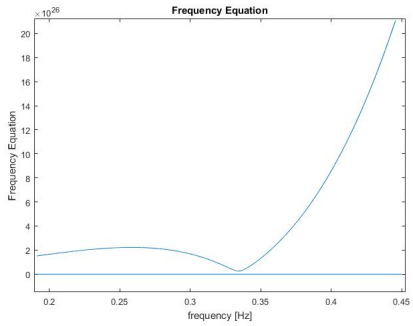

Figure 4.13: Frequency Equation Plot

The procedure to obtain the mode shape can be seen on the AppendixA. The mode shape for the first three natural frequencies of the system can be seen on the Figure4.14. In the high rise building which is induced by a wind load, it is mostly always the case that only the first mode excited by the wind load. Because the wind spectrum act in low frequency (Figure5.9).

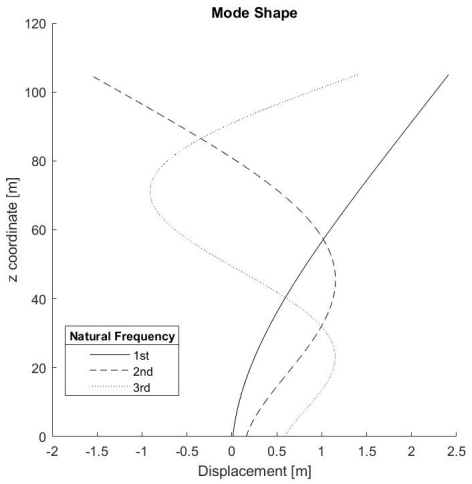

Figure 4.14: Mode Shape

4.3. TORSIONAL VIBRATION

The torsional vibration of the building is considered separately (uncoupled) from the bending vibration. Coupled Bending-Torsion vibration occurs due to the difference between the shear center of the cross-section and the center of mass. If the building cross-section is symmetrical on both of the axes, the torsion vibration can be uncoupled to the bending. If the building is symmetric on one of the cross-section, the torsional center will be located on the symmetric axis.

If we see the top view of the cross section of the EPO building including the steel frame, it can be seen that the building is symmetric in one axis which is the Y-axis. Therefore the location of the torsional axis is located in line with the Y-axis. Then the torsional motion can be determined as it is depicted in the Figure4.15.

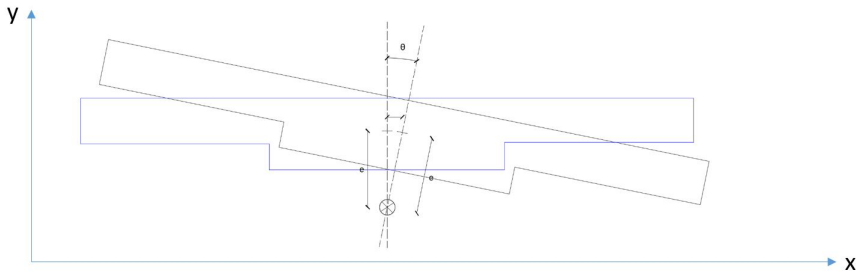

Figure 4.15: Torsional Deformation

In this building, the small rotation theory is applicable in the torsional vibration. Therefore it can be stated that the torsional movement will induce a translational deflection on the X and Y-axis. The translational deflection on X-axis is dominant while the deformation on Y-axis due to torsional movement is negligible. Thus on the vibration on Y axis, the torsion and bending can be uncoupled.

The torsional vibration of the EPO building is modeled as a torsional bar (Figure4.4 (right)). The TMD act as a torsional aborber on the top of the building. Soil structure interaction also modeled as a torsional spring and dashpot on the bottom of the bar. The equation of motion for the torsional vibration is:

$$-\omega^2 \rho J \tilde{\theta}_{(z,\omega)} - \frac{\partial}{\partial z}\left(GJ\left(1+i\omega c_\theta^*\right)\frac{\partial}{\partial z}\tilde{\theta}_{(z,\omega)}\right) = \tilde{\tau}_{(z,t)} \tag{4.19}$$

Building and soil structure properties need to be obtained to find the response for the torsional vibration. The procedure to obtain these properties is the same as the bending properties, the detail procedure can be seen in the following section.

4.3.1. STATIC CALCULATION - SUPERSTRUCTURE

The torsional stiffness of the building for the torsional bar model can be obtained through the finite element program. The torque which is applied to the building can be seen in the Figure4.16. The figure is a top view of a floor in the building.

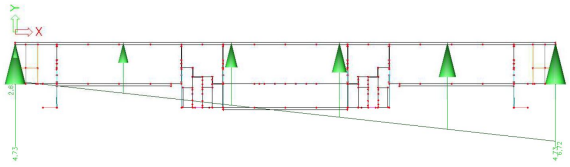

Figure 4.16: Torsional Wind Loading

The wind loading consist of two part, a constant distributed load along the width and a torque which can be seen in the Figure4.17:

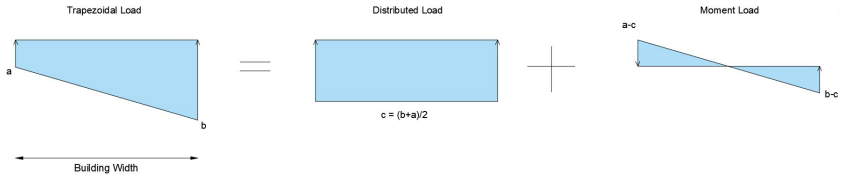

Figure 4.17: Separation of Trapezoidal Wind Load

The distributed load contributes to the bending behavior of the building while the moment load contributed to the torque. Therefore the distributed torque along the height for the torsional bar model can be calculated as:

$$\tau = \sum_{i=1}^{26} \frac{1}{6} \frac{d_i \, B^2}{105 - 11.8} = 2383.33 kNm/m \tag{4.20}$$

From Figure4.17:

$$\begin{aligned} d = b - c \quad \text{and} \quad a - c = -d \\ B = \text{Building Width} \end{aligned} \tag{4.21}$$

The torsional rotation which is obtain from the static calculation in finite element program can be seen in the Figure4.18. The graph is a top view of the building deformation due to the trapezoidal load.

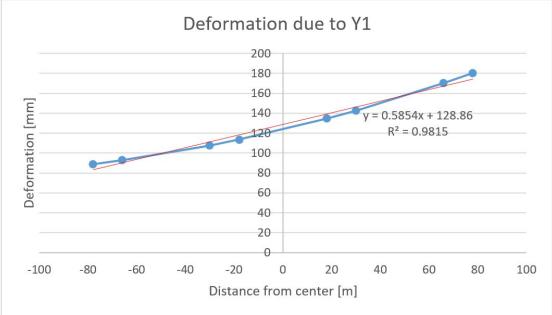

Figure 4.18: Torsional Rotation on top of the building

It can be seen that the response in static analysis is not a linear but close to a parabolic function. The red line is the linear approximation of the displacement with the equation and error on the right side of the line. From the static analysis of finite element progra, the top rotation is $5.854 * 10^{-4}$ mrad and the bottom rotation is $2.6 * 10^{-6}$. The static model of torsional bar is derived on the AppendixB.2, when the torsional deformation can be written as:

$$\begin{aligned} \theta_{1_{(0)}} &= \frac{(-L1 + L)\,\tau}{Kq} \\ K_q &= 8.5 * 10^{13} Nm/rad \\ \theta_{2_{(L)}} &= \frac{1}{GJ}\left(-1/2\,\tau\,L^2 + L\tau\,L + 1/2\,\frac{\tau\left(-KqL1^2 + 2\,GJ\,L - 2\,GJ\,L1\right)}{Kq}\right) \\ GJ &= 2.225 * 10^{13} Nm^2 \end{aligned} \tag{4.22}$$

4.3.2. SOIL STRUCTURE INTERACTION

The torsional resistance on the base of the building can be defined as the resistance of the interaction between group piles and the soil. Because the pile cap for the group piles has a large dimension on the horizontal direction (Figure4.9), then the movement of the pile cap can be assumed as equally deformed. Unlike the bending stiffness of the group pile, the torsional stiffness does not need a reduction factor due to this diaphragm behavior.

The stiffness and damping value for one pile which is used by the TNO Diana for the dynamic analysis can be seen in the Table4.5 or in the Figure4.10.

SSI Parameter			
∅610	K_{hor}	$1.57 * 10^8$	N/m
	C_{hor}	$1.7 * 10^6$	Nm/rad
∅520	K_{hor}	$1.27 * 10^8$	Ns/m
	C_{hor}	$1.2 * 10^6$	Nms/rad

Table 4.5: Horizontal Spring and Dashpot value from TNO Diana model

Therefore the value for the torsional stiffness and damping can be obtain from the equation below:

$$\begin{aligned} K_q &= \sum_{i=1}^{n_{pile}} (1.57 n_{D610} + 1.27 n_{D520}) * 10^8 = 6.7410^{13} \\ C_q &= \sum_{i=1}^{n_{pile}} (1.7 n_{D610} + 1.2 n_{D520}) * 10^6 = 7.210^{11} \end{aligned} \tag{4.23}$$

The mass density and polar moment of inertia (ρJ) of the torsional bar can be obtain by fitting this value to the given natural frequency from the finite element program. The torsional natural frequency can be seen on the Figure4.12 which is 0.285 Hz. The frequency equation can be obtained by search the determinant of the dynamic stiffness matrix in AppendixA EquationA.44 which is written as:

$$\begin{aligned} \text{Frequency Equation} = &- Cq \sin(\alpha L)\, \omega^2 C_\theta \gamma_t + Cq \sin(\alpha L)\, \omega^2 C_\theta + i GJ \cos(\alpha L)\, \alpha\, \omega\, C_\theta \gamma_t \\ &- i Cq GJ \cos(\alpha L)\, \alpha\, \omega + i Cq \sin(\alpha L)\, \omega K_\theta \gamma_t - i GJ \cos(\alpha L)\, \alpha\, \omega\, C_\theta \\ &+ i Kq \sin(\alpha L)\, \omega C_\theta \gamma_t - i Cq \sin(\alpha L)\, \omega K_\theta + GJ^2 \sin(\alpha L)\, \alpha^2 + GJ\alpha \\ &\cos(\alpha L)\, K_\theta \gamma_t - i Kq \sin(\alpha L)\, \omega C_\theta - GJ Kq \cos(\alpha L)\, \alpha - GJ \cos(\alpha L) \\ &\alpha K_\theta + Kq \sin(\alpha L)\, K_\theta \gamma_t - Kq \sin(\alpha L)\, K_\theta \end{aligned} \tag{4.24}$$

in which:

$$\begin{aligned} \alpha &= \sqrt{\frac{\omega^2 \rho J}{GJ^*}} \\ \gamma_t &= \frac{i\omega C_\theta + K_\theta}{\left(-\omega^2 J_\theta + i\omega C_\theta + K_\theta\right)} \end{aligned} \tag{4.25}$$

By set the TMD properties to zero, the only unknown in this equation is the mass density and polar moment of inertia. As the root of this equation is the natural frequency from the one dimensional model, the value of mass density and polar moment inertia is:

$$\rho J = 1.5529 * 10^9 kg\ m \tag{4.26}$$

This value is overestimate due to the linear assumption of the torsional response along the width. After the dynamic analysis is performed in the Chapter5, the dynamic acceleration can be calculated and this torsional stiffness value gives too low acceleration compared to the finite element software. A new torsional properties is introduced in the Chapter5. For the dynamic analysis in Chapter5 the value of the torsional stiffness which give the same bending + torsional vibration is:

$$GJ = 5 \times 10^{12} Nm^2 \tag{4.27}$$

The mass density and polar moment of intertia to give 0.285 Hz natural frequency is:

$$\rho J = 3.49 \times 10^8\ kg\ m \tag{4.28}$$

4.4. TMD PROOPERTIES

The TMD properties that is used in EPO building is shown in the table below:

TMD Parameter		
m_t	$4.4 * 10^5$	kg
C_t	$1.6944 * 10^6$	Ns/m
K_t	$1.394 * 10^5$	N/m

Table 4.6: TMD Properties

For the torsional model, the properties of the TMD is the bending TMD properties as in the Table4.6 multiplied by the squared of the radius. The radius is the horizontal distance between the location of TMD and the middle of the building width which is $61.5m$ in this case.

5

DYNAMIC WIND LOADING

This chapter discusses the dynamic wind loading on the one-dimensional model which is depicted in Figure4.4. The wind load analysis is done in both bending beam and torsional bar. The output of the analysis is the building acceleration in the time domain. Then afterward, the effect of the TMD application is also shown.

5.1. INTRODUCTION

In principle, the dynamic wind load can be observed in the time domain or frequency domain. The time domain analysis (time history analysis) is when the data of the pressure of the wind through time on each point of the building's facade is input as the load. This pressure data can be obtained through wind tunnel test for complex building shape. The second domain is the frequency domain analysis (spectrum analysis) when the fluctuating wind speed is modeled in frequency regime (or as known as wind speed spectrum) and input as the load. Several studies have been made to model the variance of the fluctuating wind speed which is used in practice to design a high rise building throughout the world.

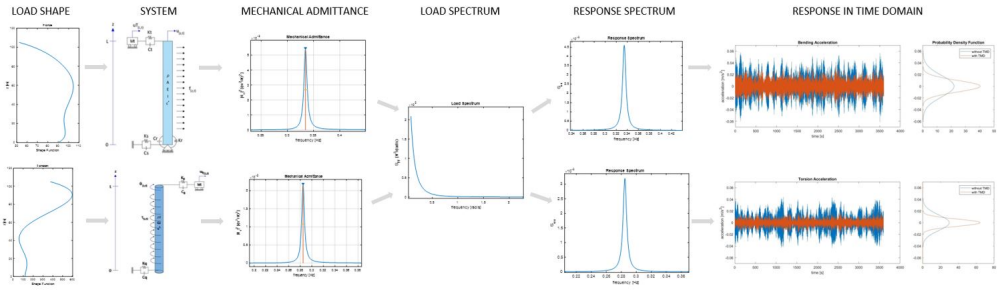

Figure 5.1: Dynamic Wind Load Procedure

The procedure to obtain the acceleration in the time domain is described in the Figure5.1 and discussed in detail in the section5.2. In this thesis, the frequency domain analysis is used. The reason is that there is a lot of information which can be obtained through the frequency domain such as damping ratio and natural frequencies. The procedure to analyze the dynamic wind loading is as follow. The response spectrum can be described through the equation below.

$$S_{uu}(z,\omega) = |H_s|^2 S_{FF} \tag{5.1}$$

where the $|H_s|^2$ is the mechanical admittance and S_{FF} is the wind load spectrum. The detailed information regarding these procedure is explained in the next following section.

5.2. WIND LOAD SHAPE FUNCTION

In the Eurocode, the shape function of the wind load is determined by the function of the wind speed because the pressure or the force of the wind load is just some constants multiplied by an exponential function which

is:

$$f_{(z)} = \ln \frac{z}{z_0} \tag{5.2}$$

But for a building with a large surface, more accurate wind speed profile can be obtained through the wind tunnel test which is shown in Figure5.2.

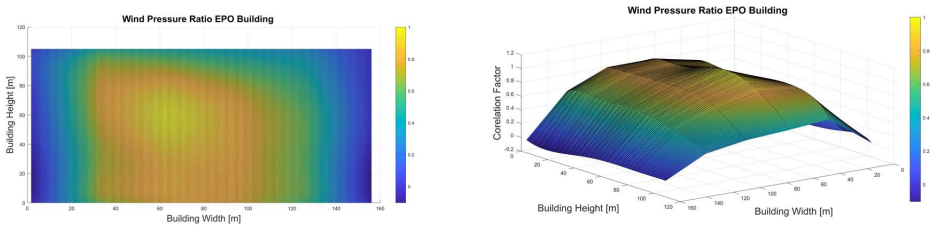

Figure 5.2: Wind pressure profile over the building height

The left figure depicts the side view of the building and the right figure depicts the 3D image of the wind pressure on the building where the building height and the building width axis are shown in the graph. This figure depicts the ratio of the wind pressure on the building surface. It can be seen that the highest value is at the middle of the building which is the point of reference for the ratio which is set to one.

Because the model is 1 dimensional (height), the load shape function for bending vibration can be obtained by integrate the value over the width. If the position along the building width is the x coordinate from 0 to B, along building height is z coordinate from 0 to L, and the wind pressure profile is a function of $p_{(x,z)}$, then the wind load shape function for bending vibration can be written as:

$$f_{b_{(z)}} = \int_0^B p_{(x,z)}\, dx \tag{5.3}$$

The integration of the 3D pressure ratio over the width is shown in the in left figure of Figure5.3. The load shape function for the torsional vibration can be obtained by multiplying the shape function for bending and the eccentricity. It can be written as:

$$\begin{aligned} \text{centroid}_{(z)} &= \frac{\int_0^B x\, p_{(x,z)}\, dx}{\int_0^B p_{(x,z)}\, dx} \\ \text{eccentricity}_{(z)} &= B/2 - \text{centroid} \\ f_{\theta_{(x,z)}} &= f_{b_{(z)}} * \text{eccentricity}_{(z)} \end{aligned} \tag{5.4}$$

The wind load shape function can be seen in the Figure5.3. The left graph is the shape function for bending vibration, the middle graph is the eccentricity function and the right graph is the shape function for torsional vibration.

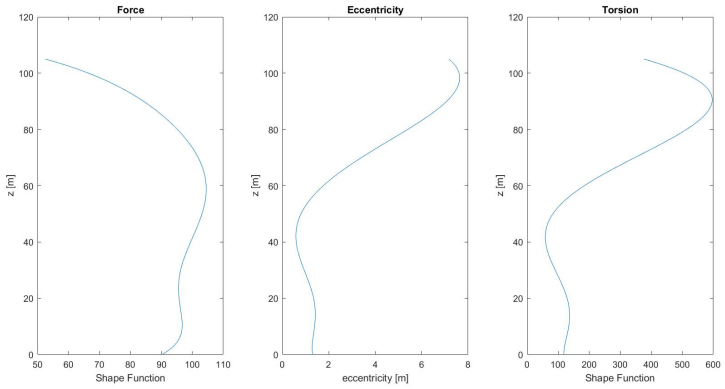

Figure 5.3: Wind Load Shape for Bending Vibration

The load shape function for bending and torsion can be also written as a sixth order polynomial equation which can be seen in the equation below:

$$\begin{aligned} f_{b_{(z)}} &= az^6 + bz^5 + cz^4 + dz^3 + ez^2 + fz + g \\ f_{\theta_{(x,z)}} &= a_t z^6 + b_t z^5 + c_t z^4 + d_t z^3 + e_t z^2 + f_t z + g_t \end{aligned} \tag{5.5}$$

$$\begin{aligned} a &= -1.96 \times 10^{-9} & a_t &= \ \ 1.99 \times 10^{-8} \\ b &= \ \ 6.64 \times 10^{-7} & b_t &= -6.74 \times 10^{-6} \\ c &= -8.66 \times 10^{-9} & c_t &= \ \ 7.60 \times 10^{-4} \\ d &= \ \ 5.20 \times 10^{-3} & d_t &= -3.25 \times 10^{-2} \\ e &= -1.43 \times 10^{-1} & e_t &= \ \ 0.43 \\ f &= \ \ 1.65 \times 10^{-9} & f_t &= -0.176 \times 10^{-9} \\ g &= \ \ 90.2 & g_t &= \ \ 1.18 \times 10^{2} \end{aligned}$$

5.3. MECHANICAL ADMITTANCE

The model for the bending and torsion vibration of the high rise building with a single TMD on top of the building can be seen in the figure 5.4 below. The TMD is connected through a spring and dashpot to the building.

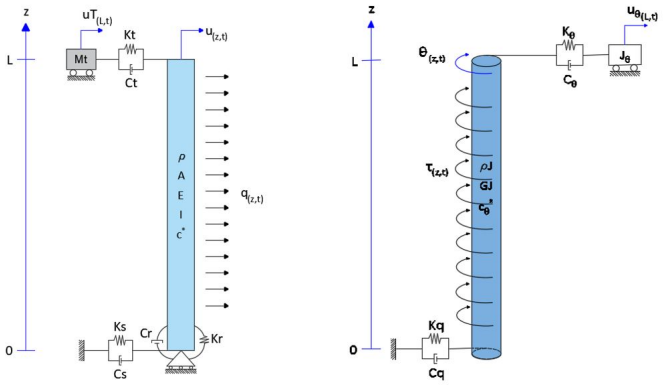

Figure 5.4: One Dimensional Model of a High-rise Building

The equation of motion for the Euler-Bernoulli beam and torsional bar can be seen respectively in the equation below:

$$\begin{aligned} \rho A \frac{\partial^2}{\partial t^2} u_{(z,t)} + \frac{\partial^2}{\partial z^2}\left(EI\left(1 + c^* \frac{\partial}{\partial t}\right)\frac{\partial^2}{\partial z^2} u_{(z,t)}\right) &= q_{(z,t)} \\ \rho J \frac{\partial^2}{\partial t^2}\theta_{(z,t)} - \frac{\partial}{\partial z}\left(GJ\left(1 + c_\theta^* \frac{\partial}{\partial t}\right)\frac{\partial}{\partial z}\theta_{(z,t)}\right) &= \tau_{(z,t)} \end{aligned} \tag{5.6}$$

The equation of motion for the TMD in bending and torsional model can be seen respectively in the equation below:

$$\begin{aligned} m_t \frac{\partial^2}{\partial t^2} u_{t_{(t)}} + C_t\left(\frac{\partial}{\partial t} u_{t_{(t)}} - \frac{\partial}{\partial t} u_{(z,t)}\right) + K_t\left(u_{t_{(t)}} - u_{(z,t)}\right) &= 0 \\ J_\theta \frac{\partial^2}{\partial t^2}\theta_{t_{(t)}} + C_\theta \frac{\partial}{\partial t}\left(\theta_{t_{(t)}} - \theta_{(z,t)}\right) + K_\theta\left(\theta_{t_{(t)}} - \theta_{(z,t)}\right) &= 0 \end{aligned} \tag{5.7}$$

The detailed analytical procedure to obtain the mechanical admittance can be seen on the AppendixA. The procedure to obtained the mechanical admittance for bending and torsion is shown in the flow chart (Figure5.5).

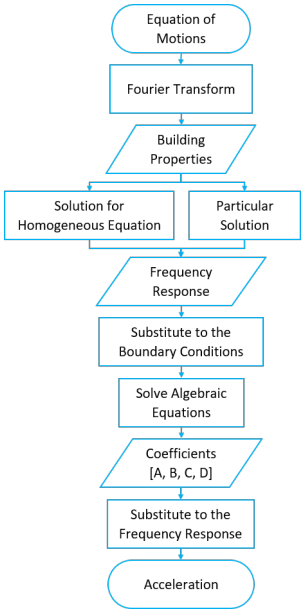

Figure 5.5: Mechanical Admittance Procedure

The frequency response for the acceleration is derived in the AppendixA:

$$\begin{aligned} \text{bending acceleration}_{(z,\omega)} &= \omega^2 \tilde{u}_{(z,\omega)} \\ \text{torsion acceleration}_{(z,\omega)} &= R\,\omega^2 \tilde{\theta}_{(z,\omega)} \end{aligned} \tag{5.8}$$

The mechanical admittance can be defined as:

$$\begin{aligned} H_s(\text{bending}) &= \left|\omega^2 \tilde{u}_{(z,\omega)}\right|^2 \\ H_s(\text{torsion}) &= \left|R\,\omega^2 \tilde{\theta}_{(z,\omega)}\right|^2 \end{aligned} \tag{5.9}$$

The mechanical admittance for the bending vibration due to the force in frequency domain ($f_{(\omega)}$) equal to 1, including the shape function for the wind (5.2) can be seen in Figure5.6 and Figure5.7.

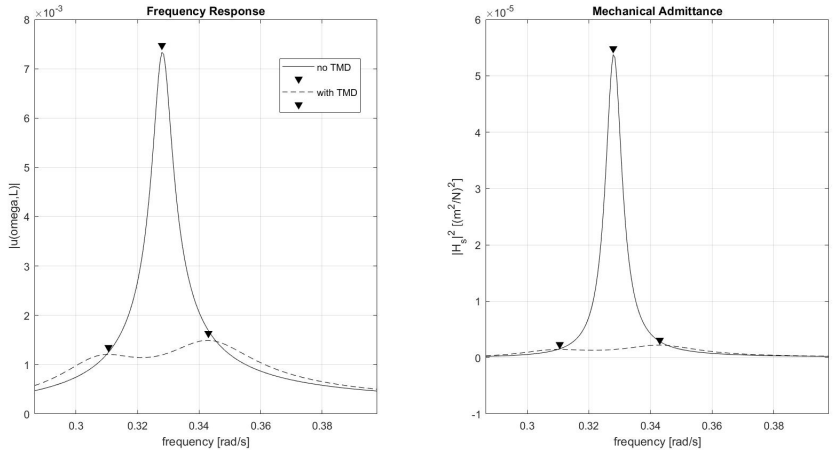

Figure 5.6: Mechanical Admittance: Bending Vibration

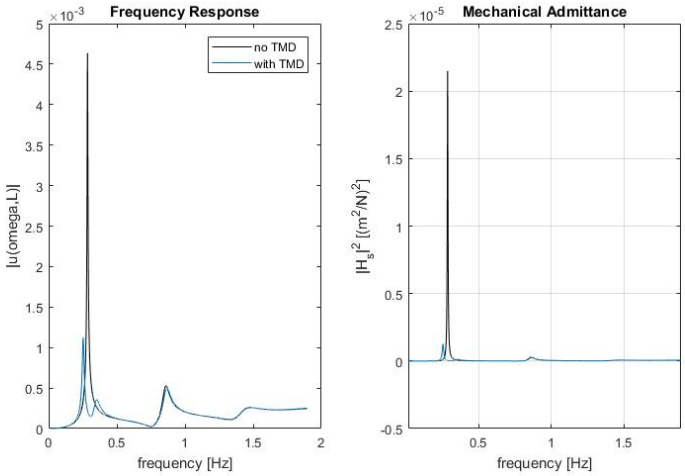

Figure 5.7: Mechanical Admittance: Torsion Vibration

5.4. WIND LOAD SPECTRUM

The wind load spectrum is a frequency function of the wind pressure. Because the building model 1 dimensional model with the space coordinate only in 1 direction which is along the height (z coordinate), the wind load is a distributed line load along the height. This distributed wind load from the fluctuating part of the wind can be obtained through multiplication of the wind speed spectrum, a load factor, and aerodynamic admittance. Which can be also written as:

$$S_{FF} = |H_a|^2 \, C_w \, S_{vv} \tag{5.10}$$

where Ha is the aerodynamic admittance, S_{vv} is the wind speed spectrum and C_w is the coefficient factor. The graph of the wind load spectrum for EPO building can be seen in Figure5.8 below:

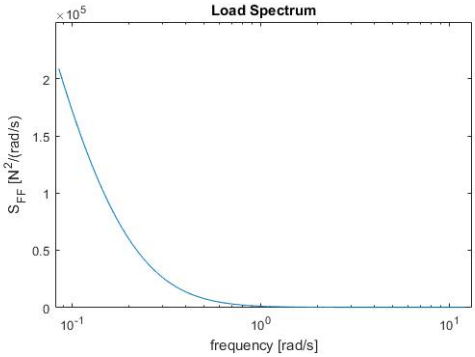

Figure 5.8: Wind Load Spectrum

The fluctuating wind pressure along the height of the building can be formulated as:

$$q_{(z,t)} = \int_0^B C_f \rho_{air} \bar{v}_{(x,z)} \tilde{v}_{(x,z,t)} \, dx \tag{5.11}$$

5.4.1. WIND SPEED SPECTRUM

Wind speed spectrum is a function of wind speed through the frequency. The previous study by shows that the wind speed in the frequency domain follows the Gaussian model. There is many model which is derrived from this assumption and in Eurocode, Solari's variance spectrum model is used to derived the wind speed spectrum. It can be seen in Figure5.9.

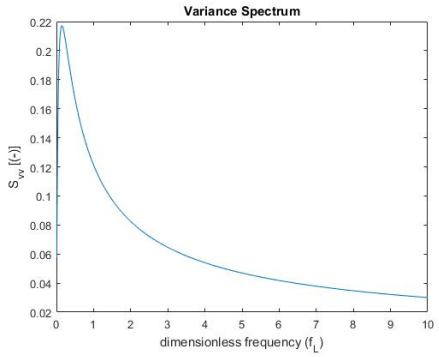

Figure 5.9: Solari's Spectrum model

This variance spectrum follows a function in the equation below:

$$S_L = \frac{6.8 f_L}{(1+10.2 f_L)^{5/3}} \tag{5.12}$$

The graph of the wind spectrum can be seen in Figure5.10 below:

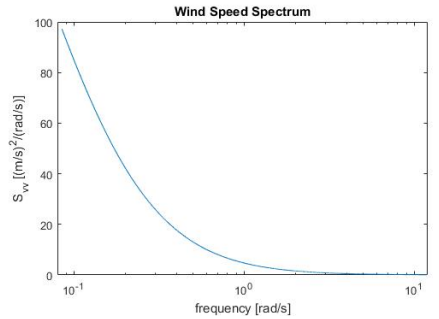

Figure 5.10: Wind Spectrum

The function for the wind speed spectrum can be seen in the equation below:

$$S_{vv} = S_L \frac{\sigma_v^2}{2\pi n} \tag{5.13}$$

The relation between dimensionless frequency and frequency in Hz is:

$$f_L = \frac{nL}{v} \tag{5.14}$$

5.4.2. AERODYNAMIC ADMITTANCE

For an object which the contact area of the wind is large, the wind velocity has different values on each point on the surface. If this wind velocity on different point is observed, the peak value of the wind velocity is not occur at the same time. Therefore, there is less variance of the total wind speed for each time. This phenomena is taking into account by the aerodynamic admittance.
Based on the Eurocode, the aerodynamic admittance can be calculated as:

$$R_{h,b} = \frac{1}{\eta_{b,h}} - \frac{1}{2(\eta_{b,h})^2}(1 - e^{-2\eta_{b,h}}) \tag{5.15}$$

in which:

$$\eta_{[b;h]} = 4.6\,[b;h]\,\frac{f_L}{L_{(z)}}$$
$$L_{(z)} = L_t\left(\frac{z}{z_t}\right)^{\alpha} \tag{5.16}$$
$$\alpha = 0.67 + 0.05\,ln(z_0)$$

The mathematical symbols of b is the building width, h is the building height, fL is the dimensionless frequency, and L(z) is the turbulence length. The plot of the aerodynamic admittance for EPO building can be seen in Figure5.11 below:

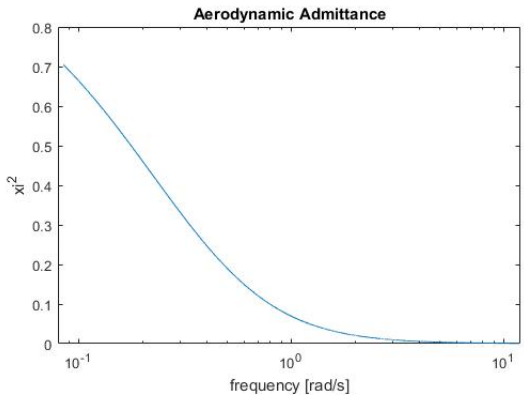

Figure 5.11: Aerodynamic admittance

5.5. SUMMARY

After obtaining all the function, now the response spectrum function (for acceleration) which is described in the equation can be obtained.

$$S_{aa_{(z,\omega)}} = |H_s|^2|H_a|^2[C_f\rho_{air}\bar{v}_0]^2\frac{6.8f_L}{(1+10.2f_L)^{5/3}}\frac{\sigma_v^2}{2\pi n} \tag{5.17}$$

The graph of the response spectrum (acceleration) for the EPO building can be seen in Figure5.12 below:

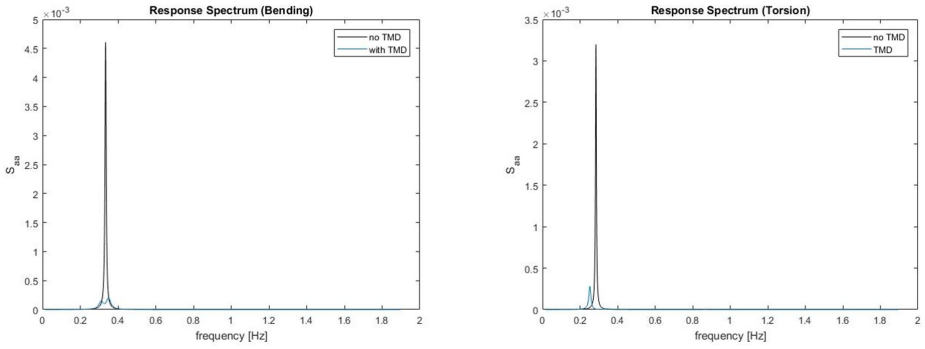

Figure 5.12: Response Spectrum

Then the standard deviation for the acceleration response, and the peak acceleration can be obtain through the following equation:

$$\sigma_a = \sqrt{\int_0^{\infty} S_{uu}\,d\omega} \tag{5.18}$$

The response in time domain can also be obtained through the Gaussian model because the model of the wind speed is also derived from this Gaussian stationary process. This method means that it is assumed that

a function can be built up by summation of sinusoidal function with random phase. This statement also can be expressed in the equation form which is:

$$u_{(t)} = \sum_{i=1}^{N} \hat{u}_{(\omega)} sin(\omega t + \phi) \tag{5.19}$$

in which:

$$\hat{u}_{(\omega)} = \sqrt{2 S_{uu_{(\omega)}} \Delta\omega} \tag{5.20}$$

The building has two directions in the horizontal axis, the longer length is the building width with 157 m and the shorter length is the building depth with 20 m. The critical vibration is the vibration of the building with the direction perpendicular to the building width. The plot of the horizontal acceleration in the time domain on this critical axis can be seen as these following figures:

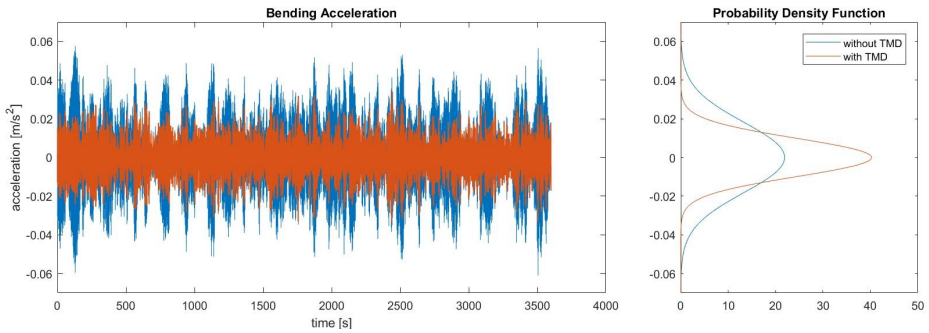

Figure 5.13: Bending Acceleration in Time Domain

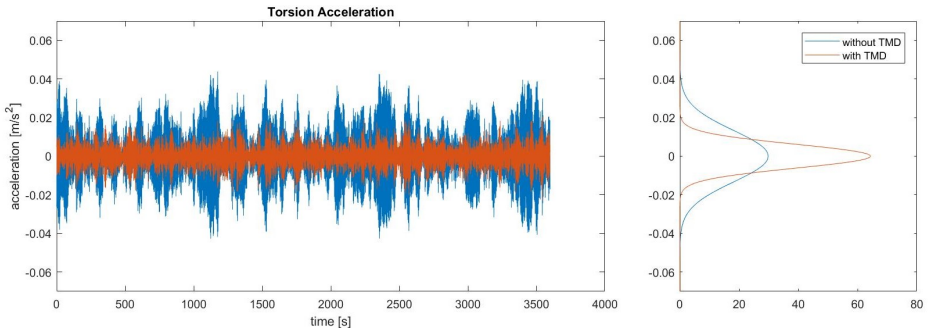

Figure 5.14: Torsion Acceleration in Time Domain

For EPO building, the peak acceleration for building with and without TMD are:

Peak Bending acceleration:

without TMD = 0.0610 m/s^2
with TMD = 0.0344 m/s^2
TMD effectiveness = 43%

Peak Torsion acceleration:

without TMD = 0.0438 m/s^2
with TMD = 0.023 m/s^2
TMD effectiveness = 47%

For the peak horizontal acceleration in the critical axis (perpendicular building width), the location is on the top corner of the building. This acceleration can be obtained by the summation of the bending and torsion acceleration in Figure5.13 and Figure5.14 as shown in Figure5.15 below: Peak total (bending + torsion) acceleration:

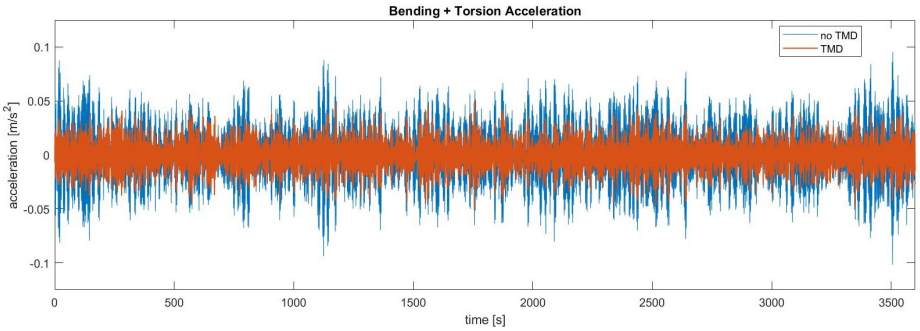

Figure 5.15: Total Acceleration in Time Domain

without TMD = 0.1018 m/s^2
with TMD = 0.05143 m/s^2
Effectiveness of TMD = 49%

5.6. FREQUENCY DEPENDENT SSI

The value of the spring stiffness and dashpot used in the finite element program to analyzed the dynamic wind loading is valid on a specific natural frequency of the EPO building. But the soil stiffness and damping is a frequency dependent value, a model for predicting the soil structure interaction is made by John.P.Wolf. An estimation base on the dimension of the foundation and CPT test of the soil is made by Mr. Sanchez Gomez which can be seen in Figure5.16 below:

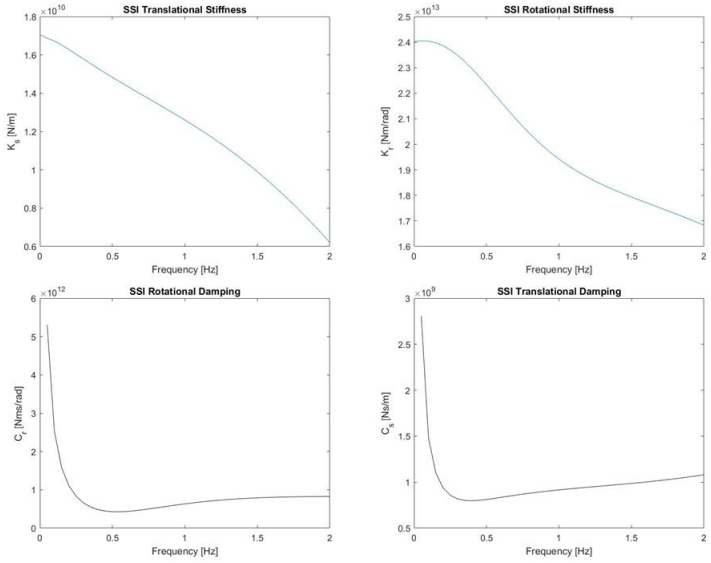

Figure 5.16: Frequency Dependent of SSI Parameter

It can be seen that the damping value has a relatively high value at lower frequency. For EPO Building case the natural frequency of the bending vibration of the building is 0.337, the value of the SSI parameter in this frequency is:

SSI Parameter		
Ks	$1.56 * 10^{10}$	N/m
Kr	$2.33 * 10^{13}$	Nm/rad
Cs	$8.04 * 10^{8}$	Ns/m
Cr	$5.74 * 10^{11}$	Nms/rad

Table 5.1: EPO SSI Properties

If the frequency dependent SSI parameter (Figure5.16) is used in the dynamic analysis, which is change the value of $[KsKrCsCr]$ to the value of $[KsKrCsCr]_{(\omega)}$. The result for the acceleration can be seen in Figure5.17 below:

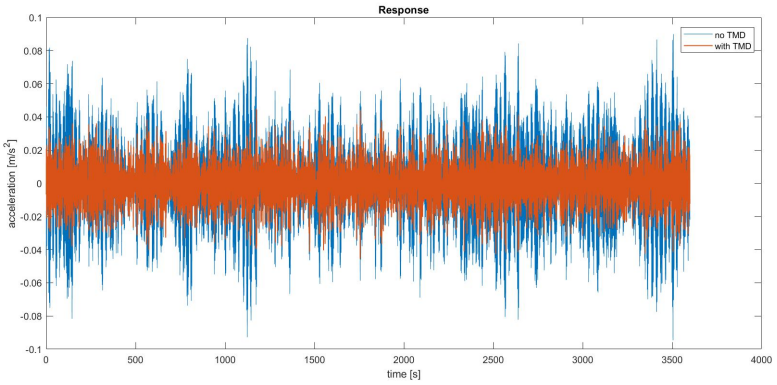

Figure 5.17: Acceleration with frequency dependent SSI

The peak acceleration is:

without TMD = 0.09463 m/s^2
with TMD = 0.04545 m/s^2
Effectiveness of TMD = 51%

The value of the peak is slightly different than the result from Figure5.15 because the natural frequency of the building is slightly changed and therefore because the load is modeled as a random load, the change of this frequency influence the peak value of the acceleration in time domain. But it can be seen that the effectiveness of the TMD is about the same with 2% difference.

5.7. COMPARISON WITH FINITE ELEMENT PROGRAM

This TMD effectiveness from the one dimensional model is over estimate compared to the analysis with finite element program. The acceleration on the top of the building in the middle of the width, which is the bending acceleration of the building, from TNO Diana can be seen in the figure below:

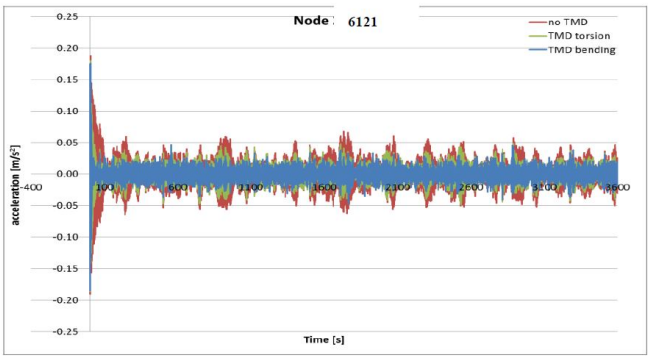

Figure 5.18: Acceleration on the top middle of the building

The peak value without TMD is $0.07 m/s^2$ and with TMD is $0.049 m/s^2$ which make the TMD is 30% effective.

The torsional vibration has a large different than the one dimensional model, as mention in the 4. The torsional behavior of the building is not linear along the width as it can be seen in Figure5.19:

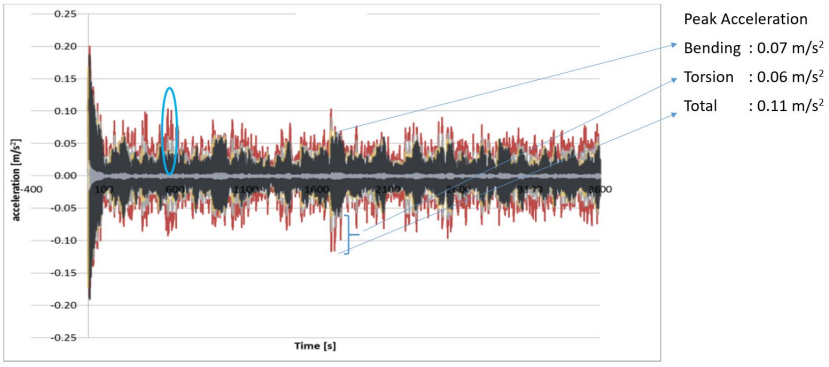

Figure 5.19: Torsional vibration from TNO Diana

The color of the graph represent the acceleration on specific location on top of the building. The black graph (point 6121) is the acceleration on the middle of the width and the red graph (point 190) is te acceleration on the furthers from the middle as it can be seen in Figure5.20.

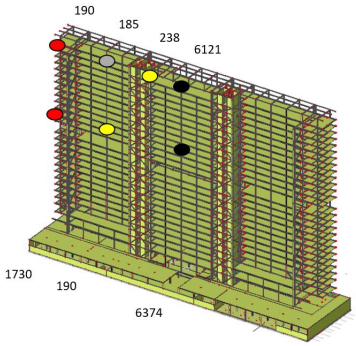

Figure 5.20: Points of observation

The torsional acceleration can be determine as the difference between the acceleration on the point 190 and 6121, the value of the acceleration on the blue circle on Figure5.19 can be seen on the Figure5.21.

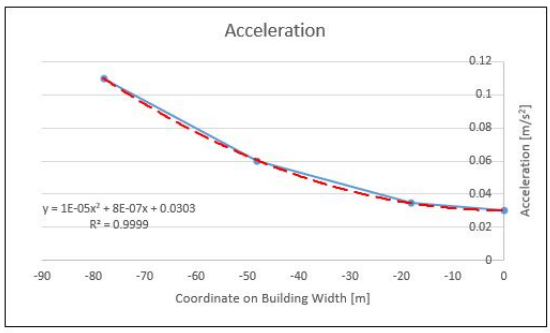

Figure 5.21: Acceleration value along the building width

It can be seen that the acceleration is not linear along the width. Therefore the torsional stiffness (ρJ) in this beam is not a realistic stiffness as in 3D model but it gives an equivalent value for this simple torsional bar model to perform similar as the critical torsional vibration of the building. The effectiveness of the TMD for EPO building in finite element program can be seen in the figure below:

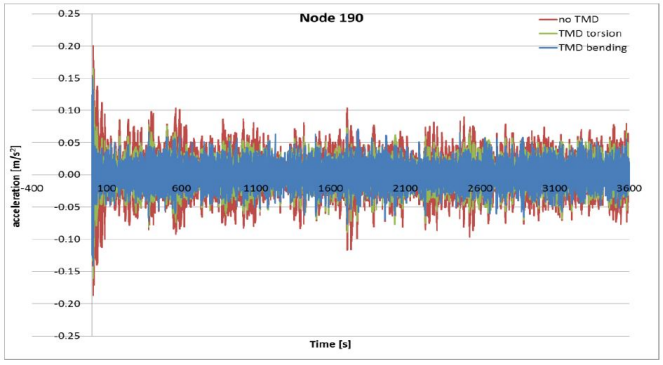

Figure 5.22: Acceleration in point 190

The peak value without TMD is $0.11 m/s^2$ and with TMD is $0.07 m/s^2$ which make the TMD is 36% effective.

5.8. APPLICATION OF WIND TURBINE

The application of wind turbine on high rise building to gain energy is becoming familiar. In the building industry, a large wind turbine has been applied in Pearl River Tower (China), Strata Tower (United Kingdom), and also Bahrain World Trade Center (Bahrain). This wind turbine does not only effect the energy gain for the electricity but also increase the aerodynamic damping of that specific location. Therefore a study of the application of a wind turbine in reducing the acceleration of the EPO Building is studied in this section. The model for this study can be seen in Figure5.23 below:

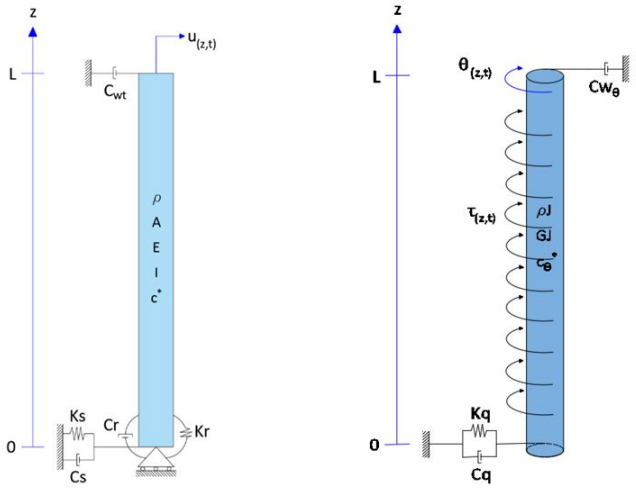

Figure 5.23: One dimensional model for building with wind turbine

The only different between this model and the basic model (building with TMD on top) is the shear boundary condition on top of the building which can be written as:

Bending Vibration:

$$(1+i\omega C^*)EI\,\frac{\partial^3}{\partial z^3}\tilde{u}_{(z,\omega)}\Big|_{z=L} - i\omega C_{wt}\,\tilde{u}_{(z,t)}\big|_{z=L} = 0$$

Torsion Vibration:

$$(1+i\omega C_\theta^*)\,\frac{\partial}{\partial z}\tilde{\theta}_{(z,\omega)}\Big|_{z=L} + i\omega C_{w\theta}\,\tilde{\theta}_{(z,\omega)}\big|_{z=L} = 0 \tag{5.21}$$

in which:

$$C_{w\theta} = C_{wt} * R^2$$

R : Length from the torsional center and position of the wind turbine along the building width (5.22)

The value of the C_{wt} can be obtain through an estimation based on the offshore wind turbine experiment and simulation result. This simulation is done by D.J.Cerda Salzmann and J. van der Tempel from TU Delft, the value of the aerodynamic damping of the offshore wind turbine is shown in Figure5.24:

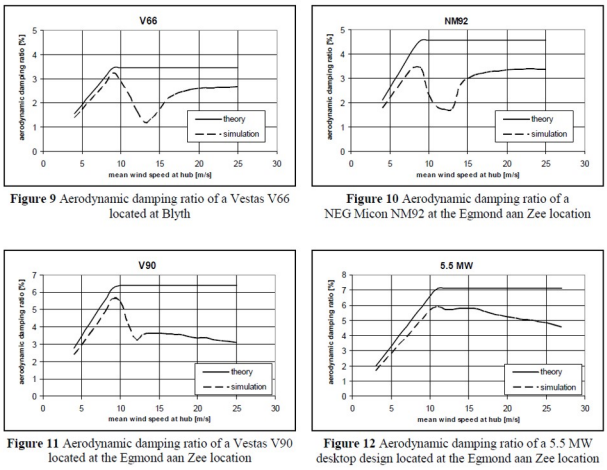

Figure 9 Aerodynamic damping ratio of a Vestas V66 located at Blyth

Figure 10 Aerodynamic damping ratio of a NEG Micon NM92 at the Egmond aan Zee location

Figure 11 Aerodynamic damping ratio of a Vestas V90 located at the Egmond aan Zee location

Figure 12 Aerodynamic damping ratio of a 5.5 MW desktop design located at the Egmond aan Zee location

Figure 5.24: Aerodynamic damping in different wind speed [7]

The design is to use the optimum added aerodynamic damping which is taken to be 6% based on the graph. This value is valid for a certain wind speed, if we look at the wind tunnel test of the EPO Building in Figure5.25:

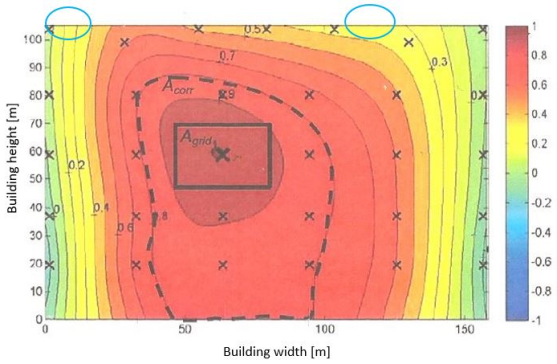

Figure 5.25: Side view of building (building width vs building height): Correlation factor

The value is the correlation factor of the wind between one point and another point, if we take the static wind load which state that:

Maximum Wind Speed at correlation factor = 1 :

$$\bar{v} = v_b\, k_r\ \ log\left(\frac{z}{z_o}\right)\Big|_{z=60m} = 25.9 m/s \tag{5.23}$$

Optimum Correlation Factor on top of the builing :

$$C_f = \frac{10}{25.9} = 0.38$$

The peformance of the wind turbine in reducing the acceleration on top of the building is depicted in Figure5.26:

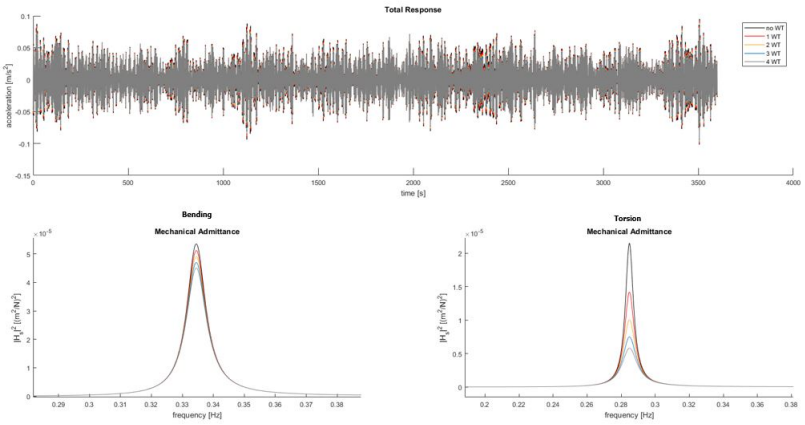

Acceleration [m/s²]		
Bending	Torsion	Total
0.0610	0.0438	0.1018
0.0605	0.0401	0.099
0.0599	0.0372	0.0967
0.0593	0.0352	0.0945
0.0588	0.0338	0.0926

Damping Ratio [%]	
Bending	Torsion
1.1	1
1.12	1.23
1.15	1.47
1.17	1.7
1.2	1.93

Figure 5.26: Total (bending+torsion) acceleration of EPO building with wind turbine

The wind turbine increase the damping of the system by 0.1% in bending and 0.93% in torsion and therefore it reduce the total acceleration from 0.1018 to $0.0926 m\ s^2$. The reason it is more optimum in the torsion vibration in this case is due to the model of the torsion which does not taking into account the distribution of mechanical stress in horizontal direction along the building width. Therefore the performance of the wind turbine in the torsional vibration can be enhance by placing the wind turbine in the longest radius from torsional center. Due to the EPO building design which has the width higher than the height, the wind turbine is more effective in reducing the torsional vibration.

6

TMD Design

Several models are made to study the effect of TMD and soft soil condition. The difference of the model can be on the different type of TMD, TMD position, and different building properties. The basic model is shown in the figure3.9, this model is usually applied in reality because often the maximum deflection is on the top of the building which the TMD is placed. The analytical solution is done in the falling sub-chapter for this basic model.

6.1. EPO Building Case

The model is modified to increase the quantity of the TMD. It is desired to study the effect of multiple TMD in the high rise building. The modified model can be seen in the Figure6.1.There are 2 motions which are $\tilde{u}_1$ for $0 \leq z \leq LTMD$ and $\tilde{u}_2$ for $LTMD \leq z \leq L$.

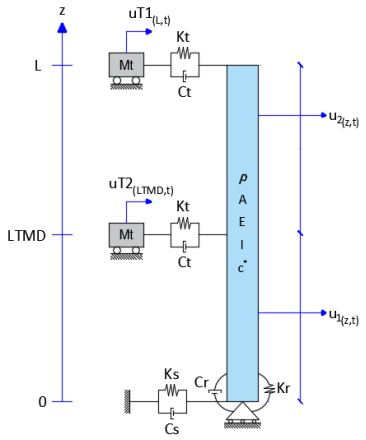

Figure 6.1: Building with 2 TMDs

The high-rise building with TMD can be modeled with the discrete system (N-DOFs system, Figure 1.1. Discrete Model of High Rise with TMD [3]Figure 1.1) and continuous system (Figure6.1). The continuous system is modeled as a Euler-Bernoulli beam with an interaction with soil condition. The soil properties can be input as translational and rotational stiffness and damping. The TMD first position on the top of the building, later in the parametric study it may be changed to different positions and quantities.

6.1.1. Equation of motion

The equation of motion (EOM) for the first and second motion can be seen in the following equation:

$$EI^* \frac{\partial^4}{\partial z^4} \tilde{u}_{1,2\,(z,\omega)} - \omega^2 \rho A \tilde{u}_{1,2\,(z,\omega)} = \tilde{q}_{1,2\,(z,\omega)} \tag{6.1}$$

The solution for the homogeneous equation and the particular solution is the same as the basic model in equation A.12 and A.14.

6.1.2. BOUNDARY AND INTERFACE CONDITION

The boundary condition of the model is the same as in equation A.18 to A.1.2 only the motion $\tilde{u}_1$ is used for $z = 0$ and $\tilde{u}_2$ for $z = L$. The interface condition at $z = L1$ can be seen in the equation below:

Displacement:

$$\tilde{u_1}_{(L1,\omega)} - \tilde{u_2}_{(L1,\omega)} = 0 \tag{6.2}$$

Rotation:

$$\frac{\partial}{\partial z}\tilde{u_1}_{(L1,\omega)} - \frac{\partial}{\partial z}\tilde{u_2}_{(L1,\omega)} = 0 \tag{6.3}$$

Bending Moment:

$$\frac{\partial^2}{\partial z^2}\tilde{u_1}_{(L1,\omega)} - \frac{\partial^2}{\partial z^2}\tilde{u_2}_{(L1,\omega)} = 0 \tag{6.4}$$

Shear Force:

$$EI^*\left(\frac{\partial^3}{\partial z^3}\tilde{u_2}_{(L1,\omega)} - \frac{\partial^3}{\partial z^3}\tilde{u_1}_{(L1,\omega)}\right) + (i\omega C_t + Kt)(\tilde{u_1}_{(L1,\omega)} - \tilde{u_t}_{(L1,\omega)}) = 0 \tag{6.5}$$

6.1.3. RESULT AND ANALYSIS

The data which is used to compare the different model of the TMD is the EPO building from Zonneveld which is describe in previous chapter. In summary, the data can be seen in the table 6.2.

Soil Parameter			Building Parameter		
Ks	$3.62x10^{10}$	N/m	EI	5^{13}	Nm^2
Kr	$7.65x10^{12}$	Nm/rad	ρA	$9.5x10^5$	kg/m
Cs	$3.9x10^8$	Ns/m	C^*	$7.5x10^{-3}$	s
Cr	$1.43x10^{11}$	Nms/rad	L	105	m

Table 6.1: EPO building data

TMD Parameter		
mt	$4.4x10^5$	kg
Ct	$1.8x10^6$	Ns/m
Kt	$1.39x10^5$	N/m

Table 6.2: EPO building TMD data

The second model proved that for the same total mass, the quantity of the TMD is not improving its effectiveness. Since the most effective position is on the top of the building, then it is better that the second mass is positioned near to the top. The graph of the frequency response function can be seen in the Figure6.2 below: The different line describe the different position of the second TMD in the building. MTMD 100m means the first TMD is on the top of the building, and the second is at 100m from the bottom (z=100).

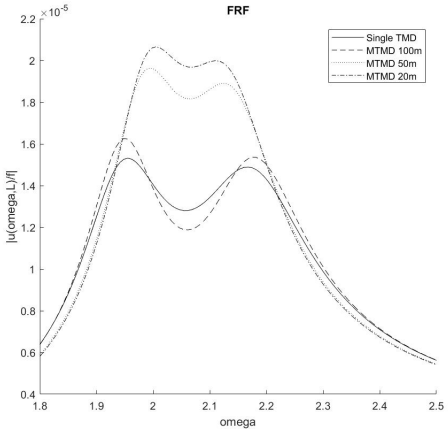

Figure 6.2: Frequency response for multiple TMD model

6.2. DISTRIBUTED TRANSLATIONAL MASS DAMPER

The model of distributed translational mass damper can be seen in the figure below:

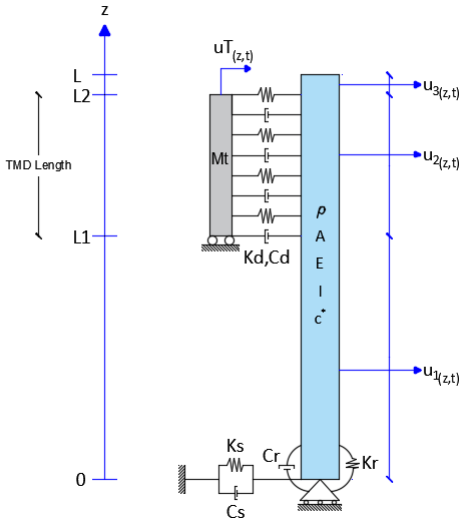

Figure 6.3: Prestressed TMD

6.2.1. EQUATION OF MOTION

TUNED MASS DAMPER

The equation of motion for the TMD can be written as:

$$-\omega^2 m_{td}\tilde{u}_{t(z,\omega)} + (i\omega C_d + K_d)(\tilde{u}_{t(z,\omega)} - \tilde{u}_{2(z,\omega)}) = 0 \tag{6.6}$$

Then the expression of the TMD motion can be obtain as such:

$$\begin{aligned} \tilde{u}_{tz,\omega} &= \gamma\, \tilde{u}_{2(z,\omega)} \\ \gamma &= \frac{i\omega C_d + K_d}{-\omega^2 m_{td} + i\omega C_d + K_d} \end{aligned} \tag{6.7}$$

BUILDING

The equation of motion for the building with TMD with distributed property can be seen in the following equation:

1. For: 0<z<L1

$$EI^* \frac{\partial^4}{\partial z^4} \tilde{u}_{1(z,\omega)} - \omega^2 \rho A \tilde{u}_{1(z,\omega)} = \tilde{q}_{1(z,\omega)} \tag{6.8}$$

2. For: L1<z<L2

$$EI^* \frac{\partial^4}{\partial z^4} \tilde{u}_{2(z,\omega)} - \omega^2 \rho A \tilde{u}_{2(z,\omega)} + (i\omega C_d + K_d)(\tilde{u}_{2(z,\omega)} - \tilde{u}_{t(z,\omega)}) = \tilde{q}_{(z,\omega)} \tag{6.9}$$

3. For: L2<z<L

$$EI^* \frac{\partial^4}{\partial z^4} \tilde{u}_{3(z,\omega)} - \omega^2 \rho A \tilde{u}_{3(z,\omega)} = \tilde{q}_{(z,\omega)} \tag{6.10}$$

In order to solve the differential equation for the second motion, substitute the equation 6.7 to the 6.9 resulting:

$$EI^* \frac{\partial^4}{\partial z^4} \tilde{u}_{2(z,\omega)} - \omega^2 \rho A \tilde{u}_{2(z,\omega)} + (i\omega C_d + K_d)(1-\gamma) \tilde{u}_{2(z,\omega)} = \tilde{q}_{(z,\omega)} \tag{6.11}$$

HOMOGENEOUS EQUATION:
First, find the solution for the homogeneous equation which can be written as:

$$\frac{\partial^4}{\partial z^4} \tilde{u}_{2(z,\omega)} - \beta_2^4 \tilde{u}_{2(z,\omega)} = 0 \tag{6.12}$$

In which:

$$\beta_2 = \left(\frac{\omega^2 \rho A + (i\omega C_d + K_d)(\gamma - 1)}{EI^*} \tilde{u}_{2(z,\omega)} \right)^{1/4} \tag{6.13}$$

Applying the same form of general solution as in equation A.8, the solution for the homogeneous equation is:

$$\tilde{u}_{2(z,\omega)} = A_2 \cosh(\beta_2 z) + B_2 \sinh(\beta_2 z) + C_2 \cos(\beta_2 z) + D_2 \sin(\beta_2 z) \tag{6.14}$$

PARTICULAR SOLUTION:
The EOM can be re-write as:

$$\frac{\partial^4}{\partial z^4} \tilde{u}_{2(z,\omega)} - \beta_2^4 \tilde{u}_{2(z,\omega)} = \frac{\tilde{q}_{(z,\omega)}}{EI^*} \tag{6.15}$$

Because the form of the loading is the same, the form of the particular solution is the same as in equation A.14. Substituting this form to the EOM resulting:

$$24A_p - \beta_2^4 \left(A_p x^4 + B_p x^3 + C_p x^2 + D_p x + E_p \right) = \frac{ax^4 + bx^3 + cx^2 + dx + e}{EI^*} \tag{6.16}$$

Then the coefficients for the particular solution can be solved through this equation. The result of the coefficients are:

$$A_p = -\frac{a}{\beta_2^4 EI^*} \; ; \; B_p = -\frac{b}{\beta_2^4 EI^*} \; ; \; C_p = -\frac{c}{\beta_2^4 EI^*} \; ; \; D_p = -\frac{d}{\beta_2^4 EI^*} \; ; \; E_p = \frac{24EI^* A_p - e}{\beta_2^4 EI^*} \tag{6.17}$$

6.2.2. BOUNDARY AND INTERFACE CONDITION

The boundary condition at the bottom of the model is the same as in equation A.18. The top boundary condition of this model can be seen as follows:
Bending Moment:

$$EI^* \frac{\partial^2}{\partial z^2} \tilde{u}_{3(L,\omega)} = 0 \tag{6.18}$$

Shear Force:

$$EI^* \frac{\partial^3}{\partial z^3} \tilde{u}_{3(L,\omega)} = 0 \tag{6.19}$$

The interface condition at $z = L1$ and $z = L2$ can be seen in the equation below:
Displacement:

$$\begin{aligned} \tilde{u}_{1(L1,\omega)} - \tilde{u}_{2(L1,\omega)} &= 0 \\ \tilde{u}_{2(L2,\omega)} - \tilde{u}_{3(L2,\omega)} &= 0 \end{aligned} \tag{6.20}$$

Rotation:

$$\begin{aligned} \frac{\partial}{\partial z}\tilde{u_1}_{(L1,\omega)} - \frac{\partial}{\partial z}\tilde{u_2}_{(L1,\omega)} = 0 \\ \frac{\partial}{\partial z}\tilde{u_2}_{(L2,\omega)} - \frac{\partial}{\partial z}\tilde{u_3}_{(L2,\omega)} = 0 \end{aligned} \tag{6.21}$$

Bending Moment:

$$\begin{aligned} \frac{\partial^2}{\partial z^2}\tilde{u_1}_{(L1,\omega)} - \frac{\partial^2}{\partial z^2}\tilde{u_2}_{(L1,\omega)} = 0 \\ \frac{\partial^2}{\partial z^2}\tilde{u_2}_{(L2,\omega)} - \frac{\partial^2}{\partial z^2}\tilde{u_3}_{(L2,\omega)} = 0 \end{aligned} \tag{6.22}$$

Shear Force:

$$\begin{aligned} \frac{\partial^3}{\partial z^3}\tilde{u_1}_{(L1,\omega)} - \frac{\partial^3}{\partial z^3}\tilde{u_2}_{(L1,\omega)} = 0 \\ \frac{\partial^3}{\partial z^3}\tilde{u_2}_{(L2,\omega)} - \frac{\partial^3}{\partial z^3}\tilde{u_3}_{(L2,\omega)} = 0 \end{aligned} \tag{6.23}$$

6.2.3. RESULT AND ANALYSIS

With the same data as the table 6.2, the performance of the distributed tuned mass damper (DTMD) model is described in this section. The frequency response for the acceleration can be seen in the Figure6.4. The figure describe a building with a DTMD placed on the top of the building. The parameter for this study is the length of the DTMD which is shown in the legend on the graph. L=20m means the distributed TMD has a length of 20 m downward from the top of the building. But it is design that the DTMD has the same total mass or in equation:

$$m_{td_1} L_1 = m_{td_2} L_2 = 4.410^5 kg \tag{6.24}$$

The value of the y coordinate of the graph is only to compare the effectiveness of the TMD models. The acceleration value can be obtain from this graph using the procedure form the chapter 1. It can be seen the optimal length of the distributed TMD is only 1m which is the same as the model 1 (single mass TMD).

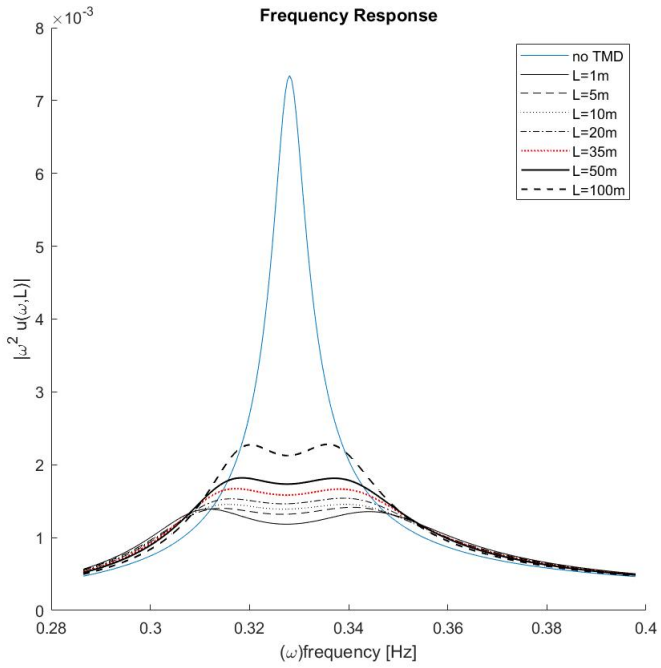

Figure 6.4: Frequency response for DTMD model

But in reality, the advantage of the DTMD is that it has a large total mass value compared to single point mass TMD. Single point mass TMD usually used some blocks of steel clamped as one mass. But in DTMD case, a

continuous long mass can be used for example in Tokyo Sky Tree, the engineer uses the emergency stair case with a continuous tubular concrete column as DTMD. This model is studied deeper in the section 5.

6.3. ROTATIONAL MASS DAMPER

The model of rotational mass damper can be seen in the figure below:

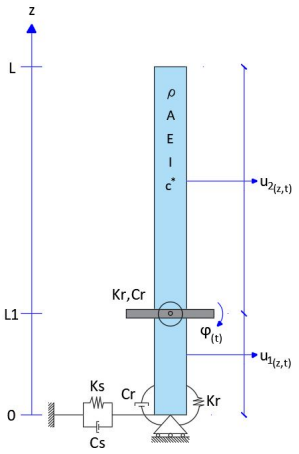

Figure 6.5: Prestressed TMD

6.3.1. EQUATION OF MOTION

While the equation of motion of the beam is the same as the Analysis in chapter 7.2, the equation of motion of the rotating TMD can be seen in the equation below:

$$\begin{aligned} ma &= \sum F \\ -\omega^2 m_{tr} R^2 \tilde{\theta}_{(\omega)} &= -(iC_{tr} + K_{tr})\left(\tilde{\theta}_{(\omega)} - \frac{\partial}{\partial z}\tilde{u}_{1(L1,\omega)}\right) \\ \tilde{\theta}_{(\omega)} &= \frac{iC_{tr} + K_{tr}}{-\omega^2 R^2 m_{tr} + i\omega C_{tr} + K_{tr}} \frac{\partial}{\partial z}\tilde{u}_{1(L1,\omega)} \end{aligned} \tag{6.25}$$

Therefore, the solution for the beam EOM is also the same as in chapter A.1.1, in summary it can be written as:

$$\begin{aligned} \tilde{u}_{1,2(z,\omega)} &= \tilde{u}_{1,2homogeneous} + \tilde{u}_{1,2particular} \\ \tilde{u}_{1,2homogeneous} &= A_{1,2}\cosh(\beta z) + B_{1,2}\sinh(\beta z) + C_{1,2}\cos(\beta z) + D_{1,2}\sin(\beta z) \\ \tilde{u}_{1,2particular} &= A_{p(1,2)}z^4 + B_{p(1,2)}z^3 + C_{p(1,2)}z^2 + D_{p(1,2)}z + E_{p(1,2)} \end{aligned} \tag{6.26}$$

6.3.2. BOUNDARY AND INTERFACE CONDITION

The boundary condition for the bottom and top can be seen in the chapter 6.2.2. The interface conditions at $z = L1$ when the rotational TMD is placed are:

Displacement:

$$\tilde{u}_{1(L1,\omega)} - \tilde{u}_{2(L1,\omega)} = 0 \tag{6.27}$$

Rotation:

$$\frac{\partial}{\partial z}\tilde{u}_{1(L1,\omega)} - \frac{\partial}{\partial z}\tilde{u}_{2(L1,\omega)} = 0 \tag{6.28}$$

Bending Moment:

$$EI^*\left(\frac{\partial^2}{\partial z^2}\tilde{u}_{2(L1,\omega)} - \frac{\partial^2}{\partial z^2}\tilde{u}_{1(L1,\omega)}\right) - (i * C_{tr} + K_{tr})\left(\frac{\partial}{\partial z}\tilde{u}_1 - \tilde{\theta}_{(\omega)}\right) = 0 \tag{6.29}$$

Shear Force:

$$\frac{\partial^3}{\partial z^3}\tilde{u}_{1(L1,\omega)} - \frac{\partial^3}{\partial z^3}\tilde{u}_{2(L1,\omega)} = 0 \tag{6.30}$$

6.3.3. PENDULUM TYPE

The model in the Figure6.6 describes a mass with a certain radius connected to a building by a rigid inextensible bar. The connection to the building is designed to transfer only bending moment by rotational spring and dashpot. The difference of this model compared to previous rotational TMD model is that the mass has a potential energy which can be positive (right figure) or negative (left figure).

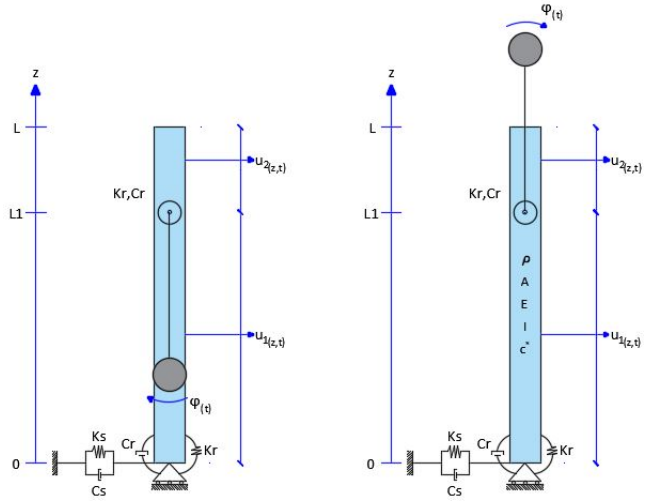

Figure 6.6: Prestressed TMD

The only change that occur in this model is in the equation of motion of the TMD which is:

$$
\begin{aligned}
-(\omega^2 R^2 \pm gR) m_{tr} \tilde{\theta}_{(\omega)} &= -(iC_{tr} + K_{tr}) \left(\tilde{\theta}_{(\omega)} - \frac{\partial}{\partial z} \tilde{u_1}_{(L1,\omega)} \right) \\
\tilde{\theta}_{(\omega)} &= \frac{iC_{tr} + K_{tr}}{-(\omega^2 R^2 \pm gR) m_{tr} + i\omega C_{tr} + K_{tr}} \frac{\partial}{\partial z} \tilde{u_1}_{(L1,\omega)}
\end{aligned}
\tag{6.31}
$$

6.4. RESULT AND ANALYSIS

The plot of the frequency response function for the acceleration of the rotational TMD (RTMD) can be seen in the Figure6.8. The model is a block of mass horizontally located at radius R from the core, a clear image can be seen in Figure6.7.

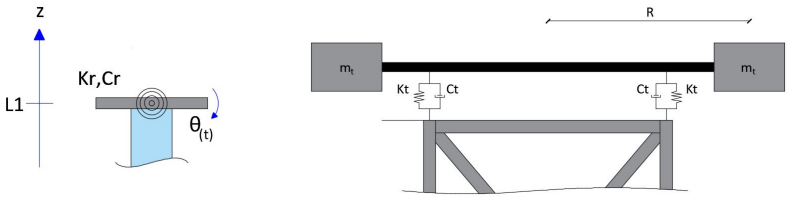

Figure 6.7: Rotational Tuned Mass Damper

In which:

$$
\begin{aligned}
K_r, C_r &= 2[K_t, C_t] R^2 \\
J &= 2 m_t R^2
\end{aligned}
\tag{6.32}
$$

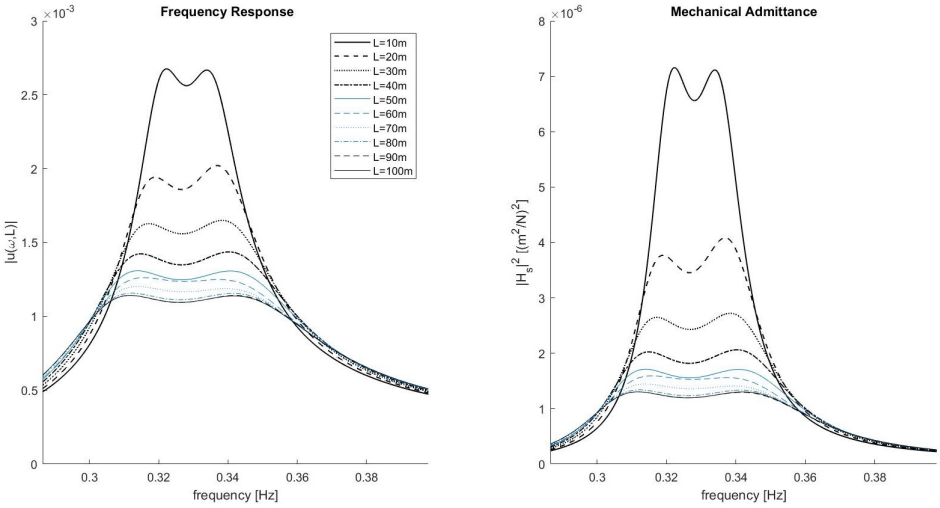

Figure 6.8: Frequency Response RTMD

Figure6.8 depicts some different positions of the RTMD on the building. It can be seen that the optimum position of RTMD is on the top of the building since the rotation is maximum on top. It s proven also from the static analysis of clamped free beam that the equation for the rotation is:

$$\frac{\partial}{\partial z}u = \frac{1}{EI}\left(\frac{1}{24}fz^4 - \frac{1}{6}fLz^3 + \frac{1}{4}fL^2z^2 + \frac{1}{2}\frac{fL^2zEI}{Kr} + \frac{fLEI}{Ks}\right) \tag{6.33}$$

Unlike the conventional TMD model, the effectiveness of the RTMD model can be improved without chang-

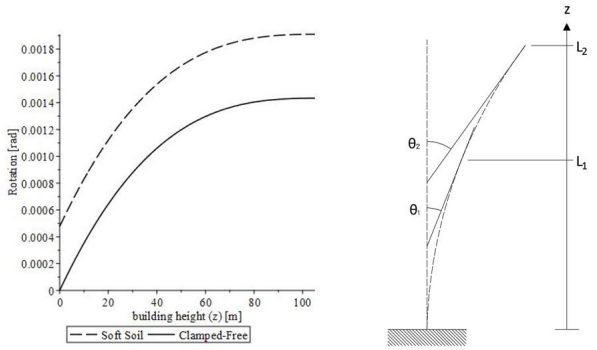

Figure 6.9: Rotation of a static beam

ing the mass but changing the radius. It has the same influence as changing the mass, but in the case of Figure6.7 changing the radius does not change the frequency of the RTMD unlike changing its mass.
But because RTMD effect on the bending moment which is not as effective as shear force in reducing the response, it needs very long radius of 100m to have the same effect of the sigle mass TMD (basic model). This can be seen in Figure6.10:

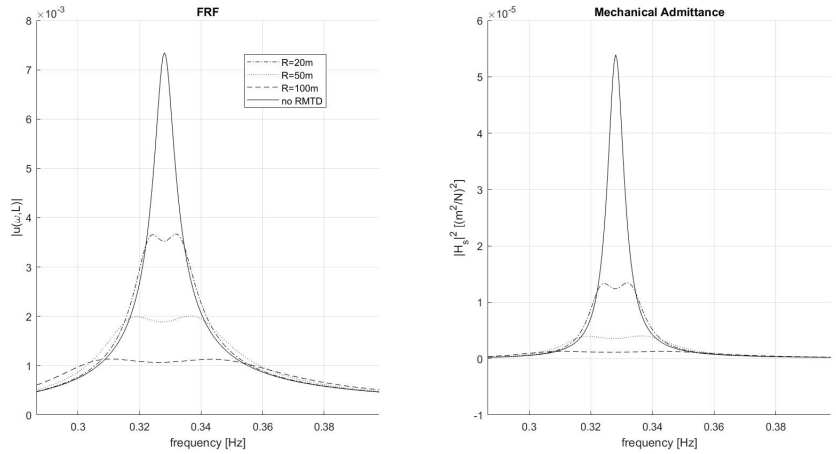

Figure 6.10: Frequency Response RTMD

This is also can be understand through static calculation. If we would like to move a building with the same deformation, we need the value of bending moment (M) 100 times larger than the value of the shear force (F).

$$u_M = \frac{1}{EI}\left(-1/6\,Fz^3 + 1/2\,FLz^2 + \frac{EI\,FLz}{Kr} + \frac{EI\,F}{Ks}\right)$$
$$u_F = \frac{1}{EI}\left(1/2\,Mz^2 + \frac{EI\,Mz}{Kr}\right) \tag{6.34}$$

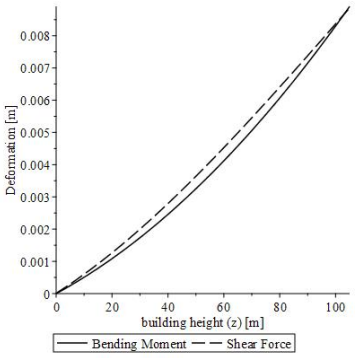

Figure 6.11: Influence of bending moment and shear force

The acceleration for the RTMD with 100m radius is $0.0278 m/s^2$. As expected it is higher than the base TMD model which has the acceleration $0.0301 m/s^2$.

6.5. ROTATIONAL AND TRANSLATIONAL MASS DAMPER

The model of rotational and translational mass damper can be seen in the figure below:

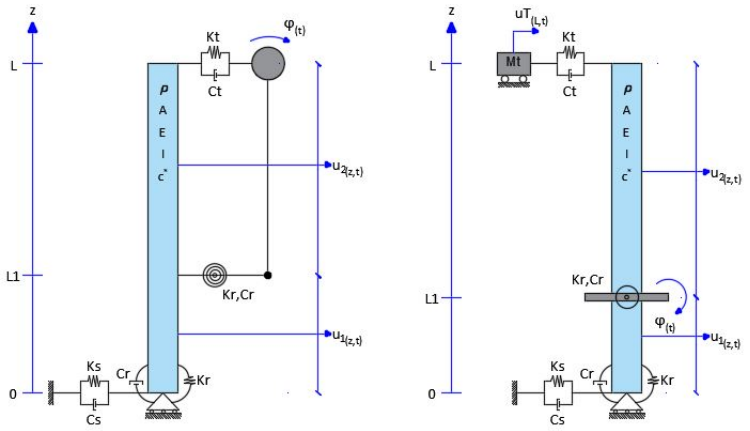

Figure 6.12: Rotational and translational mass damper

The figure on the left depicts a TMD model which the rotational and translational mass damper is connected through a pendulum. The figure on the right depicts an uncoupled system of the translational and rotational behavior of the TMD. The system has 2 masses, one for translational and the other for the rotational.

6.5.1. EQUATION OF MOTION

TUNED MASS DAMPER

For the left figure, the EOM of the TMD is:

$$-\omega^2 J\theta + (i\omega C_{rt} + K_{rt})\left(\theta_{(\omega)} - \frac{\partial}{\partial z}\tilde{u_2}_{(z,\omega)}\right) + (i\omega C_t + K_t)(\theta_{(\omega)} - R\tilde{u_2}_{(z,\omega)}) = 0 \tag{6.35}$$

Then the expression of $\tilde{\theta}$ can be through this equation:

$$\tilde{\theta_{(\omega)}} = \frac{(i\omega C_{tr} + K_{tr})\frac{\partial}{\partial z}\tilde{u_2}_{(L1,\omega)} + (i\omega C_t + K_t)R\tilde{u_2}_{(L,\omega)}}{-(\omega^2 R^2 + gR)m_t + (i\omega C_{tr} + K_{tr}) + (i\omega C_t + K_t)R^2} \tag{6.36}$$

6.5.2. BOUNDARY AND INTERFACE CONDITION:

The boundary at the bottom can be seen at the equation . The boundry condition at $z = L$ is:

Bending Moment:

$$EI^* \frac{\partial^2}{\partial(z^2)}\tilde{u_2}_{(L,\omega)} = 0 \tag{6.37}$$

Shear Force:

$$EI^* \frac{\partial^3}{\partial z^3}\tilde{u_2}_{(L,\omega)} - (i\omega C_t + K_t)(\tilde{u_2}_{(L,\omega)} - R\tilde{\theta}_{(\omega)}) = 0 \tag{6.38}$$

The interface conditions at $z = L1$ are:

Displacement:

$$\tilde{u_1}_{(L1,\omega)} - \tilde{u_2}_{(L1,\omega)} = 0 \tag{6.39}$$

Rotation:

$$\frac{\partial}{\partial z}\tilde{u_1}_{(L1,\omega)} - \frac{\partial}{\partial z}\tilde{u_2}_{(L1,\omega)} = 0 \tag{6.40}$$

Bending Moment:

$$EI^*\left(\frac{\partial^2}{\partial z^2}\tilde{u_2}_{(L1,\omega)} - \frac{\partial^2}{\partial z^2}\tilde{u_1}_{(L1,\omega)}\right) - (i * C_{tr} + K_{tr})\left(\frac{\partial}{\partial z}\tilde{u_1} - \tilde{\theta}_{(\omega)}\right) = 0 \tag{6.41}$$

Shear Force:

$$\frac{\partial^3}{\partial z^3}\tilde{u_1}_{(L1,\omega)} - \frac{\partial^3}{\partial z^3}\tilde{u_2}_{(L1,\omega)} = 0 \tag{6.42}$$

6.5.3. RESULT AND ANALYSIS

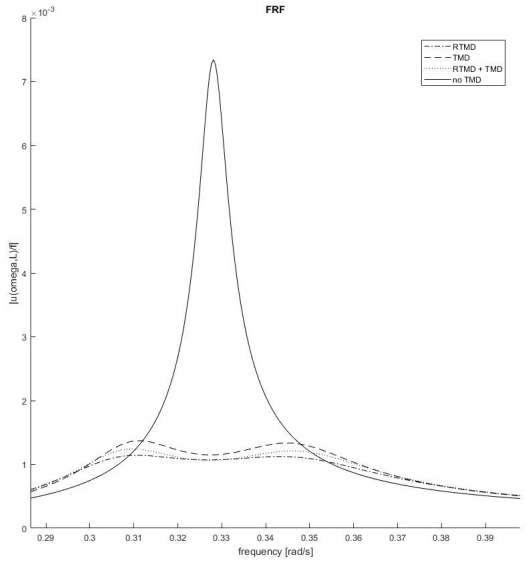

Figure 6.13: Rotational and translational mass damper (coupled)

The mass, translational spring and dashpot value is the same as the base model. Also the rotational spring and damper is the same as the RTMD model with 100m radius. The graph shows that the performance of the model with one pendulum mass is in in between the base model (single TMD mass on top of the building) and the rotational mass damper. This is influenced by the value of stiffness and damping which connect the pendulum to the building. There are 2 extreme case which are:

1. The rotational stiffness and dashpot is zero (TMD 100% RTMD 0%) - similar to base TMD model (dashed line)
2. The translational stiffness and dashpot is zero (TMD 0% RTMD 100%) - similar to rotational TMD model (dashed-dot line)

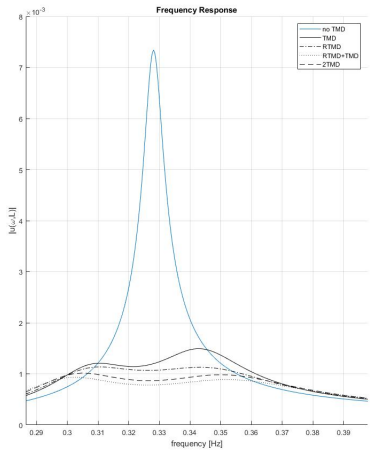

Figure 6.14: Distributed and translational mass damper (uncoupled)

As the rotational stiffness and daspot is increased from the case 1, the value of the translational stiffness and dashpot should be decreased to tuned it to have the same natural frequency of the building, it can be seen

from the equation of motion of the TMD system in equation 6.36. The result from doing this is that the graph is moved from the case 1 graph, closer to the case 2 graph. So it is reducing the performance of TMD.

In the model when there are 2 separate masses (translational and rotational), the frequency response can be seen in the Figure6.14. The value of the mass spring and damper is the same as the base model and the RTMD model with 100m radius. The rotational and translational TMD are placed on the top of the building since it is the most optimum location for both TMD performance.

It can be seen that the performance of the RTMD + TMD is better than the single TMD because it has more mass. But comparing to the 2 translational TMD mass on top of the building or double the mass of the single TMD model, the graph shows that it has similar result with RTMD+TMD model. Because the RTMD with 100m radiuse itself (dashed-dot line) has a better performance compared to the base TMD model (solid black line).

6.6. DISTRIBUTED ROTATIONAL MASS DAMPER

The distributed rotational mass damper is design to absorb the large rotational change on the bottom of the building. The model can be seen in the figure below.

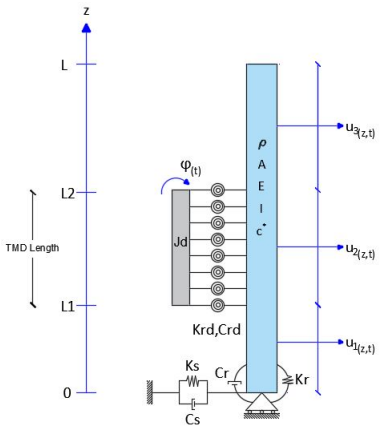

Figure 6.15: Distributed rotational mass damper

6.6.1. EQUATION OF MOTION

TUNED MASS DAMPER

The equation of motion for the TMD can be written as:

$$-\omega^2 J\tilde{\theta} + (i\omega C_r d + K_r d)\left(\tilde{\theta}_{(z,\omega)} - \frac{\partial^2}{\partial z^2}\tilde{u}_{2(z,\omega)}\right) \tag{6.43}$$

The expression of TMD's motion can be obtained from the above equation:

$$\tilde{\theta}_{(z,\omega)} = \gamma \frac{\partial^2}{\partial z^2}\tilde{u}_{2(z,\omega)} \tag{6.44}$$

in which:

$$\gamma = \frac{(i\omega C_r d + K_r d)}{-\omega^2 J + i\omega C_r d + K_r d} \tag{6.45}$$

BUILDING

The building is divided into three parts, for each part, the equation of motion is:

1. For: 0<z<L1

$$EI^* \frac{\partial^4}{\partial z^4}\tilde{u}_{1(z,\omega)} - \omega^2 \rho A \tilde{u}_{1(z,\omega)} = \tilde{q}_{(z,t)} \tag{6.46}$$

2. For: L1<z<L2

$$EI^* \frac{\partial^4}{\partial z^4}\tilde{u}_{2(z,\omega)} - \omega^2 \rho A \tilde{u}_{2(z,\omega)} + (i\omega C_r d + K_r d)\left(\frac{\partial^2}{\partial z^2}\tilde{u}_{2(z,\omega)} - \tilde{\theta}_{(z,\omega)}\right) = \tilde{q}_{(z,t)} \tag{6.47}$$

3. For: L2<z<L

$$EI^* \frac{\partial^4}{\partial z^4} \tilde{u}_{3(z,\omega)} - \omega^2 \rho A \tilde{u}_{3(z,\omega)} = \tilde{q}_{(z,t)} \tag{6.48}$$

By using the expression of the TMD's motion in equation 6.44, the second EOM in the building can be written as:

$$EI^* \frac{\partial^4}{\partial z^4} \tilde{u}_{2(z,\omega)} - \omega^2 \rho A \tilde{u}_{2(z,\omega)} + (i\omega C_r d + K_r d)(1-\gamma) \frac{\partial^2}{\partial z^2} \tilde{u}_{2(z,\omega)} = \tilde{q}_{(z,t)} \tag{6.49}$$

This equation can be solve by finding the solution for the homogeneous equation and the particular solution.

HOMOGENEOUS EQUATION:

$$\frac{\partial^4}{\partial z^4} \tilde{u}_{2(z,\omega)} + 2\alpha^2 \frac{\partial^2}{\partial z^2} \tilde{u}_{2(z,\omega)} - \beta^4 \tilde{u}_{2(z,\omega)} = 0 \tag{6.50}$$

In which:

$$\begin{aligned} \alpha &= \sqrt{\frac{(i\omega C_r d + K_r d)(1-\gamma)}{2EI^*}} \\ \beta &= \left(\frac{\omega^2 \rho A}{EI^*}\right)^{1/4} \end{aligned} \tag{6.51}$$

The general solution for this homogeneous linear differential equation is:

$$\tilde{u}_{2(z,\omega)} = \sum_{i=1}^{4} C_i e^{\lambda_i z} \tag{6.52}$$

Substituting this form of solution to the EOM resulting:

$$\lambda^4 + 2\alpha^2 \lambda^2 - \beta^4 = 0 \tag{6.53}$$

The value for λ can be obtained by finding the root of the equation. For the fourth order polynomial in the form of:

$$\begin{aligned} \lambda^2 &= -\alpha^2 \pm \sqrt{\alpha^4 + \beta^4} \\ \lambda_{a,b} &= \pm \sqrt{\sqrt{\alpha^4 + \beta^4} - \alpha^2} \\ \lambda_{c,d} &= \pm i \sqrt{\sqrt{\alpha^4 + \beta^4} + \alpha^2} \end{aligned} \tag{6.54}$$

The form of solution for the homogeneous equation now can be written as:

$$\tilde{u}_{2(z,\omega)} = A_2 \cosh \lambda 1 z + B_2 \sinh \lambda 1 z + C_2 \cos \lambda 2 z + D_2 \sin \lambda 2 z \tag{6.55}$$

In which:

$$\begin{aligned} \lambda_1 &= \sqrt{\sqrt{\alpha^4 + \beta^4} - \alpha^2} \\ \lambda_2 &= \sqrt{\sqrt{\alpha^4 + \beta^4} + \alpha^2} \end{aligned} \tag{6.56}$$

PARTICULAR SOLUTION:

Due to the change occur in the equation of motion, therefore the particular solution for the second building motion is also changed. But because the form of the load is the same, the particular solution can be found in the same form as in equation A.14. Substituting to the 2nd EOM resulting:

$$\begin{gathered} -\beta^4 (Apx^4 + Bpx^3 + Cpx^2 + Dpx + Ep) + \alpha^2 (24Apx^2 + 12Bp\alpha^2 x + 4Cp\alpha^2) + 24Ap = \\ \frac{az^4 + bz^3 + cz^2 + dz + e}{EI^*} \end{gathered} \tag{6.57}$$

Therefore the constant for the particular solution can be written as:

$$\begin{aligned} A_p &= -\frac{a}{EI^*\beta^4} \\ B_p &= -\frac{b}{EI^*\beta^4} \\ C_p &= \frac{24A_pEI^*\alpha^2 - c}{EI^*\beta^4} \\ D_p &= \frac{12B_pEI^*\alpha^2 - d}{EI^*\beta^4} \\ E_p &= \frac{4C_pEI^*\alpha^2 + 24A_pEI^* - e}{EI^*\beta^4} \end{aligned} \tag{6.58}$$

6.6.2. BOUNDARY AND INTERFACE CONDITIONS

The four dynamic boundary conditions can be written as:

Shear Force:

$$EI^*\frac{\partial^3}{\partial z^3}\tilde{u_1}_{(0,\omega)} + (i\omega C_s + K_s)\tilde{u_1}_{(0,\omega)} = 0 \tag{6.59}$$

Bending Moment:

$$EI^*\frac{\partial^2}{\partial z^2}\tilde{u_1}_{(0,\omega)} + (i\omega C_r + K_r)\frac{\partial}{\partial z}\tilde{u_1}_{(0,\omega)} = 0 \tag{6.60}$$

Shear Force:

$$EI^*\frac{\partial^3}{\partial z^3}\tilde{u_3}_{(L,\omega)} = 0 \tag{6.61}$$

Bending Moment:

$$EI^*\frac{\partial^3}{\partial z^3}\tilde{u_3}_{(L,\omega)} = 0 \tag{6.62}$$

The eight interface conditions can be written as:

Displacement:

$$\begin{aligned} \tilde{u_1}_{(L1,\omega)} - \tilde{u_2}_{(L1,\omega)} &= 0 \\ \tilde{u_2}_{(L2,\omega)} - \tilde{u_3}_{(L2,\omega)} &= 0 \end{aligned} \tag{6.63}$$

Rotation:

$$\begin{aligned} \frac{\partial}{\partial z}\tilde{u_1}_{(L1,\omega)} - \frac{\partial}{\partial z}\tilde{u_2}_{(L1,\omega)} &= 0 \\ \frac{\partial}{\partial z}\tilde{u_2}_{(L2,\omega)} - \frac{\partial}{\partial z}\tilde{u_3}_{(L2,\omega)} &= 0 \end{aligned} \tag{6.64}$$

Bending Moment:

$$\begin{aligned} \frac{\partial^2}{\partial z^2}\tilde{u_1}_{(L1,\omega)} - \frac{\partial^2}{\partial z^2}\tilde{u_2}_{(L1,\omega)} &= 0 \\ \frac{\partial^2}{\partial z^2}\tilde{u_2}_{(L2,\omega)} - \frac{\partial^2}{\partial z^2}\tilde{u_3}_{(L2,\omega)} &= 0 \end{aligned} \tag{6.65}$$

Shear Force:

$$\begin{aligned} \frac{\partial^3}{\partial z^3}\tilde{u_1}_{(L1,\omega)} - \frac{\partial^3}{\partial z^3}\tilde{u_2}_{(L1,\omega)} &= 0 \\ \frac{\partial^3}{\partial z^3}\tilde{u_2}_{(L2,\omega)} - \frac{\partial^3}{\partial z^3}\tilde{u_3}_{(L2,\omega)} &= 0 \end{aligned} \tag{6.66}$$

6.6.3. RESULT AND ANALYSIS

The DRMD (distributed rotational mass damper) model is design to influence the curvature of the building. Because the building is modeled as a beam, the curvature of the beam is defined as the rate of change of the rotation which can be seen in the figure with $d\theta$.

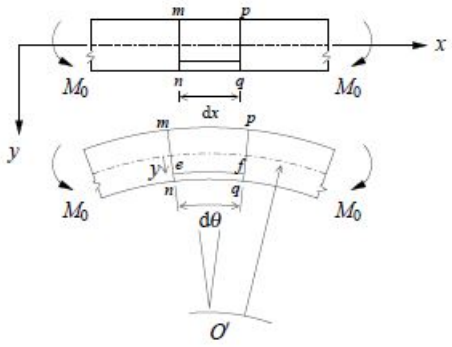

Figure 6.16: Curvature of a beam

The optimum position of the DRMD must be determined first. The DRMD is modeled with the length of 1 m and a total mass of $4.410^5 kg$ with a radius of 100m. It can be seen in the Figure6.18 that the optimum position is placed at 50m from the bottom.

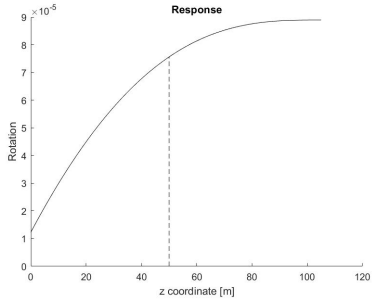

Figure 6.17: Response Function along the Building's Height

This can be understood by seeing the rotation plot along the beam as it can be seen in Figure6.17. Because the rate of change of the rotation occurs also at the location 50 m from the bottom.

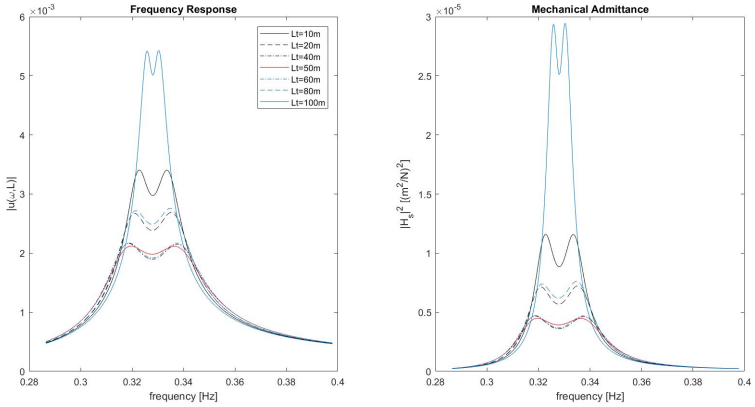

Figure 6.18: Position Parameter

The comparison of the frequency response function and mechanical admittance of the distributed rotational mass damper with the base TMD model can be seen in the Figure6.19. The acceleration of the DRMD model

with 100m radius and position at 50m from the bottom is $0.0375 m/s^2$. As expected it is lower than the base TMD model which has the acceleration $0.0301 m/s^2$.

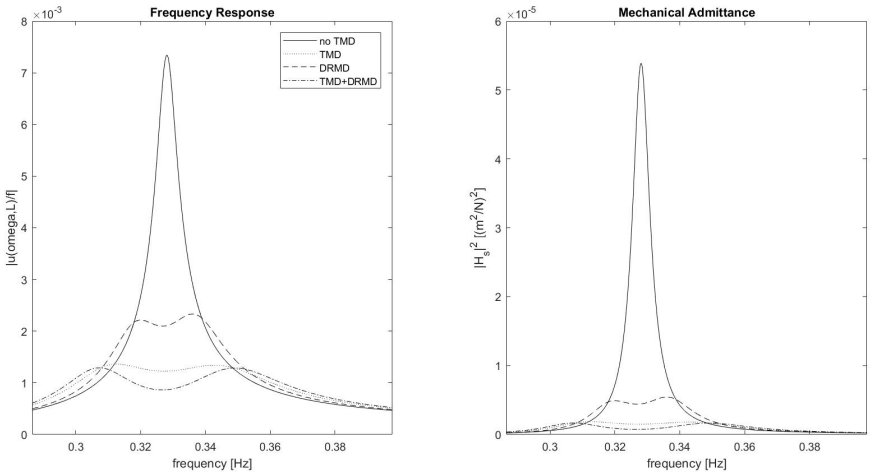

Figure 6.19: Frequency Response Distributed Rotational Mass Damper

6.7. RIGID BAR MASS DAMPER

The model of rigid bar as a mass damper can be seen in the figure below:

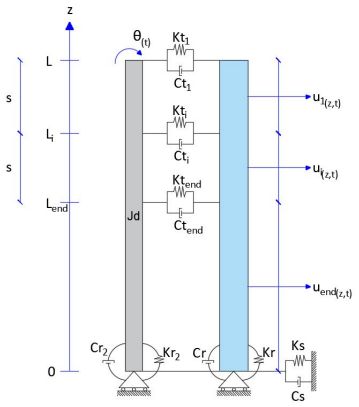

Figure 6.20: Rigid bar as a mass damper

6.7.1. EQUATION OF MOTION

The equation of motion of the TMD can be written as:

$$-\omega^2 J\tilde{\theta}_{(\omega)} + (i\omega C_{r2} + K_{r2})\tilde{\theta}_{(\omega)} + \sum_{i=1}^{end}(i\omega C_{ti} + K_{ti})\left(L_i^2\tilde{\theta}_{(\omega)} - L_i\tilde{u}_{2(L_i,\omega)}\right) = 0 \tag{6.67}$$

In which:

$$L_i = L - is \tag{6.68}$$

The equation of motion of the beam can be written as:

$$EI^* \frac{\partial^4}{\partial z^4}\tilde{u}_{i\,(z,\omega)} - \omega^2 \rho A \tilde{u}_{i\,(z,\omega)} = \tilde{q}_{(z,t)} \tag{6.69}$$

The Boundary condition can be written as:

Shear Force:

$$EI^* \frac{\partial^3}{\partial z^3}\tilde{u}_{end\,(0,\omega)} + (i\omega C_s + K_s)\tilde{u}_{end\,(0,\omega)} = 0 \tag{6.70}$$

Bending Moment:

$$EI^* \frac{\partial^2}{\partial z^2} \tilde{u}_{end\,(0,\omega)} + (i\omega C_r + K_r) \frac{\partial}{\partial z} \tilde{u}_{end\,(0,\omega)} = 0 \tag{6.71}$$

Shear Force:

$$EI^* \frac{\partial^3}{\partial z^3} \tilde{u}_{1\,(L,\omega)} - (i\omega C_t + K_t)(\tilde{u}_{(L,\omega)} - \tilde{u}_{t\,(\omega)}) = 0 \tag{6.72}$$

Bending Moment:

$$EI^* \frac{\partial^2}{\partial z^2} \tilde{u}_{1\,(L,\omega)} = 0 \tag{6.73}$$

Interface condition for each point at $z = L_i$ can be written as:
Displacement:

$$\tilde{u}_{i\,(L_i,\omega)} - \tilde{u}_{i+1\,(L_i,\omega)} = 0 \tag{6.74}$$

Rotation:

$$\frac{\partial}{\partial z} \tilde{u}_{i\,(L_i,\omega)} - \frac{\partial}{\partial z} \tilde{u}_{i+1\,(L_i,\omega)} = 0 \tag{6.75}$$

Bending Moment:

$$\frac{\partial^2}{\partial z^2} \tilde{u}_{i\,(L_i,\omega)} - \frac{\partial^2}{\partial z^2} \tilde{u}_{i+1\,(L_i,\omega)} = 0 \tag{6.76}$$

Shear Force:

$$EI^* \left(\frac{\partial^3}{\partial z^3} \tilde{u}_{i+i\,(L_i,\omega)} - \frac{\partial^3}{\partial z^3} \tilde{u}_{i\,(L_i,\omega)} \right) + (i\omega C_{ti} + K_{ti})(\tilde{u}_{i\,(L_i,\omega)} - \tilde{u}_{ti}) = 0 \tag{6.77}$$

6.7.2. RESULT AND ANALYSIS

The frequency response for the acceleration due to wind load in frequency domain ($f_{(\omega)} = 1$) and the mechanical admittance for the rigid bar TMD can be seen in the Figure6.21. The rigid bar has a mass of $4.4 * 10^5 kg$

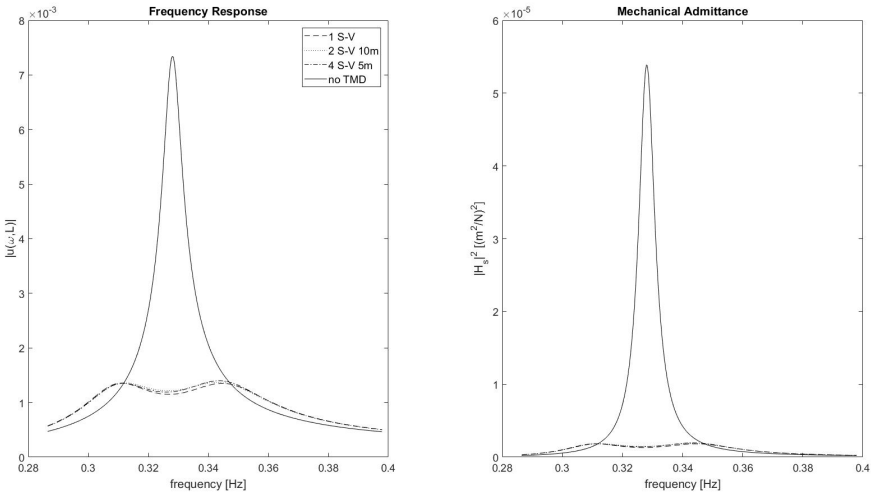

Figure 6.21: Frequency response of a rigid bar TMD

and connected with different quantity of viscous damper and spring stiffness. In the legend of the graph, 2 S-V 5m describe that the rigid bar connected with 2 spring stiffness and viscous damper. The first is always on top of the building, and the second has a 5m spacing below it. It can be conclude that the amount of the viscous damper and spring stiffness does not influence the performance of the TMD. But it influences the value of each the spring stiffness and damper. With more spring and damper, the value for a single spring-damper can be reduced.
This model is beneficial to take advantage of using an element of the building which does not have a major contribution to the structural stability. For example the shaft for emergency escape can be used as a rigid

TMD from the bottom to the top of the building. Which is also contribute to the total cost because the cost of the mass is 50% of the total cost of buy and install TMD. The European Patent Office (EPO) which is designed by Zonneveld has two emergency shaft with a total weight of $2.2 * 10^6 kg$ as it can be seen in the Figure6.22.

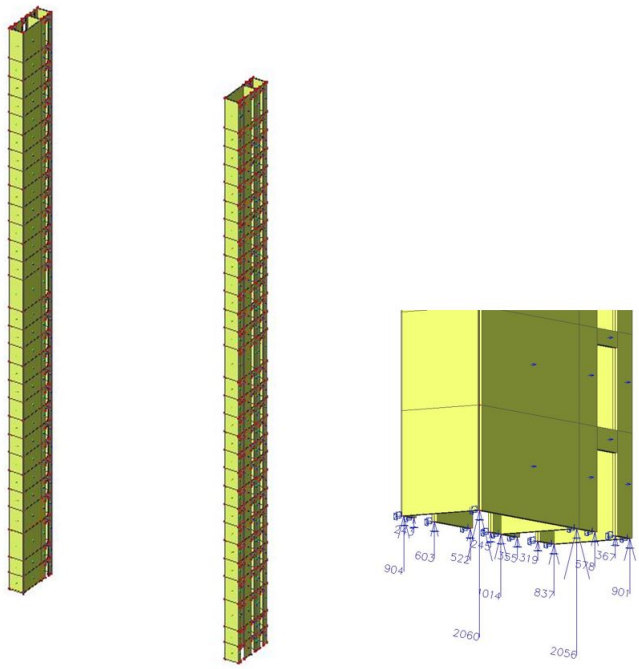

Figure 6.22: EPO Building Emergency Shaft

With this emergency shaft as a rigid bar TMD connected to the building through viscous damper and spring stiffness, the performance of the TMD can be increased as it is shown in Figure6.23. The performance using

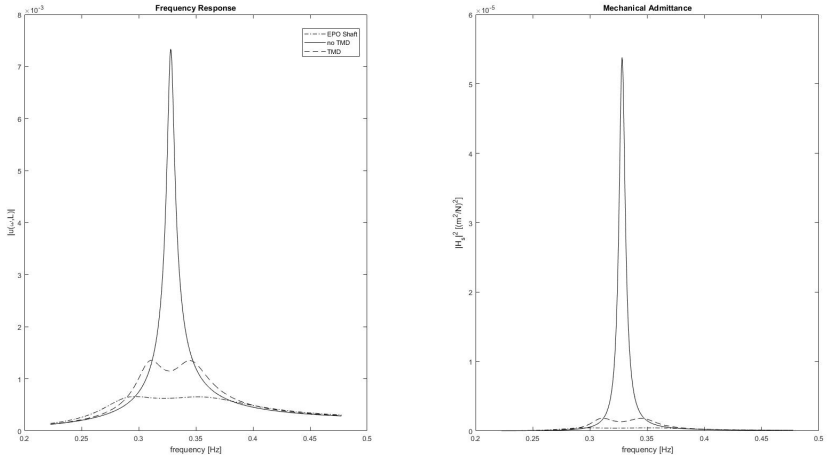

Figure 6.23: Frequency response of a EPO's emergency shaft as a rigid bar TMD

the emergency shaft as TMD is significant, with this shaft as the TMD, the acceleration of the building due to the bending vibration is $0.0212 m/s^2$. While the acceleration due to the basic TMD model (single TMD mass on top of the building) is $0.0301 m/s^2$.

III

ANALYSIS

7

COST ANALYSIS

Besides the TMD performance, cost is a significant parameter in designing a TMD. A comparison in using the TMD and increasing the dimension of the steel profile is made in this chapter. Then further analysis in the cost analysis can explain more about the beneficial of the TMD and on which building properties it is favored.

7.1. INTRODUCTION

The main idea of the cost analysis is to compare the cost of reducing building acceleration by applying TMD and increasing the dimension of the steel profile. The procedure of the cost analysis is shown in Figure7.1:

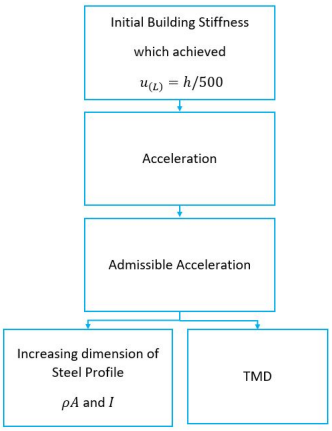

Figure 7.1: Cost analysis procedure

1. Reduce the building stiffness by decreasing the steel profile dimension. The minimum limitation of this decrement is the displacement limit of the building which is $h/500$.

2. Do the dynamic analysis to obtain the acceleration of this reduced properties.

3. Reduce the acceleration of the building by increasing the dimension of the steel profile.

4. Reduce the acceleration of the building by applying TMD.

Static analysis is used to determine the stiffness of the building. There are 2 properties which the building has that influence the maximum deflection of the building, which are the bending property and torsional property. The total deflection at one point of the building can be obtained by the summation of bending and torsion deflection. The model which is used for the static analysis can be seen in the figure below:

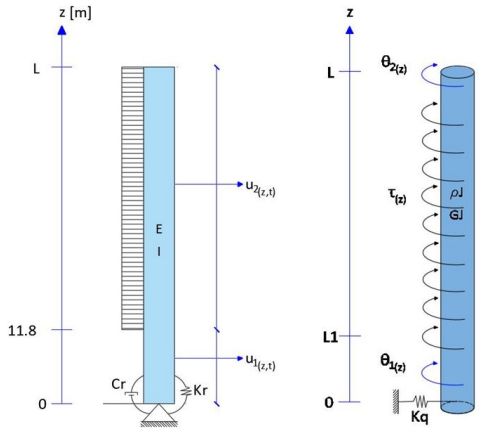

Figure 7.2: Bending Beam Model

The bending deflection can be seen in following equation:

$$u_{2(z)} = \frac{1}{EI}\Big(1/24\,qz^4 + \frac{1}{6}(-Lq-P)z^3 + \frac{1}{4}L(Lq+2P)z^2 + \frac{1}{6}\frac{\Big(-Kr\,Ll^3q + 3\,EI\,L^2q - 3\,EI\,Ll^2q + 6\,EI\,LP\Big)z}{Kr} + \frac{1}{24}qLl^4\Big) \tag{7.1}$$

The torsional rotation of the building with very stiff torsional base K_q, that the torsional deformation at the base equal to zero, can be seen in the following equation:

$$\theta_2 = \frac{-1/2\,\tau\,z^2 + L\tau\,z - 1/2\,\tau\,Ll^2}{GJ} \tag{7.2}$$

7.2. ANALYSIS

Based on the static analysis in Equation7.1 with the wind load in Figure4.17, the bending and torsional stiffness of the building which is needed to fulfill the deformation limit of $h/500 = 0.21m$ is:

$$\begin{aligned} q &= 226.11kN/m \\ P &= 2007kN \\ \tau &= 2383.33kNm/m \\ EI &= 3.5\times10^{13}Nm^2 \\ GJ &= 1.9\times10^{13} \end{aligned} \tag{7.3}$$

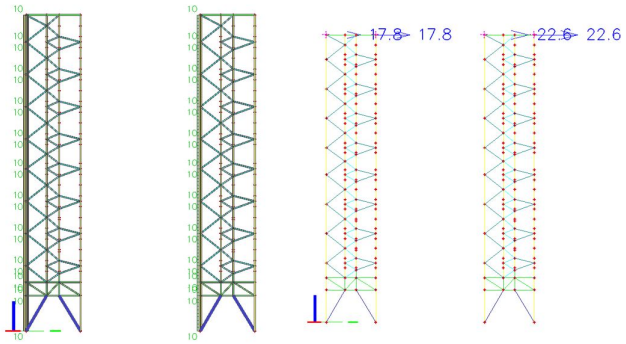

Figure 7.3: Steel Frame SCIA Engineer

Comparing this value to the initial EPO building properties ($EI = 4.7\times10^{13}\ Nm^2$) in Table4.4, this reduce of

the building stiffness is made by decreasing the dimension of steel profile which is also decrease the building mass. This condition is modeled in SCIA Engineering finite element program to calculate the decrement of the mass which can be seen in Figure7.3.

Because the steel frame core is the structural element which resist the horizontal stability of the building, the stiffness of the building due to horizontal wind loading can be obtain through calculating the stiffness of the 6 steel frame cores. There are two types of steel frame in EPO building, these two frame is depicted in the two figures from the left side of Figure7.3. There are 2 type 1 steel frame and 4 type 2 steel frame in the EPO building. The model of the steel frame which is loaded by $10kN/m$ horizontal force. The deformation formula for the Euler-Bernoulli Beam which is:

$$\begin{aligned} u_{(L)} &= \frac{qL^4}{8EI} \\ EI &= \frac{qL^4}{8u_{(L)}} \end{aligned} \tag{7.4}$$

The deformation on top of the steel frame is obtained through the SCIA Engineering program which is shown in Figure7.3 (two figures on the right side), then the stiffness of one steel frame can be calculated as:

$$\begin{aligned} EI_1 &= 1.707 \times 10^{12} Nm^2 \\ EI_2 &= 6.906 \times 10^{12} Nm^2 \\ EI_{total} &= 2 * EI_1 + 4 * EI_2 = 4.5 \times 10^{13} Nm^2 \end{aligned} \tag{7.5}$$

The total mass for the 6 steel frames model in Figure7.3 is $6.288ton$ which is obtain from the finite element program. With the same procedure, the steel profile dimension is decreased to obtained the $EI_{total} = 3.5 \times 10^{13} Nm^2$. The total mass for 6 steel frames of the reduced dimension is $4.938ton$. It reduces the steel frame mass by $1.35ton$, then the ρA becomes $8.57 \times 10^5 kg/m$ from $8.7 \times 10^5 kg/m$. Which is less than 1%, the mass from the change of steel profile dimension is relatively mall because the majority of the mass is located on the concrete floor and imposed load of non-structural elements.

Then the total acceleration with the building with stiffness as in Equation7.3 and mass per unit length of $8.57 \times 10^5 kg/m$ can be seen in the blue graph on the figure below:

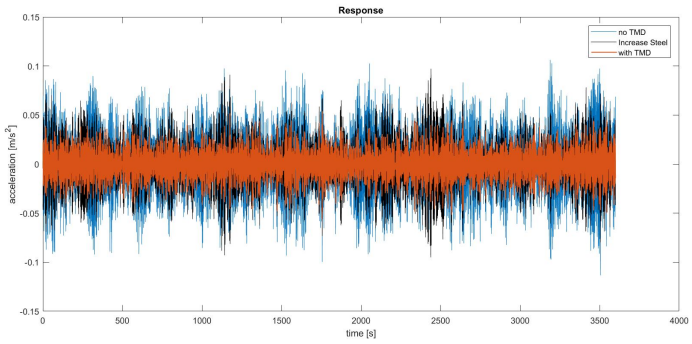

Figure 7.4: Acceleration

The black graph represent the building with the properties as in Chapter4, and the orange graph represent the building with TMD properties in Table4.6. The peak for each graph are:

$$\begin{aligned} \text{Blue} &= 0.1134 m/s^2 \\ \text{Black} &= 0.1 m/s^2 \\ \text{Orange} &= 0.056 m/s^2 \end{aligned} \tag{7.6}$$

It can be seen that the increase of steel profile dimension gives a small influence in the building acceleration compared to the TMD. The EPO building is already required the comfort criteria for a building based on figure which is $0.17 m/s^2$. But the building also need to required the user requirement such as the client in performance based design. A further reference for the acceleration of the building is made, the figure below

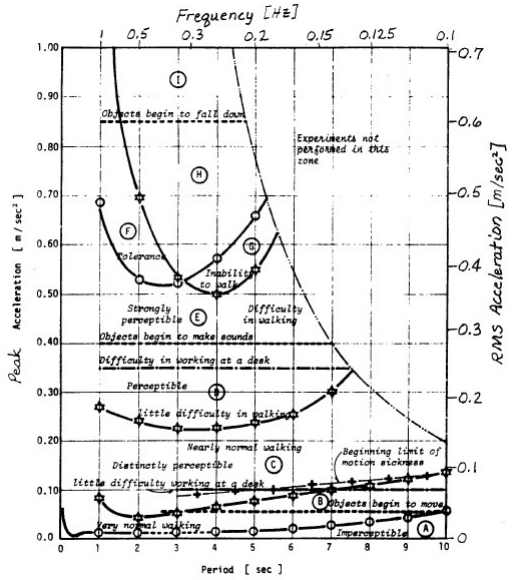

Figure 7.5: Comfort Criteria [D. Boggs]

shows an experiment of how people experience the building acceleration.

The building period for EPO is 3.5 second, and if the criteria of 0.1 for little difficult of working is made in this case. Then the additional steel is enough to fulfill the standard performance. In this case the EPO building is already close to the limit therefore the increase of steel dimension can be consider to be applied. The price of the $1350 ton$ steel is 1713 euro/ton, the cost for this enhancement is 2,312,550 euro. For this case, the reduce of the acceleration through the stiffness gives the same amount with the total cost from the TMD which is $2x10^7$ euro. But if we compare to the same amount reduction, the mass of TMD can be reduce to achieve the same acceleration as the increase of the steel profile dimension. With the TMD mass of $1 \times 10^5 kg$ the peak acceleration is $0.939 m/s^2$ as it can be seen in Figure7.6:

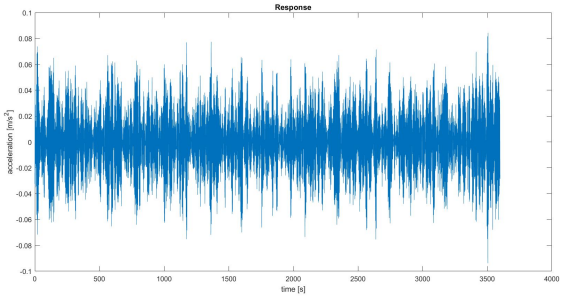

Figure 7.6: Acceleration with lower TMD mass

The steel mass of $4.4 \times 10^5 kg$ is 814,800 euro, then the price can be reduced by 629,618 euro which makes the TMD application more advantageous.

8

SENSITIVITY STUDY

The sensitivity study is done to understand the influence of the building, soil, and TMD properties in the dynamic behavior of the structure. The procedure is to change one property of the system in the one dimensional model and see the influence in term of the acceleration of the building.

8.1. BUILDING PROPERTIES

One of the most important and sensitive property of the building which correlated to the acceleration is the damping. Since it is more difficult to predict then the stiffness or mass of the building, there are a lot uncertainty in the value of the building damping. In this section, the damping which is studied is the damping of the building which in the one dimensional model, is represented by the value of C^*.

To measure the damping value of the building which is influenced by the C^*, the soil structure interaction (SSI) is changed to the rigid base on the one dimensional model. This properties can be seen in the table below:

SSI Parameter: Rigid Base		
Ks	$1 * 10^{100}$	N/m
Kr	$1 * 10^{100}$	Nm/rad
Cs	0	Ns/m
Cr	0	Nms/rad

Table 8.1: SSI Paramter for One Dimensional Model (Figure4.4)

Then the damping is measured by inputing the force equal to one in the frequency domain and plot the power spectral density as it is done in the Section4.2.1. The C^* value for the bending beam and torsional rod which give the material damping the same value for the bending and torsion can be seen in the Table8.2.

	Torsion	Bending
Damping	C_θ*	C*
0.374	4.17E-03	3.18E-03
0.539	6.02E-03	4.60E-03
0.704	7.87E-03	6.01E-03
0.870	9.72E-03	7.42E-03
1.035	1.16E-02	8.83E-03
1.201	1.34E-02	1.02E-02
1.367	1.53E-02	1.17E-02
1.533	1.71E-02	1.31E-02
1.699	1.90E-02	1.45E-02
1.865	2.08E-02	1.59E-02
2.031	2.27E-02	1.73E-02
2.197	2.45E-02	1.87E-02
2.364	2.64E-02	2.01E-02

	Torsion	Bending
Damping	C_θ*	C*
2.530	2.82E-02	2.15E-02
2.697	3.01E-02	2.29E-02
2.865	3.19E-02	2.44E-02
3.032	3.38E-02	2.58E-02
3.199	3.56E-02	2.72E-02
3.367	3.75E-02	2.86E-02
3.536	3.93E-02	3.00E-02
4.607	5.15E-02	3.89E-02
5.691	6.38E-02	4.79E-02
6.793	7.60E-02	5.68E-02
7.915	8.82E-02	6.58E-02
9.064	1.00E-01	7.47E-02
10.239	1.13E-01	8.37E-02

	Torsion	Bending
Damping	C_θ*	C*
11.450	1.25E-01	9.26E-02
12.700	1.37E-01	1.02E-01
13.998	1.49E-01	1.11E-01
15.343	1.61E-01	1.19E-01
16.751	1.74E-01	1.28E-01
18.228	1.86E-01	1.37E-01
19.784	1.98E-01	1.46E-01
21.431	2.10E-01	1.55E-01
23.183	2.23E-01	1.64E-01
25.059	2.35E-01	1.73E-01
27.080	2.47E-01	1.82E-01
29.273	2.59E-01	1.91E-01
31.671	2.71E-01	2.00E-01

Table 8.2: C^* value for the bending and torsion model(4.4) to obtain the same damping ratio

Then to obtain the acceleration at the top of the building, with the C^* value from the Table8.2, change the SSI properties back to the Table4.3. With the same procedure as the Chapter4 the peak acceleration (bending+torsion) of the building on the top corner can be obtained. Then the influence of the building damping (C^*) to the peak acceleration can be seen in the Figure8.1. It can be seen that the damping ratio has a significant influence from the value of zero to 4.5% which can reduce the peak acceleration from 0.13 to 0.06m/s^2. Therefore an accurate prediction for the damping of the building need to be developed.

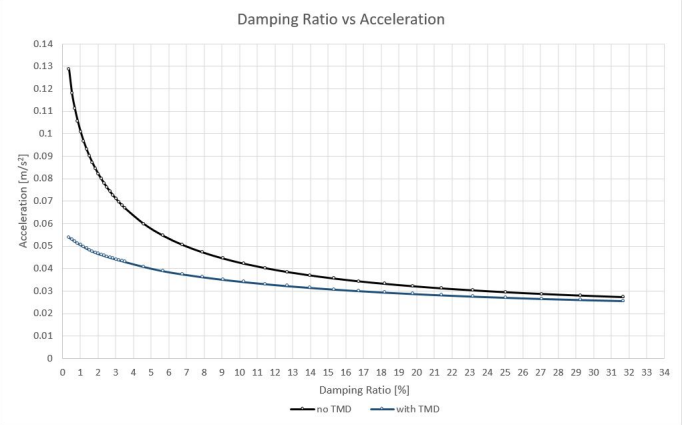

Figure 8.1: Influence of C^* on Peak Acceleration

8.2. TMD PROPERTIES

The passive TMD rely solely on the mass (this can be interpreted different way such as the Prestressed TMD), while the spring and dashpot is just a value which need to be tuned so that the mass give the optimum performance in absorbing the vibration. Therefore the sensitivity study in the TMD properties is done by changing the value of the TMD mass. The parameter of the TMD mass often mention in the form of the mass ratio (μ), which is the ratio of the TMD mass with the Building mass. The value of the mass ratio, TMD mass, and the spring-dashpot properties which is tuned to the optimum value can be seen in the Table8.3.

μ	Mt	Ct	Kt
0	0	0	0
0.001	9.14E+04	1.00E+04	4.03E+05
0.002	1.83E+05	2.50E+04	8.04E+05
0.003	2.74E+05	5.50E+04	1.20E+06
0.004	3.65E+05	9.00E+04	1.60E+06
0.005	4.57E+05	1.30E+05	2.00E+06
0.006	5.48E+05	1.80E+05	2.39E+06

μ	Mt	Ct	Kt
0.007	6.39E+05	2.28E+05	2.78E+06
0.008	7.31E+05	2.70E+05	3.18E+06
0.009	8.22E+05	3.20E+05	3.57E+06
0.01	9.14E+05	3.60E+05	3.95E+06
0.015	1.37E+06	6.50E+05	5.58E+06
0.02	1.83E+06	9.00E+05	7.37E+06
0.04	3.65E+06	2.50E+06	1.19E+07

Table 8.3: Value of TMD Properties for Sensitivity Study

In this thesis the optimum value of spring-dashpot of the TMD is defined as the value which gives the Building acceleration to the lowest point. For the spring stiffness, Den Hartog has derived the optimum tuning value of K which can be obtain through the Equation3.23.

$$\frac{\omega_{TMD}}{\omega_{building}} = \frac{1}{1+\mu} \qquad K_t = \omega_{TMD}^2 * m_t \tag{8.1}$$

In this case, this equation is applicable until $\mu = 0.01$, this equation is slightly modified trough a multiplication by a constant factor in larger TMD mass. The reason that the tuning ratio is not applicable is because the frequency of the wind has a high value in low frequency (Figure5.9). Therefore for the large TMD mass, the distance of the first and the second peak is larger when plotting the response in the frequency domain. Then it is more optimum that the second peak (peak which has larger frequency value) has higher value than the first peak. This condition can be seen in the plot of the mechanical admittance in the Figure8.2.

The Figure8.2 is the result of the basic model and procedure in the Section5. The figure on the right is the squared value of the figure on the left which is the mechanical admittance or can be also called the power spectral density. This value is take into account the shape function of the wind load but without taking into account the frequency function. The frequency load which is used in this graph is a constant value of one. The full calculation of the dynamic wind load is done for the bending and torsional model to obtain the peak acceleration at the top corner of the building as that is the critical location. The acceleration plot for different mass ratio can be seen in the Figure8.5

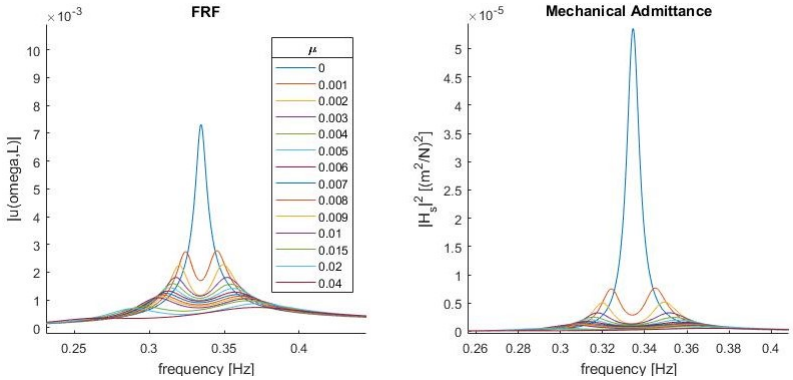

Figure 8.2: Mechaniccal Admittance: TMD Mass Parameter

The optimum value of the dashpot (C_t) is obtained through trial and error. The value from the trial and error can be plot as a graph to find C_t value for different TMD mass. The figure shows that the optimum value of Ct can be obtain trhough the second or third order polynomial function with an error less than 0.1%.

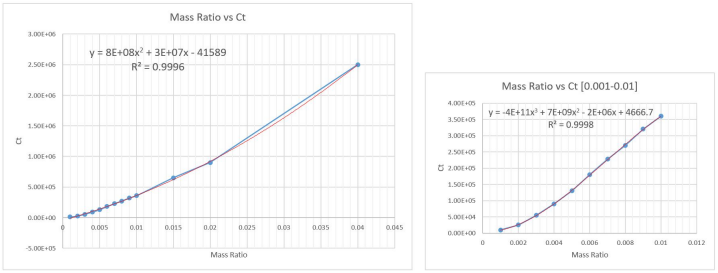

Figure 8.3: Optimum Ct for each Mass Ratio

Because the TMD is tuned to the bending natural frequency of the building, then the optimum C_t value is when the bending vibration (acceleration) is at the lowest value. Therefore it can be seen on the Figure8.4 that the bending plot is smooth while the torsion is not. The Figure8.4 shows that th effective mass ratio in the EPO building bending vibration is 0.003. Because after TMD mass is larger than 0.003 of the building mass, the influence of increasing the mass to reduce the acceleration is significantly drop.

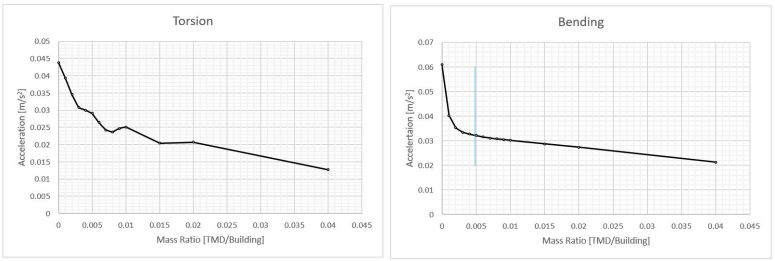

Figure 8.4: Acceleration for Bending and Torsion with different Mass Ratio

The bending combine with torsion acceleration at the top corner of the building which is represented by the model in Figure4.4 can be seen in the Figure8.5.

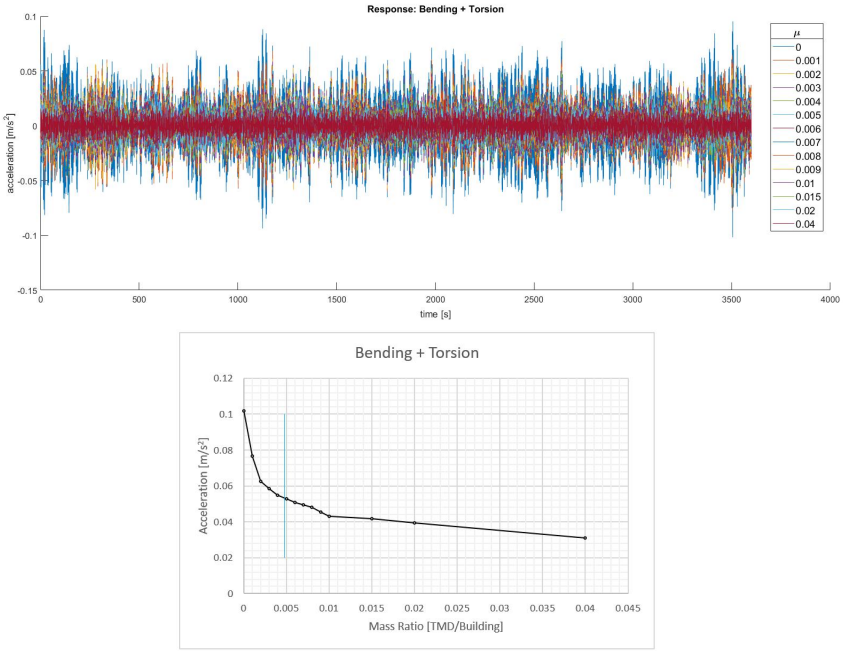

Figure 8.5: Acceleration for Building+Torsion with different Mass Ratio

The figure on the bottom represent the peak value from the top figure for each mass ratio. The vertical blue line on the bottom figure shows the mass ratio value of the EPO building ($\mu = 0.0048$). It can be concluded that the TMD design for the EPO building is effective since after 0.005 the increase of the TMD mass is not significant.

8.3. SOIL STRUCTURE INTERACTION

This chapter discuss how the soil structure interaction (SSI) properties change the sensitivity graph of the building and TMD properties. To understand the characteristics of the four SSI properties, the Figure8.6 shows the influence of the SSI damping on the damping ratio of the one dimensional model.

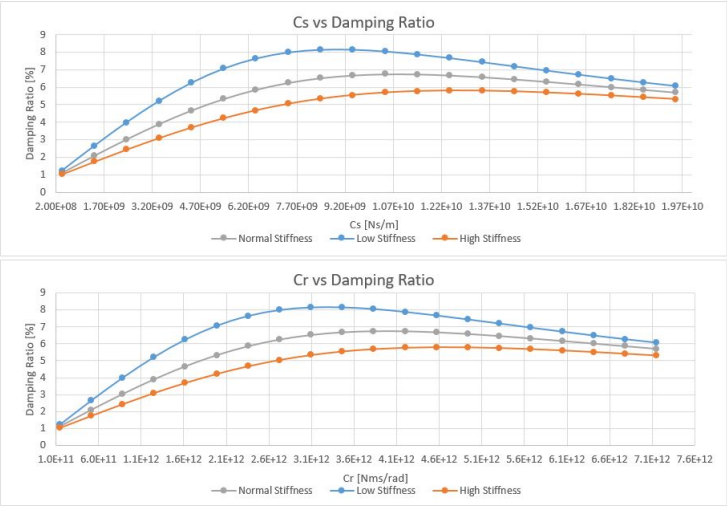

Figure 8.6: SSI Damping (Cs Cr) Influence on the Model Damping

The graph is obtain from the bending model only, with the Cs and Cr changed at the same time. So for example, the damping of 4% on the grey graph (normal stiffness Kr Ks Table4.3) is the result of the $Cs = 3.41 * 10^9$ and $Cr = 1.25 * 10^{12}$ together. With the same understanding of the dashpot characteristic as in Section3.3.2, a high value of dashpot means that the support becomes rigid. So there is an optimum value of the damping in SSI properties which gives a high damping ratio. This damping value can be changed also based on the foundation design, a rigid wall pile and soft ground can produce a larger damping ability [Konishi, 2011]. This topic needs further modeling and analysis to be done. But since there is corelation between foundation design and damping of the SSI, if the TMD is applied on the structure, low SSI is wanted for the better performance of the TMD (3.4).

The influence of the stiffness also affect the damping ratio of the total high rise building, a higher stiffness restrict the relative displacement at the base and therefore it limits the damping ability. Note that this stiffness is a value which represent the soil structure interaction so it takes into account both of the foundation and soil properties.

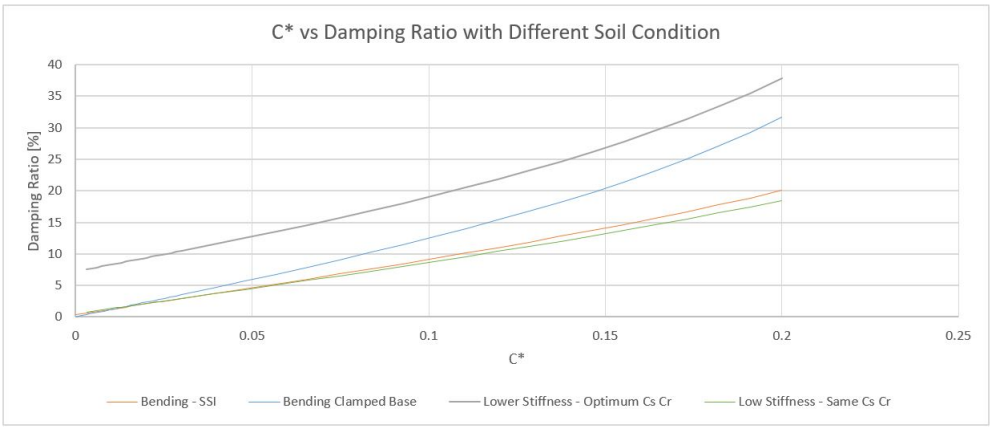

Figure 8.7: SSI damping influence in Building Damping Parameter

The relation between acceleration and damping ratio remain unchanged whether the damping ratio comes

from the SSI or C^* (building) properties. It is because what matter for the response is the area of the mechanical admittance, a 1% damping has the same mechanical admittance graph whether it comes from SSI or the building damping. But the damping from the SSI has an influence on the sensitivity of the building damping (C^*) which is shown in the Figure8.7.

It can be seen that on the contrary with the damping gain from the Cs and Cr, the building damping gives lower value with the decrease of the Kr and Ks (20% decrease (green line)). This is because the C^* gives more damping ability if the deformation difference along the beam is increase and lower base stiffness reduce the difference between internal deformation of the beam.

9

SLENDER HIGH RISE

9.1. STATIC WIND LOADING

The procedure to obtain the wind pressure on the building's facade is based on The Netherlands building code NEN-EN 1991-1-4 which is also according to Eurocode. This building code is only applicable for building height under 200 m, therefore an additional information for the wind pressure above 200 m is obtained through The Netherlands building code NTA4614-3. The input values in accordance with the NEN-EN 1991-1-4 can be seen in the Table9.1.

Wind Data Properties			
Basic wind velocity	v_b	27	m/s
Orography factor	c_o	1	
Minimum Height	z_{min}	10	m
Maximum Height	z_{max}	200	m
Roughness length	z_o	1	m
Roughness length terrain category II	$z_{o,\mathrm{II}}$	0.05	m
Reference height	z_t	200	m
Length scale	L_t	300	m
Turbulence factor	k_l	1	
Air Density	ρ_{air}	1.25	kg/m^3
Building height	h	270	m
Building width (in plane with wind load)	b	25.5	m
Building depth (out of plane with wind load)	d	25.5	m

Table 9.1: Basic Value for Wind Load

9.1.1. PEAK VELOCITY PRESSURE

The reference height (z_e) to calculate the velocity pressure for building with its height larger than twice its width can be seen in the Figure9.1. The procedure in the section below can be followed to calculate the peak velocity pressure.

MEAN WIND VELOCITY

The mean wind speed function over the height can be obtained through the equation below:

$$v_m(z) = c_r(z)\, c_o(z)\, v_b \tag{9.1}$$

where $c_r(z)$ is a roughness factor and k_r is a terrain factor which can be calculated as:

$$\begin{aligned} c_r(z) &= k_r\, ln\left(\frac{z}{z_o}\right) \\ k_r &= 0.19\left(\frac{z_o}{z_o, II}\right)^{0.07} \end{aligned} \tag{9.2}$$

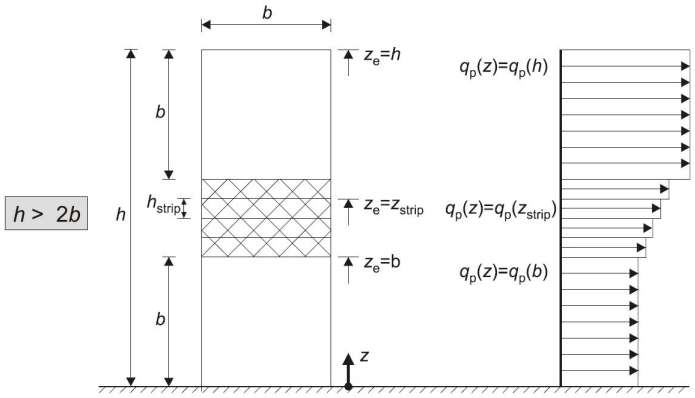

NOTE The velocity pressure should be assumed to be uniform over each horizontal strip considered.

Figure 9.1: Reference height and velocity pressure profile

WIND TURBULENCE

The turbulence intensity is defined as the standard deviation of the turbulence divided by the mean wind velocity.

$$I_v(z) = \frac{\sigma_v}{v_m(z)} \tag{9.3}$$

in which:

$$\sigma_v = k_r \; k_l \; v_b \tag{9.4}$$

PEAK VELOCITY PRESSURE

The peak velocity pressure can be written in the equation below:

$$q_p(z) = (1 + 7I_v(z)) \; \frac{1}{2} \; \rho \; v_m^2(z) \tag{9.5}$$

Based on the Figure9.1, the profile for the peak velocity pressure along the height of the building can be seen in the Figure9.2. In which the wind speed and turbulence intensity is a function of height and their values can be seen in the table (left side of the figure).

h	vm	Iv	qp
[m]	[m/s]		[kN/m2]
0			0.829603705
25.5	20.4907	0.30877	0.829603705
34.8125	22.4603	0.28169	0.936992081
44.125	23.9601	0.26406	1.022019163
53.4375	25.1716	0.25135	1.092756029
62.75	26.188	0.24159	1.153515405
72.0625	27.0634	0.23378	1.206886791
81.375	27.8324	0.22732	1.254552905
90.6875	28.5179	0.22186	1.297671826
100	29.1364	0.21715	1.337076159
109.313	29.6997	0.21303	1.373385467
118.625	30.217	0.20938	1.407073802
127.938	30.6951	0.20612	1.438512318
137.25	31.1397	0.20318	1.467997275
146.563	31.555	0.2005	1.495769082
155.875	31.9448	0.19806	1.522025619
165.188	32.3119	0.19581	1.546931789
174.5	32.6589	0.19373	1.570626523
174.5			1.630206468
200	33.5218	0.18874	1.630206468

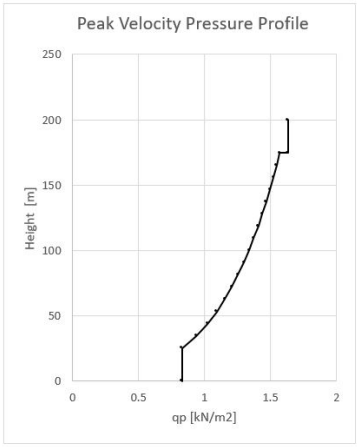

Figure 9.2: peak velocity pressure over height

9.1.2. WIND FORCES ON STRUCTURES

The wind forces for the building with $h/d > 5$ can be determined through the force coefficient as written in the equation below:

$$F_w(z) = c_s c_d \; c_f \; q_p(z_e) \; b \tag{9.6}$$

FORCE COEFFICIENT

The force coefficient for structural elements with rectangular sections can be calculated as:

$$c_f = c_{f,0}\,\psi_r\,\psi_\lambda \tag{9.7}$$

Where the $c_{f,0}$ is the force coefficient for rectangular section with sharp corners and without free-end flow. This value can be determined through Figure9.3. The slender high rise which is considered has the same width and depth. Therefore the value for the force coefficient can be taken as:

$$\begin{aligned} d/b &= 1 \\ c_{f,0} &= 2.1 \end{aligned} \tag{9.8}$$

The ψ_r and ψ_λ respectively are the reduction factor for section with rounded corner and the end-effect factor for elements with free-end flow. Because the building has a sharp corner and attach to the ground, the value for both factor can be taken as one. Then the force coefficient can be determined as:

$$c_f = 2.1 \tag{9.9}$$

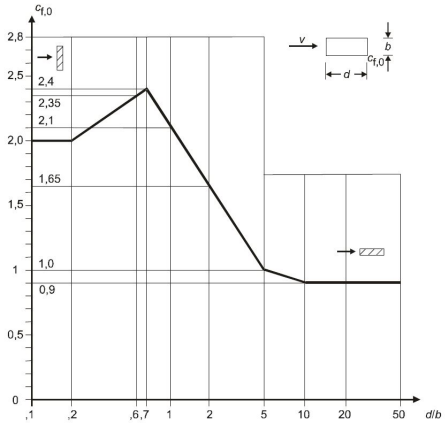

Figure 9.3: Force coefficient $c_{f,0}$

STRUCTURAL FACTOR

The structural factor can be separated into two elements, which are the size factor (c_s) and the dynamic factor (c_d). These factors take into account the fact that the peak of the wind pressure on a surface is not occur simultaneously. The formula for the structural factor can be seen in the equation below:

$$c_s c_d = \frac{1 + 2\,k_p\,I_v(z_s)\sqrt{B^2 + R^2}}{1 + 7\,I_v(z_s)} \tag{9.10}$$

z_s is the reference height and can be determined as:

$$\begin{aligned} z_s &= 0.6\,h \geqslant z_{min} \\ &= 120\ m \end{aligned} \tag{9.11}$$

Then the turbulence intensity at the reference height z_s can be calculated as:

$$I_v(z_s) = \frac{k_r * 1 * v_b}{k_r \ln\frac{z_s}{z_o} * 1 * v_b} = \frac{1}{\ln\frac{z_s}{z_o}} = 0.2088 \tag{9.12}$$

B^2 is the background factor which taking into account the fact that the wind pressure is not constantly distributed in a surface. This factor can be calculated as:

$$B^2 = \frac{1}{1 + 0.9\left(\frac{b+h}{L(z_s)}\right)^{0.63}} = 0.7193 \tag{9.13}$$

Where $L(z_s)$ is the turbulent length scale which can be calculated as:

$$\begin{aligned} L(z_s) &= L_t \left(\frac{z_s}{z_t}\right)^{\alpha} \quad \text{for} \quad z_s \geqslant z_{min} \\ L(z_s) &= 213.051\ m \\ \alpha &= 0.67 + 0.05\ \ln(z_o) = 0.67 \end{aligned} \tag{9.14}$$

R^2 is the resonance response factor which taking into account the resonance between the frequency of the fluctuating wind and the building's natural frequency. This factor can be calculated as:

$$R^2 = \frac{\pi^2}{2\,\delta}\, S_L\left(z_s, nf_1\right)\, R_h(\eta_h)\, R_b(\eta_b) \tag{9.15}$$

where $R_h\ R_b$ is the aerodynamic admittance and can be calculated as:

$$\begin{aligned} R_{h,b} &= \frac{1}{\eta_{h,b}} - \frac{1}{2\,\eta_{h,b}^2}\left(1 - e^{-2\,\eta_{h,b}^2}\right) \\ R_h R_b &= 0.19937 * 0.70852 = 0.14126 \end{aligned} \tag{9.16}$$

δ is the total logarithmic decrement of damping which can be calculated as summation for the logarithmic decrement of structural damping, aerodynamic damping and artificial damping. The aerodynamic damping can be neglected because according to the equation:

$$\delta_a = \frac{c_f \rho\, v_m(z_s)}{2 n_f \mu_e} \tag{9.17}$$

It produce a very small value because μ_e is the mass per unit area of the structure is relatively large (10^5) compared to the wind speed. The total logarithmic decrement for steel building without TMD can be calculated as:

$$\delta = \delta_s + \delta_a + \delta_d = 0.05 \tag{9.18}$$

S_L is the wind's power spectral density as a function of the non-dimensional frequency ($f_L(z_s, nf_1)$). This function is expressed by Solari as:

$$\begin{aligned} S_L(z_s, nf_1) &= \frac{6.8 f_L(z_s, nf_1)}{\left(1 + 10.2\ f_L(z_s, nf_1)\right)^{5/3}} = 0.119 \\ f_L(z_s, nf_1) &= \frac{nf_1\ L(z_s)}{v_m(z_s)} = 1.031 \\ nf_1 &= 0.14\ Hz \end{aligned} \tag{9.19}$$

The first natural frequency of the building (nf_1) is obtained through an iteration process. For a Euler-Bernoulli beam model with a clamped base, the first natural frequency can be calculated as:

$$nf_1 = \frac{3.52}{h^2}\sqrt{\frac{EI}{\rho A}} \tag{9.20}$$

The building height is a known constant and the mass is also known because the floor has the major contribution of the building mass. The first assumption is made for the building stiffness. As later the wind force is determined, a static calculation can be made to check whether the deformation of the building is exceeded the admissible deformation limit or not.

k_p is the peak factor which is the ratio of the maximum value of the fluctuation part of the building response to its standard deviation. This factor can be written as:

$$k_p = \sqrt{2\ln(\nu T)} + \frac{0.6}{\sqrt{2\ln(\nu T)}} = 3.123 \tag{9.21}$$

T is the averaging time for the mean wind velocity which can be taken as 600 seconds and ν is the up-crossing frequency which can be calculated as:

$$\nu = nf_1\sqrt{\frac{R^2}{B^2 + R^2}} = 0.1175 \tag{9.22}$$

Then all the inputs for the structural factor is calculated, then the value for the structural factor is:

$$c_s c_d = 1.157 \tag{9.23}$$

9.1.3. WIND FORCE

The wind force profile $F_w(z)$ based on Equation9.6 along the building height can be seen in the Figure9.4

h	qp	Fw
m	kN/m2	kN/m
0	0.8296	51.4114
25.5	0.8296	51.4114
34.8125	0.93699	58.0663
44.125	1.02202	63.3355
53.4375	1.09276	67.7192
62.75	1.15352	71.4845
72.0625	1.20689	74.792
81.375	1.25455	77.7459
90.6875	1.29767	80.418
100	1.33708	82.8599
109.313	1.37339	85.1101
118.625	1.40707	87.1978
127.938	1.43851	89.146
137.25	1.468	90.9732
146.563	1.49577	92.6943
155.875	1.52203	94.3214
165.188	1.54693	95.8649
174.5	1.57063	97.3333
174.5	1.63021	101.026
200	1.63021	101.026

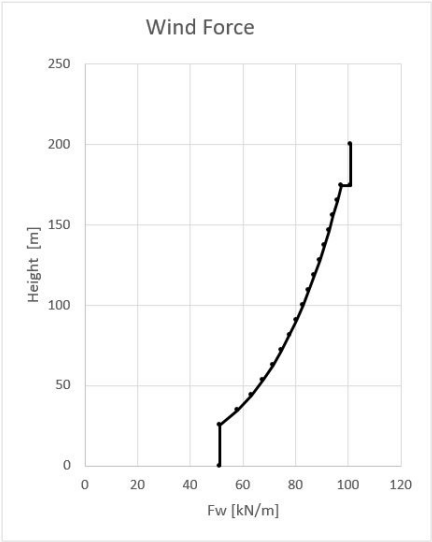

Figure 9.4: Force coefficient $c_{f,0}$

Because the building is above 200 m, the building code NTA4614 gives directly the wind pressure for building up to 300 m. The comparison between the wind pressure from NEN-EN1991 up to 200m and NTA4614 up to 270 m can be seen in middle figure of Figure9.5 below:

NTA4614	
h	Pressure
[m]	[kN/m2]
150	1.48
160	1.5
170	1.52
180	1.54
190	1.56
200	1.58
225	1.62
250	1.66
270	1.684

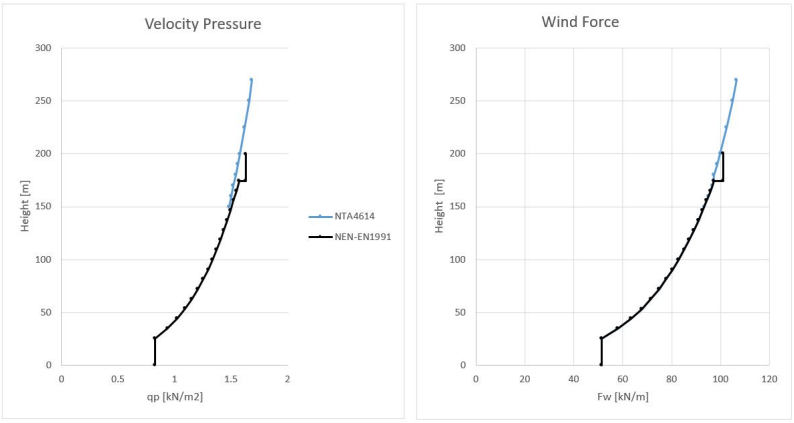

Figure 9.5: Wind Pressure Comparison

Then the wind pressure for the building up to 270 m can be obtained by modifying the value from NTA4614 to the wind pressure from the NEN-EN1991. The value for the wind force still use the same Equation9.6, which is basically some constants multiplied by the wind pressure and the building width. This wind force profile can be seen on the right figure on Figure9.5.

9.2. BUILDING PROPERTIES

There are five properties which is needed for the dynamic analysis of this slender high-rise building namely:

1. Building mass per unit height
2. Building stiffness
3. Building damping
4. Soil Structure Interaction
5. Dynamic wind load

9.2.1. BUILDING MASS

The total building mass can be calculated as the total mass from the structural elements, and the imposed load which is the contribution of non-structural elements. The dimension of the structural element can be seen on the floor-plan in the Figure9.6.

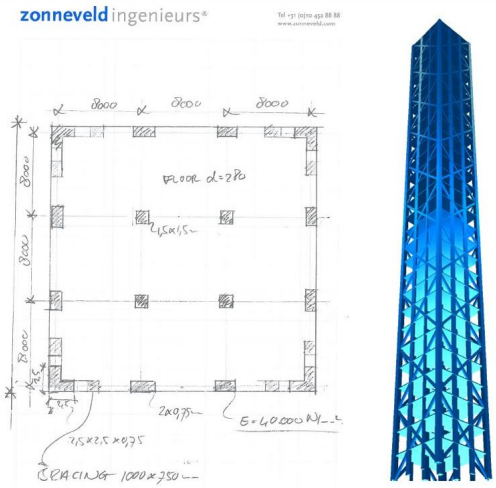

Figure 9.6: High-rise Floor plan and Structure

Then the total structural volume can be calculated as:

Total Volume Column	$=(8*(2*0.75)+4*(1.5*1.5)+$
	$4*(2.5*0.75+0.75*(2.5-0.75)))*270$
	$=9112.5\ m^3$
Total Volume Floor	$=((25.5*25.5)-33.75)*0.28*90=15535.8\ m^3$
Total Volume Bracing	$=(1*0.75)*25.632*240=4613.76\ m^3$
Total Volume	$=29262.06\ m^3$

The imposed load for an office building is $3.5kN/m^2$ for an office building. The mass per unit height can be calculated as:

$$\begin{aligned}\rho A &= \frac{29262.06\ m^3 * 2400\ kg/m^3}{270m} + \frac{616.5*90*3.5*101.94}{270} \\ &= 3.33\times10^5 kg/m\end{aligned} \tag{9.24}$$

9.2.2. BUILDING STIFFNESS

The building stiffness is obtained through the static calculation. The model for this calculation is a bending beam which can be seen in Figure9.7.

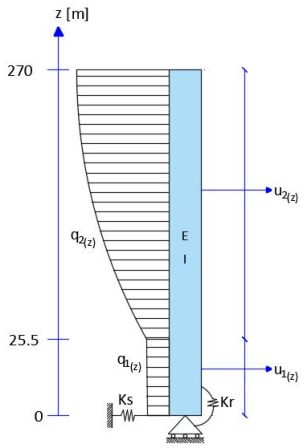

Figure 9.7: Bending Beam Model

in which:

$$q_{2(z)} = a\,z^6 + b\,z^5 + c\,z^4 + d\,z^3 + e\,z^2 + f\,z + g$$

$$\begin{bmatrix} a \\ b \\ c \\ d \\ e \\ f \\ g \end{bmatrix} = \begin{bmatrix} -2.415 \times 10^{-12} \\ 2.33 \times 10^{-9} \\ -8.99 \times 10^{-7} \\ 1.79 \times 10^{-4} \\ -2.05 \times 10^{-2} \\ 1.568 \\ 23.803 \end{bmatrix} \tag{9.25}$$

The detailed procedure to derive the response for this model is shown in the AppendixB.3. The deformation on the top of the building can be written according to the EquationB.43 which is:

$$\begin{aligned} u_{2(L)} = \frac{1}{EI}\Bigg(&\frac{aL^{10}}{5040} + \frac{bL^9}{3024} + \frac{cL^8}{1680} + \frac{dL^7}{840} + \frac{eL^6}{360} + \frac{fL^5}{120} + \frac{1}{24}gL^4 - \frac{L}{2520}\Big(60\,aL^6 + 70\,bL^5 + 84 \\ &cL^4 + 105\,dL^3 + 140\,eL^2 + 210\,fL + 420\,g\Big)L^3 + \frac{L^2}{1680}\Big(105\,aL^6 + 120\,bL^5 + 140\,cL^4 + \\ &168\,dL^3 + 210\,eL^2 + 280\,fL + 420\,g\Big)L^2 + \frac{1}{5040\,K_r}\Big(-280\,K_r\,L1^9\,a + 630\,EI\,L^8\,a - 630 \\ &EI\,L1^8\,a - 315\,K_r\,L1^8\,b + 720\,EI\,L^7\,b - 720\,EI\,L1^7\,b - 360\,K_r\,L1^7\,c + 840\,EI\,L^6\,c - 840\,EI \\ &L1^6\,c - 420\,K_r\,L1^6\,d + 1008\,EI\,L^5\,d - 1008\,EI\,L1^5\,d - 504\,K_r\,L1^5\,e + 1260\,EI\,L^4\,e - 1260 \\ &EI\,L1^4\,e - 630\,K_r\,L1^4\,f + 1680\,EI\,L^3\,f - 1680\,EI\,L1^3\,f - 840\,K_r\,L1^3\,g + 840\,K_r\,L1^3\,q1 + \\ &2520\,EI\,L^2\,g - 2520\,EI\,L1^2\,g + 2520\,EI\,L1^2\,q1\Big)L + \frac{1}{15120\,K_s}\Big(252\,K_s\,L1^{10}\,a + 280\,K_s\,L1^9\,b \\ &+ 315\,K_s\,L1^8\,c + 2160\,EI\,L^7\,a - 2160\,EI\,L1^7\,a + 360\,K_s\,L1^7\,d + 2520\,EI\,L^6\,b - 2520\,EI\,L1^6 \\ &b + 420\,K_s\,L1^6\,e + 3024\,EI\,L^5\,c - 3024\,EI\,L1^5\,c + 504\,K_s\,L1^5\,f + 3780\,EI\,L^4\,d - 3780\,EI\,L1^4 \\ &d + 630\,K_s\,L1^4\,g - 630\,K_s\,L1^4\,q1 + 5040\,EI\,L^3\,e - 5040\,EI\,L1^3\,e + 7560\,EI\,L^2\,f - 7560 \\ &EI\,L1^2\,f + 15120\,EI\,Lg - 15120\,EI\,L1\,g + 15120\,EI\,L1\,q1\Big)\Bigg) \end{aligned} \tag{9.26}$$

The deformation limit for the building is requested to be 570 mm. To achieve this limit, EquationB.43 can be used with z equal to L (deformation at the top of the building). The soil structure interaction is assumed to be rigid in this case, this can be done by substituting a very high number (10^{100}) to K_r and K_s.Then after all the known constants is input, EquationB.43 becomes:

$$\frac{6.73\times10^{10}+9.65\times10^{-92}EI}{EI}=0.57$$
$$EI=1.18\times10^{11}N/m^2 \tag{9.27}$$

9.3. DYNAMIC ANALYSIS

After the building properties is obtained through the static calculation, the dynamic analysis with the same procedure as in Chapter5 is performed. But there are some differences in comparison to the EPO building case, these differences is explained in detail in the following sections. The model for the slender high rise building can be seen in Figure9.8 where $L_1 = 25.5\ m$.

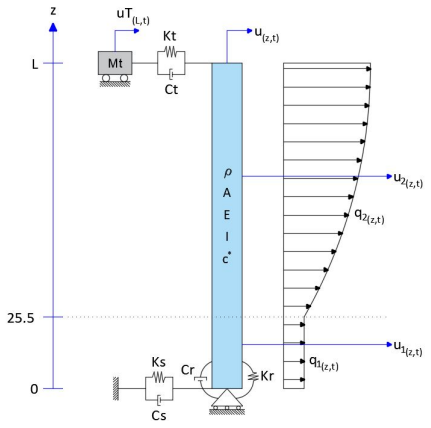

Figure 9.8: One Dimensional Model for High Rise Building

The soil structure interaction (SSI) is assumed to be rigid with small damping effect (clamped base), therefore the value of the SSI parameters can be written as:

SSI Parameter		
Ks	$1*10^{100}$	N/m
Kr	$1*10^{100}$	Nm/rad
Cs	0	Ns/m
Cr	0	Nms/rad

Table 9.2: SSI Properties for One Dimensional Model

9.3.1. DYNAMIC WIND LOAD

Because the wind tunnel test is not performed for this slender high rise, the shape function for the wind load is obtained through the assumption based on Eurocode. The assumption is the wind load follows a function of natural logarithm through the height which can be written as:

$$\begin{aligned} \text{for } 0\leqslant z\leqslant L_1 \quad &: \quad f_{1_{(z)}}=\ln b/z_o \\ \text{for } L_1\leqslant z\leqslant h \quad &: \quad f_{2_{(z)}}=\ln z/z_o \end{aligned} \tag{9.28}$$

Equation9.28 can be plot along the building height as it is shown in Figure9.9 below:

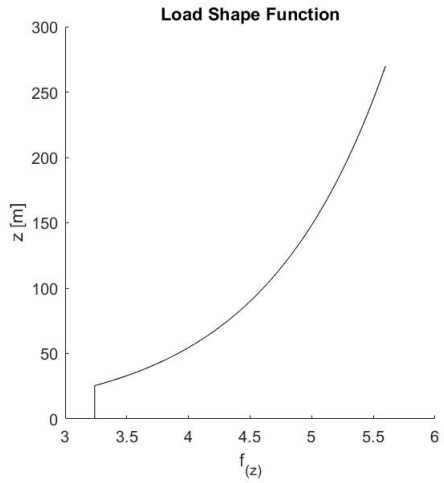

Figure 9.9: Load Shape Function

This change of the load shape function ($f_{(z)}$) influence the mechanical admittance (H_s) because it changes the coefficients of the particular solution in the section A.4.1 AppendixA. The shape function consist of two part, the constant part and the second part which follows the function of natural logarithm. To make it easier for finding the particular solution, the function in the second part can be approximate by the sixth order polynomial equation which is:

$$f_{2_{(z)}} = az^6 + bz^5 + cz^4 + dz^3 + ez^2 + fz + g \tag{9.29}$$

The particular solution for the exponential function is the same sixth order polynomial equation as shown in EquationA.62. The difference is located on the value of the coefficients which now can be determined as:

$$\begin{aligned} a &= -6.47 \times 10^{-14} & e &= -7.90 \times 10^{-4} \\ b &= 6.63 \times 10^{-11} & f &= 6.53 \times 10^{-2} \\ c &= -2.77 \times 10^{-8} & g &= 2.007 \\ d &= 6.14 \times 10^{-6} \end{aligned}$$

Then with the same procedure as Chapter5 the top acceleration for this slender high-rise building can be seen in Figure9.10. The peak acceleration can be written as:

without TMD = 0.1889 m/s^2
with TMD = 0.0919 m/s^2
Effectiveness of TMD = 51.35%

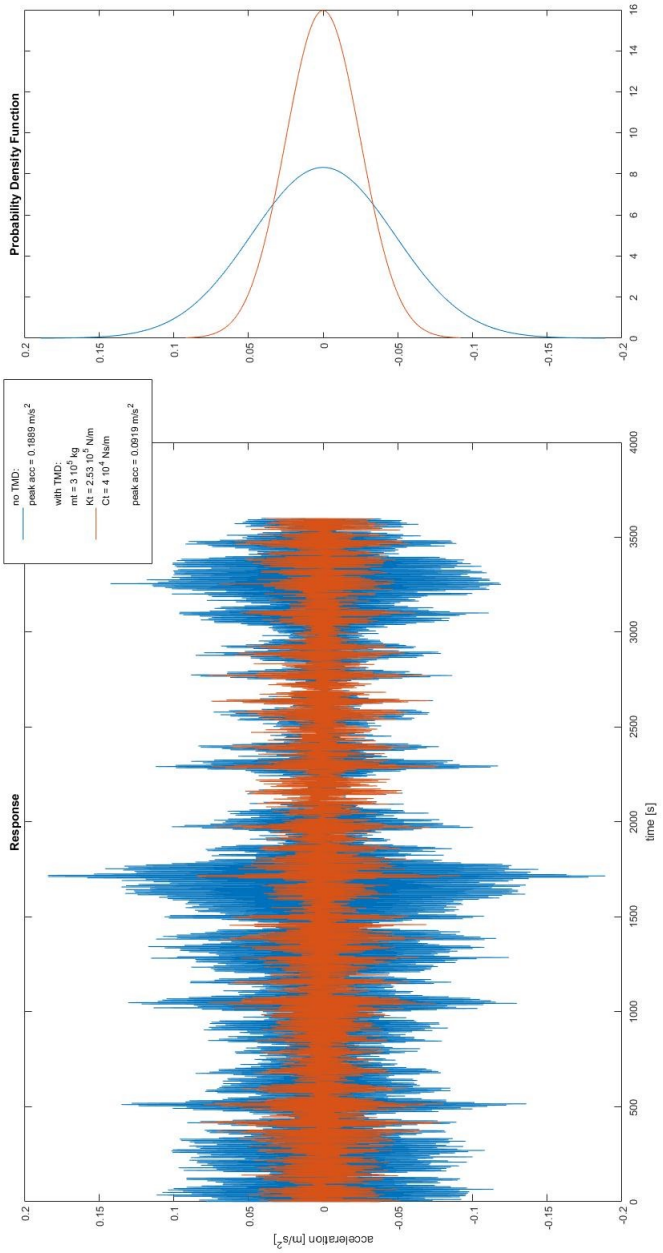

Figure 9.10: Top Acceleration

10

CONCLUSION

There is numerous way to reduce the acceleration of the building. The damping can be enhanced by damping devices such as a viscous damper, magnetic damper, frictional damper and metallic yield device[9]. Also, the controlled force can be applied to the structure by devices such as active tendon system and active brace system. While the damping devices have a limited energy dissipation which is related to the material, also the active devices have a limitation because it depends on the power source. The advantages of the application of TMD in reducing structural vibration is that it resonates with the same frequency as the structure but on the opposite direction of the structure in which the energy of the building can be transfer to the mass of TMD which can absorb more energy than the damping devices.

The analytical model gives a higher effectiveness of the TMD compared to the finite element program. The difference is the analytical model only consider one direction of stress distribution while the finite element program can consider in 3 dimensions. Also, the properties of the building and soil need to be estimated in this analytical model, the stiffness and mass considered to be homogeneous along the height. The SSI modeled as a single spring and dashpot while in the finite element program there is a correlation between the piles and the flexibility of the concrete plate in the bottom. But the drawback is the most influence on the torsional model of the building. The building does not have a straight line along the width in the acceleration response. An approximation is made by lowering the torsional stiffness of the torsional bar which results in the same peak acceleration on the building, but the value along the building width cannot represent the acceleration response as in the finite element program.

The model of damping in this thesis uses the Kelvin-Voigt model which can give a damping ratio that depends on the frequency. This damping is a material damping model which it can be seen in the equation that the material properties of modulus elasticity (E) contributes to the damping. This model is not a complete representation of the damping in the building because damping can also come from the structural joint which behaves as a friction damping[1]. In the analysis of the building properties, this model gives a linear correlation to the increase of the inertia. The increase of the inertia of the building influence directly the damping properties of the system.

Application of TMD in Building

The performance of the TMD is dependent on the value of its mass, and the stiffness and damping are tuned so that the mass can give its optimum performance. The higher the ratio of the mass between the TMD and the building, the higher the effectiveness of the TMD (Figure8.5).

The effectiveness of TMD can be influenced by the damping of the building. The effect of damping ratio on the acceleration is sensitive in the lower damping ratio value (8.1). This characteristic creates a condition that the TMD (and also any damping devices) can reduce the damping of the building drastically when the building has low damping ratio. Therefore in the sense of material, a material with low damping such as steel is preferred than concrete in the application of TMD.

Damping of the building can be increased by soil structure interaction also reduce the effectiveness of TMD. The parameter in the SSI is frequency dependent. Therefore the building's natural frequency influences the damping obtained by the SSI. In the EPO Building case, lower frequency gives an optimum value for the dashpot (Figure8.6), but it also provides a high stiffness which reduces the damping ratio of the total system.

Therefore a building with a low natural frequency is preferable in the TMD application and the slender high rise is a preferred case because it has a low frequency. To predict the performance accurately in the design phase, an accurate prediction of the damping, which may come from different sources in the building, should be developed.

Types of TMD

The different types of the TMD which contribute to the different response of the building such as displacement, rotation, and curvature is modeled. The most effective way to reduce the acceleration is the translational TMD which contribute to the displacement in the horizontal direction. It can understand that to give the same displacement in the static beam model; a horizontal force needs lower value than the bending moment. The rotational TMD can have the same performance with translational TMD but with a tremendous moment arm which is almost equal to the building height. This model is challenging to construct because the structure for the arm should be stiff enough to transfer the rotation to the rotational spring and dashpot at the top of the building.If the TMD mas the same total amount of mass regardless its quantities, then the quantities do not influence in reducing the top peak acceleration on the building because the total energy transferred to the mass is the same since it has the same total value of mass. The mass of the TMD can be anything; some buildings use storage tank as the TMD. A nonstructural element may also be used as a mass, in this thesis, the idea comes from the Tokyo Sky tree which uses the emergency shaft as a TMD. This system is beneficial because the concrete shaft has a large mass. Therefore, it can be effective to reduce the acceleration. We do not need to buy or place a new mass such as a block of steel in the building if we use a part of the building such as emergency exit as the TMD. But further investigation about the safety of the people in emergency situation should be evaluated more.

Cost Analysis

TMD is more cost efficient when reducing the acceleration than increasing the dimension of the steel. But not every building case need to reduce the acceleration as much as when TMD is applied such as the EPO building. The design process often determines the stiffness to require the deformation limit first then check the acceleration. A building which has a low acceleration ($\pm 0.02 m/s^2$ the acceleration limit Figure2.2) when using the value of this stiffness (stiffness which require deformation limit h/500) is not suitable for TMD application. It is the case because the acceleration can be reduced by increasing the dimension of the profiles.

11

REMAINING CHALLENGES

Besides the result and conclution for the study of the TMD in this thesis, there are limitation as a result of the assumption or the important aspect which has not been studied. Some recomendations and remaining challenge which is important to be studied is mention in this chapter.

1. This thesis is only consider a building acceleration due to wind load. A different loading type such as earthquake is a very important aspect to be studied.
   (a) The loading characteristic has a longer period than the wind which may excite multiple mode of the building. This condition give an opportunities to the other type of the TMD because the shape of the higher mode than the first has another maximum position of the displacement.
   (b) The passive TMD system has a limitation not be able to tuned to multiple frequency, and also need a certain time to activate. This aspect is more significant in the case of earthquake. Earthquake has a limited duration of time and a quick TMD response might has a significant influence of the response. Enhance of TMD system such as hybrid, semi-active, and active is also benefitial to tuned the TMD to multiple frequency.
   (c) While the vibration of the wind is influence the serviceability limit (acceleration), the earthquake loading is a natural disaster which correlated to the safety (ultimate limit state) such as building collapse. This gives a very different perspective and analysis. Because the a big earthquake has a long return period, civil engineer usually does not design the building to be elastic because it is too costly (depend on the function of the building), therefore non linearity due to the elastoplastic of the structure may has great influence and challenging to be studied.
2. The 2 dimensional model for the torsional vibration need to be developed. The torsional model gives a drawback in predict the acceleration along the width of the building. The stiffness of the torsion is also cannot be predict through the static analysis which gives a limitation in study the torsional behavior and effect of TMD in reducing torsional behavior.
3. Variation of building cases need to be studied in order to understand an important point which is not present in the case in EPO building. The building has a unique torsional characteristic but the effect of SSI is not play a significant role in this case. A deeper study about the model of the SSI and the design of the foundation of different type of soil data related to the building acceleration, damping, and the effect of TMD application is important to be studied.
4. There are numerous devices which may be beneficial to reduce the acceleration. A study about the damping devices and active control device is important to compare the best solution to reduce building vibration and response. A cost analysis and the preferred building case for each of the device is important parameter in this study.
5. It is still a challenge to design a new type of TMD which has more effective than the conventional TMD. The fact that the TMD depend on the value of the mass is very limiting. A detailed creative design

regarding the uses of the space of the TMD is also present in building industry and also a challenge. A creative use of the active force in the TMD, or more advance technology such as artificial intelligent might be the key to the future design of TMD.

A

MECHANICAL ADMITTANCE

A.1. EULER-BERNOULLI BEAM

The high rise building with single TMD on top of the building is modeled as a one dimensional model which can be seen in the figure 5.4 below. The TMD is connected through a spring and dashpot to the building and the building is modeled as a Euler-Bernoulli beam model.

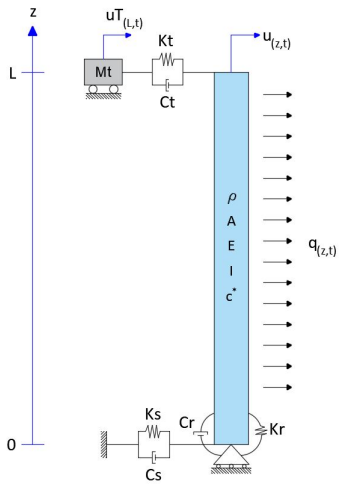

Figure A.1: Model 1: Single TMD

A.1.1. EQUATION OF MOTION

The high rise building is modeled as an Euler-Bernoulli beam, therefore the equation of motion of the system is:

$$\rho A \frac{\partial^2}{\partial t^2} u_{(z,t)} + \frac{\partial^2}{\partial z^2}\left(EI\left(1 + c^* \frac{\partial}{\partial t}\right)\frac{\partial^2}{\partial z^2} u_{(z,t)}\right) = q_{(z,t)} \tag{A.1}$$

To solve the partial differential equation (PDE) in equation of motion, Fourier Transfer is used. The reason to choose Fourier Transform is it can simplified the equation to ordinary differential equation (ODE) and there are a lot of information which can be obtain in the frequency domain. But there are condition which should be satisfied due to the assumption in the theory of Fourier Transform. FT can't handle initial conditions but since the excitation due to initial condition is not relevant in this situation, then this condition is satisfied. The system is limited to a linear system due to the application of superposition. The equation A.1 becomes:

$$-\omega^2 \rho A \tilde{u}_{(z,\omega)} + EI^* \frac{\partial^4}{\partial z^4} \tilde{u}_{(z,\omega)} = \tilde{q}_{(z,\omega)} \tag{A.2}$$

In which:

$$\begin{aligned} EI^* &= EI\left(1+i\omega c^*\right) \\ \tilde{u}_{(z,\omega)} &= \int_{-\infty}^{\infty} u_{(z,t)} e^{-i\omega t}\, dt \\ \tilde{q}_{(z,\omega)} &= \int_{-\infty}^{\infty} q_{(z,t)} e^{-i\omega t}\, dt \end{aligned} \tag{A.3}$$

For the TMD, the equation of motion can be seen in the equation below:

$$-\omega^2 m_t \tilde{u}_{t(\omega)} + (i\omega C_t + K_t)(\tilde{u}_{t(\omega)} - \tilde{u}_{(L,\omega)}) = 0 \tag{A.4}$$

From this equation, the expression of $\tilde{u}_t$ can be derived such as:

$$\tilde{u}_{t(\omega)} = \frac{i\omega C_t + K_t}{-\omega^2 m_t + i\omega C_t + K_t} \tilde{u}_{(L,\omega)} \tag{A.5}$$

HOMOGENEOUS EQUATION

The equation of motion can be separated to a homogeneous equation and a particular solution while the summation of both is the total solution. The homogeneous equation of the EOM can be written as:

$$\frac{\partial^4}{\partial z^4} \tilde{u}_{(z,\omega)} - \beta \tilde{u}_{(z,\omega)} = 0 \tag{A.6}$$

In which:

$$\beta = \left(\frac{\omega^2 \rho A}{EI^*}\right)^{1/4} \tag{A.7}$$

The general solution for this homogeneous linear differential equation is:

$$\tilde{u}_{(z,\omega)} = \sum_{i=1}^{4} C_i e^{\lambda_i z} \tag{A.8}$$

Substituting this form of solution to the homogeneous equatiokn resulting:

$$\sum_{i=1}^{4} C_i (\lambda_i^4 - \beta^4) e^{\lambda_i z} = 0 \tag{A.9}$$

We would like to find the non-trivial solution of this equation which are:

$$\begin{aligned} \lambda^4 &= \beta^4 \\ \lambda_{a,b}^2 &= \pm\beta^2 \\ \lambda_{1,2} &= \pm\beta \\ \lambda_{3,4} &= \pm i\beta \end{aligned} \tag{A.10}$$

Substituting these value back to the general solution resulting:

$$\tilde{u}_{(z,\omega)} = C_1 e^{\beta z} + C_2 e^{-\beta z} + C_3 e^{i\beta z} + C_4 e^{-i\beta z} \tag{A.11}$$

Because we know that the response (deformation) is a real value, we can write the solution in real value form using Euler formula which is:

$$\tilde{u}_{(z,\omega)} = A\cosh(\beta z) + B\sinh(\beta z) + C\cos(\beta z) + D\sin(\beta z) \tag{A.12}$$

PARTICULAR SOLUTION

The particular solution is related to the loading on the system. The loading on the high rise building which is considered in this thesis is the wind loading. The wind loading have a function of time (frequency) and space which can be separated as written in the equation below:

$$q_{(z,\omega)} = f_{(\omega)} f_{(z)} \tag{A.13}$$

The value of the wind load is not constant over height and it can be obtained from the wind speed. The shape function ($f_{(z)}$)of the wind pressure from the wind tunnel test can be seen in the the Figure5.2 and Figure5.3. The load shape function can be seen in Equation5.5, then the particular solution can also be found on the same form as the load therefore it can be written that the solution is:

$$\tilde{u}_{particular} = A_p z^6 + B_p z^5 + C_p z^4 + D_p z^3 + E_p z^2 + F_p z + G_p \tag{A.14}$$

Substitute the particular solution to the EOM resulting:

$$\begin{aligned} EI^*\left(360A_p z^2 + 120B_p z + 24C_p\right) - \omega^2 \rho A\left(A_p z^6 + B_p z^5 + C_p z^4 + D_p z^3 + E_p z^2 + F_p z + G_p\right) \\ = az^6 + bz^5 + cz^4 + dz^3 + ez^2 + fz + g \end{aligned} \tag{A.15}$$

The value of the constants can be derrived from this equation which are:

$$\begin{aligned} A_p = \frac{-a}{\omega^2 \rho A}\,;\, B_p = \frac{-b}{\omega^2 \rho A}\,;\, C_p = \frac{-c}{\omega^2 \rho A}\,;\, D_p = \frac{-d}{\omega^2 \rho A}\,;\, E_p = \frac{360EI^* A_p - e}{\omega^2 \rho A} \\ F_p = \frac{120EI^* B_p - f}{\omega^2 \rho A}\,;\, G_p = \frac{24EI^* C_p - g}{\omega^2 \rho A} \end{aligned} \tag{A.16}$$

Then the total solution for the bending vibration can be written as:

$$\begin{aligned} \tilde{u}_{(z,\omega)} = A\cosh(\beta z) + B\sinh(\beta z) + C\cos(\beta z) + D\sin(\beta z) \\ + A_p z^6 + B_p z^5 + C_p z^4 + D_p z^3 + E_p z^2 + F_p z + G_p \end{aligned} \tag{A.17}$$

A.1.2. BOUNDARY CONDITIONS

To find the value of the coefficient (A, B, C, D), the boundary conditions are used. The number of the conditions should satisfied the number of the unknowns. In this case there are 4 dynamic boundary conditions which are:

BC1-Shear Force:

$$EI^* \frac{\partial^3}{\partial z^3} \tilde{u}_{(z,\omega)}\Big|_{z=0} + (i\omega C_s + K_s)\tilde{u}_{(z,\omega)}\big|_{z=0} = 0 \tag{A.18}$$

BC2-Bending Moment:

$$EI^* \frac{\partial^2}{\partial z^2} \tilde{u}_{(z,\omega)}\Big|_{z=0} - (i\omega C_r + K_r)\frac{\partial}{\partial z}\tilde{u}_{(z,\omega)}\Big|_{z=0} = 0 \tag{A.19}$$

BC3-Shear Force:

$$EI^* \frac{\partial^3}{\partial z^3} \tilde{u}_{(z,\omega)}\Big|_{z=L} - (i\omega C_t + K_t)\left(\tilde{u}_{(z,\omega)} - \tilde{u}_{t_{(\omega)}}\right)\big|_{z=L} = 0 \tag{A.20}$$

BC4-Bending Moment:

$$EI^* \frac{\partial^2}{\partial z^2} \tilde{u}_{(z,\omega)}\Big|_{z=L} = 0 \tag{A.21}$$

The expression of $\tilde{u}_{t(\omega)}$ can be substituted to the beam motion $\tilde{u}_{(L,\omega)}$ from the equation A.5. To obtain the response ($\tilde{u}_{(z,\omega)}$), there are 4 unknowns [A, B, C, and D] need to be obtained. Therefore the 4 boundary conditions is used to obtain the unknowns. After substituting the expression of $\tilde{u}$ in equation A.12 to the boundary condition, the 4 equations can be put in matrix form:

$$\underline{\underline{K_D}} * \underline{C} = \underline{F} \tag{A.22}$$

Matrix K_D is called the dynamic stiffness matrix which can be seen in the equation A.23. Vector $\underline{C}$ consist of the coefficient [A, B, C, and D], and vector F is the value which does not contain any coefficient [A, B, C, D] in the boundary condition equation.

$$\underline{\underline{K_D}} = \begin{bmatrix} Ks + i\omega Cs & \beta^3 EI^* & Ks + i\omega Cs & -\beta^3 EI^* \\ EI^*\beta^2 & -(Kr + i\omega Cr)\beta & -EI^*\beta^2 & -(Kr + i\omega Cr)\beta \\ \gamma\cosh(\beta L) + EI^*\beta^3\sinh(\beta L) & \gamma\sinh(\beta L) + EI^*\beta^3\cosh(\beta L) & \gamma\cos(\beta L) + EI^*\beta^3\sin(\beta L) & \gamma\sin(\beta L) - EI^*\beta^3\cos(\beta L) \\ EI^*\beta^2\cosh(\beta L) & EI^*\beta^2\sinh(\beta L) & -EI^*\beta^2\cos(\beta L) & -EI^*\beta^2\sin(\beta L) \end{bmatrix} \tag{A.23}$$

In which:

$$\gamma = (i\omega C_t + K_t)\left(\frac{i\omega C_t + K_t}{-\omega^2 m_t + i\omega C_t + K_t} - 1\right) \tag{A.24}$$

$$\underline{F} = \begin{bmatrix} -6\,Dp\,EI\_star - (Ks + i\,\omega\,Cs)\,Gp \\ -2\,EI\_star\,Ep - (-Kr - i\,\omega\,Cr)\,Fp \\ -\left(\gamma L^6 + 120\,EI\_star\,L^3\right)Ap - \left(\gamma L^5 + 60\,EI\_star\,L^2\right)Bp - \left(\gamma L^4 + 24\,EI\_star\,L\right)Cp - \left(\gamma L^3 + 6\,EI\_star\right)Dp - \gamma L^2 Ep - \gamma LFp - \gamma Gp \\ -30\,L^4\,EI\_star\,Ap - 20\,EI\_star\,L^3\,Bp - 12\,EI\_star\,L^2\,Cp - 6\,EI\_star\,LDp - 2\,EI\_star\,Ep \end{bmatrix} \tag{A.25}$$

Then the coefficient vector $\underline{C}$ can be solved by:

$$\underline{C} = \underline{\underline{K_D}}^{-1}\underline{F} \tag{A.26}$$

The coefficients substitute again to equation A.12 to obtain the response in frequency domain. In order to get the acceleration of the building the equation below is used:

$$\text{acceleration} = \omega^2 \tilde{u}_{(z,\omega)} \tag{A.27}$$

A.2. MODEL FOR DAMPING IDENTIFICATION

The procedure to identify the damping is to apply a hammer test on the structure. In an analytical model such as one dimensional model, the hammer test is represent by a point load which has a very high force in a very short time. In the frequency domain, this load is a constant load of 1N over the frequency which also called the white noise spectrum. This model can be seen in the FigureA.2.

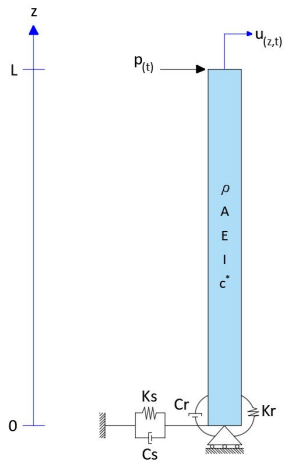

Figure A.2: Model 1: Damping Identification

The equation of motion of the model is the same as the previous model in section A.1, the only change is that the boundary condition of the TMD is change to a point load. This boundary condition at the top of the model can be seen in the equation below: **BC3-Shear Force:**

$$EI^* \frac{\partial^3}{\partial z^3}\tilde{u}_{(z,\omega)}\bigg|_{z=L} + P_{(\omega)} = 0 \tag{A.28}$$

A.3. TORSIONAL BAR

The torsional motion of the building is modeled as a torsional bar which can be seen in the FigureA.3. The TMD is also absorb the vibration in torsional degree of freedom. The TMD gives a torque which is equal to the horizontal force multiplied by the arm from the torsional center rotation (middle of the width).

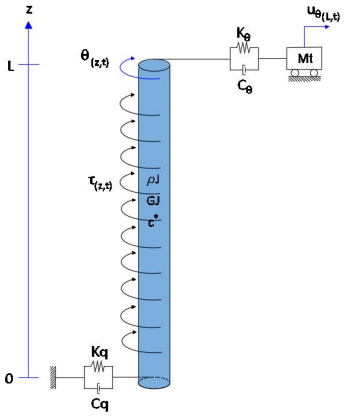

Figure A.3: Model 1: Torsional Bar Model

A.3.1. EQUATION OF MOTION

The equation of motion of a torsional bar can be seen in the figure below:

$$\begin{aligned} \rho J \frac{\partial^2}{\partial t^2}\theta_{(z,t)} - \frac{\partial}{\partial z}\left(GJ\left(1 + c_\theta^* \frac{\partial}{\partial t}\right)\frac{\partial}{\partial z}\theta_{(z,t)}\right) &= \tau_{(z,t)} \\ -\omega^2 \rho J \tilde{\theta}_{(z,\omega)} - \frac{\partial}{\partial z}\left(GJ\left(1 + i\omega c_\theta^*\right)\frac{\partial}{\partial z}\tilde{\theta}_{(z,\omega)}\right) &= \tilde{\tau}_{(z,t)} \end{aligned} \tag{A.29}$$

The equation of motion of the TMD in torsional degree of freedom is:

$$\begin{aligned} J_\theta \frac{\partial^2}{\partial t^2}\theta_{t_{(t)}} + C_\theta \frac{\partial}{\partial t}\left(\theta_{t_{(t)}} - \theta_{(z,t)}\right) + K_\theta\left(\theta_{t_{(t)}} - \theta_{(z,t)}\right) &= 0 \\ \left(-\omega^2 J_\theta + i\omega C_\theta + K_\theta\right)\tilde{\theta}_{t_{(\omega)}} &= \left(i\omega C_\theta + K_\theta\right)\tilde{\theta}_{(z,\omega)} \\ \tilde{\theta}_{t_{(\omega)}} &= \frac{i\omega C_\theta + K_\theta}{\left(-\omega^2 J_\theta + i\omega C_\theta + K_\theta\right)}\tilde{\theta}_{(z,\omega)} \end{aligned} \tag{A.30}$$

The solution for the equation of motion can be separated into two components which is the solution for the homogeneous part and the particular solution.

HOMOGENEOUS EQUATION

The homogeneous equation of the equation of motion can be written as:

$$\begin{aligned} -\omega^2 \rho J \tilde{\theta}_{(z,\omega)} - \frac{\partial^2}{\partial z^2}\left(GJ\left(1 + i\omega c_\theta^*\right)\tilde{\theta}_{(z,\omega)}\right) &= 0 \\ -\left(\frac{\omega^2 \rho J}{GJ^*}\right)\tilde{\theta}_{(z,\omega)} - \frac{\partial^2}{\partial z^2}\tilde{\theta}_{(z,\omega)} &= 0 \\ \frac{\partial^2}{\partial z^2}\tilde{\theta}_{(z,\omega)} + \alpha^2 \tilde{\theta}_{(z,\omega)} &= 0 \end{aligned} \tag{A.31}$$

in which:

$$\begin{aligned} GJ^* &= GJ\left(1 + i\omega c_\theta^*\right) \\ \alpha &= \sqrt{\frac{\omega^2 \rho J}{GJ^*}} \end{aligned} \tag{A.32}$$

The general solution for this homogeneous linear differential equation is:

$$\tilde{\theta}_{(z,\omega)} = \sum_{i=1}^{2} C_i e^{\lambda_i z} \tag{A.33}$$

Substituting this form of solution to the homogeneous equation resulting:

$$\sum_{i=1}^{2} C_i \left(\alpha^2 + \lambda_i^2\right) e^{\lambda_i z} = 0 \tag{A.34}$$

We would like to find the non-trivial solution of this equation which are:

$$\begin{aligned} \lambda^2 &= -\alpha^2 \\ \lambda_{1,2} &= \pm i\alpha \end{aligned} \tag{A.35}$$

Substituting these value back to the general solution resulting:

$$\begin{aligned} \tilde{\theta}_{(z,\omega)} &= C_1 e^{i\alpha z} + C_2 e^{-i\alpha z} \\ &= (C_1 + C_2)\cos(\alpha z) + i(C_1 - C_2)\sin(\alpha z) \\ &= A\cos(\alpha z) + B\sin(\alpha z) \end{aligned} \tag{A.36}$$

PARTICULAR SOLUTION

The load shape function for the torsional vibration can be seen in Equation5.5 (bottom). Then the particular solution can be written as:

$$\tilde{\theta}_{particular} = A_{p2} z^6 + B_{p2} z^5 + C_{p2} z^4 + D_{p2} z^3 + E_{p2} z^2 + F_{p2} z + G_{p2} \tag{A.37}$$

Substitute the particular solution to the EOM resulting:

$$\begin{aligned} -GJ^*\left(30A_{p2}z^2 + 20B_{p2}z + 12C_{p2} + 6D_{p2} + 2E_{p2}\right) - \omega^2 \rho J e^2 \Big(A_{p2}z^6 + B_{p2}z^5 + C_{p2}z^4 + D_{p2}z^3 \\ + E_{p2}z^2 + F_{p2}z + G_{p2}\Big) = a_t z^6 + b_t z^5 + c_t z^4 + d_t z^3 + e_t z^2 + f_t z + g_t \end{aligned} \tag{A.38}$$

The value of the constants can be derrived from this equation which are:

$$\begin{gathered} A_{p2} = \frac{-a_t}{\omega^2 \rho J}\,;\, B_{p2} = \frac{-b_t}{\omega^2 \rho J}\,;\, C_{p2} = \frac{30GJ^* A_{p2} + c_t}{\omega^2 \rho J}\,;\, D_{p2} = \frac{20GJ^* B_{p2} + d_t}{\omega^2 \rho J}\,;\, E_{p2} = \frac{12GJ^* C_{p2} + e_t}{\omega^2 \rho J} \\ F_{p2} = \frac{6GJ^* D_{p2} + f_t}{\omega^2 \rho J}\,;\, G_{p2} = \frac{4GJ^* E_{p2} + g_t}{\omega^2 \rho J} \end{gathered} \tag{A.39}$$

Then the total solution from the homogeneous equation and the particular solution can be written as:

$$\begin{aligned} \tilde{\theta}_{(z,\omega)} = &A\cos(\alpha z) + B\sin(\alpha z) \\ &+ A_{p2} z^6 + B_{p2} z^5 + C_{p2} z^4 + D_{p2} z^3 + E_{p2} z^2 + F_{p2} z + G_{p2} \end{aligned} \tag{A.40}$$

A.3.2. BOUNDARY CONDITIONS

There are two boundary conditions which are needed to solve the two unknowns from the solution of homogeneous equation. These boundary condition can be seen in the equations below:

BC1-Torque

$$GJ^* \frac{\partial}{\partial z}\tilde{\theta}_{(z,\omega)}\Big|_{z=0} - \left(i\omega C_q + K_q\right)\tilde{\theta}_{(z,\omega)}\big|_{z=0} = 0 \tag{A.41}$$

BC2-Torque

$$GJ^* \frac{\partial}{\partial z}\tilde{\theta}_{(z,\omega)}\Big|_{z=L} + \left(i\omega C_\theta + K_\theta\right)\left(\tilde{\theta}_{(z,\omega)} - \tilde{\theta}_{t(z,\omega)}\right)\big|_{z=L} = 0 \tag{A.42}$$

After substituting the total solution to the boundary conditions, one can put the equations to a matrix form of:

$$\underline{\underline{K_{D\theta}}} + \underline{C_\theta} = \underline{T} \tag{A.43}$$

The dynamic stiffness matrix for the torsional vibration can be written as:

$$\underline{\underline{K_{D\theta}}} = \begin{bmatrix} -iCq\omega - Kq & GJ\alpha \\ -(\gamma_t - 1)(K_\theta + i\omega C_\theta)\cos(\alpha L) - GJ\alpha \sin(\alpha L) & GJ\alpha\cos(\alpha L) - (\gamma_t - 1)(K_\theta + i\omega C_\theta)\sin(\alpha L) \end{bmatrix} \tag{A.44}$$

in which:

$$\gamma_t = \frac{i\omega C_\theta + K_\theta}{\left(-\omega^2 J_\theta + i\omega C_\theta + K_\theta\right)} \tag{A.45}$$

Then the vector T on the right side of the equation which is obtained from the particular solution can be written as:

$$\underline{T} = \begin{bmatrix} -F_{p2}GJ + \left(+iCq\omega + Kq\right)G_{p2} \\ -\left(L^6\gamma_{t2} + 6GJL^5\right)A_{p2} - \left(\gamma_{t2}L^5 + 5GJL^4\right)B_{p2} - \left(\gamma_{t2}L^4 + 4GJL^3\right)C_{p2} - \left(\gamma_{t2}L^3 + 3GJL^2\right)D_{p2} - \left(\gamma_{t2}L^2 + 2GJL\right)E_{p2} - \left(L\gamma_{t2} + GJ\right)F_{p2} - G_{p2}\gamma_{t2} \end{bmatrix} \tag{A.46}$$

in which:

$$\gamma_{t2} = \left(i\omega C_\theta + K_\theta\right)\left(1 - \gamma_t\right) \tag{A.47}$$

Then the coefficient vector $\underline{C_\theta}$ can be solved by:

$$\underline{C_\theta} = \underline{\underline{K_{D\theta}}}^{-1}\underline{T} \tag{A.48}$$

The coefficients can be substituted to equation A.40 to obtain the response in frequency domain. In order to get the acceleration of the building the equation below is used:

$$\text{acceleration} = R\omega^2\tilde{\theta}_{(z,\omega)} \tag{A.49}$$

in which R is the radius from the center of rotation in which we would like to observed. In the EPO building case, the maximum acceleration located on the corner of the building or $R = 78m$.

A.4. SLENDER HIGH-RISE BUILDING

The model for the dynamic analysis of the slender high-rise building is shown in FigureA.4 below:

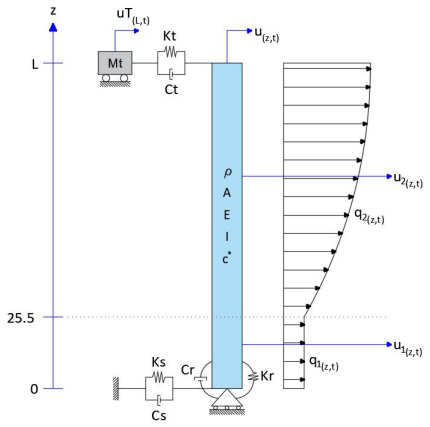

Figure A.4: One Dimensional Model for High Rise Building

in which:

$$L_1 = 25.5\ m \tag{A.50}$$

A.4.1. EQUATION OF MOTION

The high rise building is modeled as an Euler-Bernoulli beam, therefore the equation of motion of the system is:

for $0 \leqslant z \leqslant 25.5$:

$$\rho A\frac{\partial^2}{\partial t^2}u_{1_{(z,t)}} + \frac{\partial^2}{\partial z^2}\left(EI\left(1 + c^*\frac{\partial}{\partial t}\right)\frac{\partial^2}{\partial z^2}u_{1_{(z,t)}}\right) = q_{1_{(z,t)}} \tag{A.51}$$

for $25.5 \leqslant z \leqslant L$:

$$\rho A\frac{\partial^2}{\partial t^2}u_{2(z,t)} + \frac{\partial^2}{\partial z^2}\left(EI\left(1 + c^*\frac{\partial}{\partial t}\right)\frac{\partial^2}{\partial z^2}u_{2(z,t)}\right) = q_{2(z,t)} \tag{A.52}$$

To solve the partial differential equation (PDE) in equation of motion, Fourier Transform is used, which transform the equation A.51 and A.52 into:

$$-\omega^2 \rho A \tilde{u}_{1,2_{(z,\omega)}} + EI^* \frac{\partial^4}{\partial z^4} \tilde{u}_{1,2_{(z,\omega)}} = \tilde{q}_{1,2_{(z,\omega)}} \tag{A.53}$$

For the TMD, the equation of motion can be seen in the equation below:

$$-\omega^2 m_t \tilde{u}_{t(\omega)} + (i\omega C_t + K_t)(\tilde{u}_{t(\omega)} - \tilde{u}_{2_{(L,\omega)}}) = 0 \tag{A.54}$$

From this equation, the expression of $\tilde{u}_t$ can be derived such as:

$$\tilde{u}_{t(\omega)} = \frac{i\omega C_t + K_t}{-\omega^2 m_t + i\omega C_t + K_t} \tilde{u}_{2_{(L,\omega)}} \tag{A.55}$$

HOMOGENEOUS EQUATION

The equation of motion can be separated to a homogeneous equation and a particular solution while the summation of both is the total solution. The homogeneous equation of the EOM can be written as:

$$\frac{\partial^4}{\partial z^4} \tilde{u}_{1,2_{(z,\omega)}} - \beta \tilde{u}_{1,2(z,\omega)} = 0 \tag{A.56}$$

In which:

$$\beta = \left(\frac{\omega^2 \rho A}{EI^*}\right)^{1/4} \tag{A.57}$$

The general solution for this homogeneous linear differential equation is:

$$\tilde{u}_{1,2(z,\omega)} = \sum_{i=1}^{4} C_i e^{\lambda_i z} \tag{A.58}$$

which it is known that the solution form is:

$$\tilde{u}_{1,2(z,\omega)} = A_{1,2}\cosh(\beta z) + B_{1,2}\sinh(\beta z) + C_{1,2}\cos(\beta z) + D_{1,2}\sin(\beta z) \tag{A.59}$$

PARTICULAR SOLUTION

The particular solution is related to the loading on the system. The wind loading have a function of time (frequency) and space which can be separated as written in the equation below:

$$q_{1,2_{(z,\omega)}} = f_{1,2_{(\omega)}} f_{1,2_{(z)}} \tag{A.60}$$

The frequency characteristic of the wind load is taking into account by the Solari wind spectrum, therefore the value of $f_{1,2_{(\omega)}}$ is equal to one in this mechanical admittance. The shape function $f_{1_{(z)}}$ can be seen in top equation of Equation9.28 and the shape function $f_{2_{(z)}}$ can be seen in Equation9.29. The particular solution can also be found on the same form as the load therefore it can be written that the solution is:

$$\tilde{u}_{particular1} = A_{p1} \tag{A.61}$$

$$\tilde{u}_{particular2} = A_p z^6 + B_p z^5 + C_p z^4 + D_p z^3 + E_p z^2 + F_p z + G_p \tag{A.62}$$

Substitute the particular solution to the EOM resulting:

$$\begin{gathered} -\omega^2 \rho A\, A_{p1} = \ln L_1 \\ EI^*\left(360A_p z^2 + 120B_p z + 24C_p\right) - \omega^2 \rho A\left(A_p z^6 + B_p z^5 + C_p z^4 + D_p z^3 + E_p z^2 + F_p z + G_p\right) \\ = az^6 + bz^5 + cz^4 + dz^3 + ez^2 + fz + g \end{gathered} \tag{A.63}$$

The value of the constants can be derrived from this equation which are:

$$\begin{gathered} A_{p1} = \frac{\ln L_1}{-\omega^2 \rho A} \\ A_p = \frac{-a}{\omega^2 \rho A}\,;\, B_p = \frac{-b}{\omega^2 \rho A}\,;\, C_p = \frac{-c}{\omega^2 \rho A}\,;\, D_p = \frac{-d}{\omega^2 \rho A}\,;\, E_p = \frac{360EI^* A_p - e}{\omega^2 \rho A} \\ F_p = \frac{120EI^* B_p - f}{\omega^2 \rho A}\,;\, G_p = \frac{24EI^* C_p - g}{\omega^2 \rho A} \end{gathered} \tag{A.64}$$

Then the total solution for the bending vibration can be written as:

$$\begin{aligned}\tilde{u}_{1_{(z,\omega)}} &= A1\cosh(\beta z) + B1\sinh(\beta z) + C1\cos(\beta z) + D1\sin(\beta z) + A_{p1} \\ \tilde{u}_{2_{(z,\omega)}} &= A2\cosh(\beta z) + B2\sinh(\beta z) + C1\cos(\beta z) + D1\sin(\beta z) \\ &\quad + A_p z^6 + B_p z^5 + C_p z^4 + D_p z^3 + E_p z^2 + F_p z + G_p\end{aligned} \tag{A.65}$$

A.4.2. BOUNDARY CONDITIONS

To find the value of the 8 coefficients $(A_{1,2}, B_{1,2}, C_{1,2}, D_{1,2})$, the boundary and interface conditions are used. The number of the conditions should satisfied the number of the unknowns. In this case there are 4 dynamic boundary conditions and interface conditions which are:

BC1-Shear Force:

$$EI^* \frac{\partial^3}{\partial z^3}\tilde{u}_{1_{(z,\omega)}}\Big|_{z=0} + (i\omega C_s + K_s)\tilde{u}_{1_{(z,\omega)}}\big|_{z=0} = 0 \tag{A.66}$$

BC2-Bending Moment:

$$EI^* \frac{\partial^2}{\partial z^2}\tilde{u}_{1_{(z,\omega)}}\Big|_{z=0} - (i\omega C_r + K_r)\frac{\partial}{\partial z}\tilde{u}_{1_{(z,\omega)}}\Big|_{z=0} = 0 \tag{A.67}$$

BC3-Shear Force:

$$EI^* \frac{\partial^3}{\partial z^3}\tilde{u}_{2_{(z,\omega)}}\Big|_{z=L} - (i\omega C_t + K_t)\left(\tilde{u}_{2_{(z,\omega)}} - \tilde{u}_{t_{(\omega)}}\right)\big|_{z=L} = 0 \tag{A.68}$$

BC4-Bending Moment:

$$EI^* \frac{\partial^2}{\partial z^2}\tilde{u}_{2_{(z,\omega)}}\Big|_{z=L} = 0 \tag{A.69}$$

IC1-Deformation:

$$\tilde{u}_{2_{(L_1,\omega)}} - \tilde{u}_{2_{(L_1,\omega)}} = 0 \tag{A.70}$$

IC2-Rotation:

$$\frac{\partial}{\partial z}\tilde{u}_{2_{(z,\omega)}}\Big|_{z=L_1} - \frac{\partial}{\partial z}\tilde{u}_{1_{(z,\omega)}}\Big|_{z=L_1} = 0 \tag{A.71}$$

IC3-Bending Moment:

$$EI^* \frac{\partial^2}{\partial z^2}\tilde{u}_{2_{(z,\omega)}}\Big|_{z=L_1} - EI^* \frac{\partial^2}{\partial z^2}\tilde{u}_{1_{(z,\omega)}}\Big|_{z=L_1} = 0 \tag{A.72}$$

IC4-Shear Force:

$$EI^* \frac{\partial^3}{\partial z^3}\tilde{u}_{2_{(z,\omega)}}\Big|_{z=L_1} - EI^* \frac{\partial^3}{\partial z^3}\tilde{u}_{1_{(z,\omega)}}\Big|_{z=L_1} = 0 \tag{A.73}$$

The expression of $\tilde{u}_{t(\omega)}$ can be substituted to the beam motion $\tilde{u}_{(L,\omega)}$ from the equation A.55. To obtain the response $(\tilde{u}_{1,2(z,\omega)})$, there are 8 unknowns [A1, B1, C1, D1, A2, B2, C2, D2] need to be obtained. Therefore the 4 boundary conditions and 4 interface conditions is used to obtain the unknowns. After substituting the expression of $\tilde{u}$ in equation A.59 to the boundary condition, the 4 equations can be put in matrix form:

$$\underline{\underline{K_D}} * \underline{C} = \underline{F} \tag{A.74}$$

Matrix K_D is called the dynamic stiffness matrix and vector $\underline{C}$ consist of the coefficient [A1, B1, C1, D1, A2, B2, C2, D2], and vector F is the value which does not contain any coefficient [A1, B1, C1, D1, A2, B2, C2, D2] in the equations of boundary conditions and interface conditions. Then the coefficient vector $\underline{C}$ can be solved by:

$$\underline{C} = \underline{\underline{K_D}}^{-1}\underline{F} \tag{A.75}$$

The coefficients substitute again to equation A.59 to obtain the response in frequency domain. In order to get the acceleration of the building the equation below is used:

$$\text{acceleration}_{1,2} = \omega^2 \tilde{u}_{1,2_{(z,\omega)}} \tag{A.76}$$

B

STATIC ANALYSIS OF A BEAM

B.1. EULER-BERNOULLI BEAM

The model which is used as the case to solve the statics of the Euler-Bernoulli beam is shown in the Figure4.6 below:

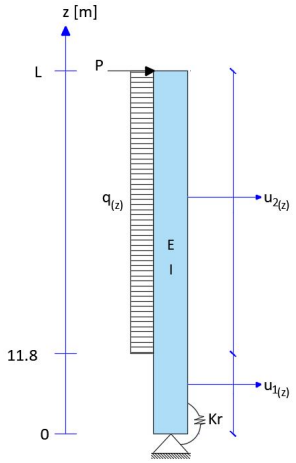

Figure B.1: Static: Bending Beam

There are two equations of motion which is separate after L1 = 11.8 m. The first equation which represent the motion of the beam on the bottom can be derived as:

$$
\begin{aligned}
\text{For } 0 \leqslant z \leqslant L1: \quad EI\frac{\partial^4 u_{1_{(z)}}}{\partial z^4} &= 0 \\
EI\frac{\partial^3 u_{1_{(z)}}}{\partial z^3} &= A_1 \\
EI\frac{\partial^2 u_{1_{(z)}}}{\partial z^2} &= A_1 z + B_1 \\
EI\frac{\partial u_{1_{(z)}}}{\partial z} &= \frac{1}{2}A_1 z^2 + B_1 z + C_1 \\
EI\, u_{1_{(z)}} &= \frac{1}{6}A_1 z^3 + \frac{1}{2}B_1 z^2 + C_1 z + D_1
\end{aligned}
\tag{B.1}
$$

The second equation which represent the motion of the beam on the top can be derived as:

$$\begin{aligned}
\text{For } L1 \leqslant z \leqslant L: \quad EI\frac{\partial^4 u_{2(z)}}{\partial z^4} &= q \\
EI\frac{\partial^3 u_{2(z)}}{\partial z^3} &= qz + A_2 \\
EI\frac{\partial^2 u_{2(z)}}{\partial z^2} &= \frac{1}{2}qz^2 + A_2 z + B_2 \\
EI\frac{\partial u_{2(z)}}{\partial z} &= \frac{1}{6}qz^3 + \frac{1}{2}A_2 z^2 + B_2 z + C_2 \\
EI\, u_{2(z)} &= \frac{1}{24}qz^4 + \frac{1}{6}A_2 z^3 + \frac{1}{2}B_2 z^2 + C_2 z + D_2
\end{aligned} \tag{B.2}$$

The boundary conditions of the static can be seen in the equations below:
BC1-Deformation:

$$u_{1(0)} = 0 \tag{B.3}$$

BC2-Bending Moment:

$$EI\frac{\partial^2 u_{1_{(0)}}}{\partial z^2}\bigg|_{z=0} - K_r\frac{\partial u_{1_{(0)}}}{\partial z}\bigg|_{z=0} = 0 \tag{B.4}$$

BC3-Shear Force:

$$EI\frac{\partial^3 u_{2(z)}}{\partial z^3}\bigg|_{z=L} + P = 0 \tag{B.5}$$

BC4-Rotation:

$$EI\frac{\partial^2 u_{2(z)}}{\partial z^2}\bigg|_{z=L} = 0 \tag{B.6}$$

The interface conditions of the system can be seen in the equation below:
IC1-Deformation:

$$u_{1_{(L_1)}} - u_{2_{(L_1)}} = 0 \tag{B.7}$$

IC2-Rotation:

$$\frac{\partial u_{1(z)}}{\partial z}\bigg|_{z=L_1} - \frac{\partial u_{2(z)}}{\partial z}\bigg|_{z=L_1} = 0 \tag{B.8}$$

IC3-Bending Moment:

$$EI\frac{\partial^2 u_{1(z)}}{\partial z^2}\bigg|_{z=L_1} - EI\frac{\partial^2 u_{2(z)}}{\partial z^2}\bigg|_{z=L_1} = 0 \tag{B.9}$$

IC4-Shear Force:

$$EI\frac{\partial^3 u_{1(z)}}{\partial z^3}\bigg|_{z=L_1} - EI\frac{\partial^3 u_{2(z)}}{\partial z^3}\bigg|_{z=L_1} = 0 \tag{B.10}$$

By substituting the equation B.1 and B.2 to the boundary and interface conditions, we can put these eight equation in the matrix form:

$$\underline{\underline{K_S}}\,\underline{C_S} = \underline{F_S} \tag{B.11}$$

In which K_S is a matrix which contains all the value in front of the coefficient vector C_S [A1,B1,C1,D1,A2,B2,C2,D2]. The vector F_S is the component which does not contain any coefficients in the vector C_S. The K_S and F_S can

be seen in the following equation:

$$\underline{\underline{K_S}} = \begin{bmatrix} 0 & 0 & 0 & EI^{-1} & 0 & 0 & 0 & 0 \\ 0 & 1 & -\frac{Kr}{EI} & 0 & 0 & 0 & 0 & 0 \\ 0 & 0 & 0 & 0 & \frac{L}{EI} & EI^{-1} & 0 & 0 \\ 0 & 0 & 0 & 0 & 1 & 0 & 0 & 0 \\ 1/6\,\frac{L1^3}{EI} & 1/2\,\frac{L1^2}{EI} & \frac{L1}{EI} & EI^{-1} & -1/6\,\frac{L1^3}{EI} & -1/2\,\frac{L1^2}{EI} & -\frac{L1}{EI} & -EI^{-1} \\ 1/2\,\frac{L1^2}{EI} & \frac{L1}{EI} & EI^{-1} & 0 & -1/2\,\frac{L1^2}{EI} & -\frac{L1}{EI} & -EI^{-1} & 0 \\ L1 & 1 & 0 & 0 & -L1 & -1 & 0 & 0 \\ 1 & 0 & 0 & 0 & -1 & 0 & 0 & 0 \end{bmatrix} \tag{B.12}$$

$$\underline{F_S} = \begin{bmatrix} 0 \\ 0 \\ -1/2\,\frac{qL^2}{EI} \\ -Lq - P \\ 1/24\,\frac{qL1^4}{EI} \\ 1/6\,\frac{qL1^3}{EI} \\ 1/2\,qL1^2 \\ L1\,q \end{bmatrix} \qquad \underline{C_S} = \begin{bmatrix} A_1 \\ B_1 \\ C_1 \\ D_1 \\ A_2 \\ B_2 \\ C_2 \\ D_2 \end{bmatrix} \tag{B.13}$$

The coefficient vector C_S can be solved by using matrix operation:

$$\underline{C_S} = \underline{\underline{K_S}}^{-1} \underline{F_S}$$

$$\underline{C_S} = \begin{bmatrix} -Lq + L1\,q - P \\ 1/2\,qL^2 - 1/2\,qL1^2 + LP \\ 1/2\,\frac{(qL^2 - qL1^2 + 2\,LP)EI}{Kr} \\ 0 \\ -Lq - P \\ 1/2\,L\left(Lq + 2\,P\right) \\ 1/6\,\frac{-Kr\,L1^3 q + 3\,EI\,L^2 q - 3\,EI\,L1^2 q + 6\,EI\,LP}{Kr} \\ 1/24\,qL1^4 \end{bmatrix} \tag{B.14}$$

Substituting this coefficients to the equation B.1 and B.2, we can obtain the equation for the deformation of the building:

$$\begin{aligned} u_1 = &\frac{1}{EI}(1/6\,(-Lq + L1\,q - P)z^3 + 1/2\,(1/2\,qL^2 - 1/2\,qL1^2 + LP)z^2 + \\ &1/2\,\frac{(qL^2 - qL1^2 + 2\,LP)EI\,z}{Kr}) \\ u_2 = &\frac{1}{EI}(1/24\,qz^4 + 1/6\,(-Lq - P)z^3 + 1/4\,L(Lq + 2\,P)z^2 + 1/6 \\ &\frac{(-Kr\,L1^3 q + 3\,EI\,L^2 q - 3\,EI\,L1^2 q + 6\,EI\,LP)z}{Kr} + 1/24\,qL1^4) \end{aligned} \tag{B.15}$$

The bottom rotation is the first derivative of the u_1 which can be written as:

$$\frac{\partial u_1}{\partial z} = \frac{1}{EI}\left(1/2\left(-Lq + L1\,q - P\right)z^2 + \left(1/2\,qL^2 - 1/2\,qL1^2 + LP\right)z + 1/2\,\frac{\left(qL^2 - qL1^2 + 2\,LP\right)EI}{Kr}\right) \tag{B.16}$$

B.2. TORSIONAL BAR

The torsional bar model for the static calculation can be seen in the FigureB.2 below:

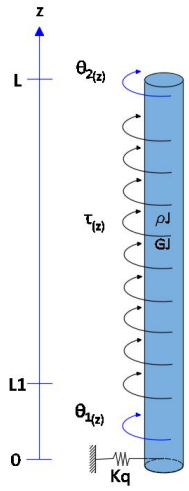

Figure B.2: Static: Torsional Bar

The governing equations for the bottom part of the bar for $0 \leqslant z \leqslant L_1$:

$$\begin{aligned} GJ\,\frac{\partial^2}{\partial z^2}\theta_{1_{(z)}} &= 0 \\ GJ\,\frac{\partial}{\partial z}\theta_{1_{(z)}} &= -A_1 \\ GJ\,\theta_{1_{(z)}} &= -A_1\,z - B_1 \end{aligned} \tag{B.17}$$

The governing equation for the top part of the bar for $L_1 \leqslant z \leqslant L$:

$$\begin{aligned} GJ\,\frac{\partial^2}{\partial z^2}\theta_{2_{(z)}} &= \tau \\ GJ\,\frac{\partial}{\partial z}\theta_{2_{(z)}} &= \tau\,z - A_2 \\ GJ\,\theta_{2_{(z)}} &= -\frac{1}{2}\tau\,z^2 - A_2\,z - B_2 \end{aligned} \tag{B.18}$$

The boundary conditions of the static can be seen in the equations below:

BC1-Torque

$$GJ\frac{\partial}{\partial z}\theta_{1_{(z)}}\Big|_{z=0} - K_q\,\theta_{1_{(z)}}|_{z=0} = 0 \tag{B.19}$$

BC2-Torque

$$GJ\frac{\partial}{\partial z}\theta_{2_{(z)}}\Big|_{z=L} = 0 \tag{B.20}$$

IC1-Torsion

$$\theta_{1_{(L_1)}} - \theta_{2_{(L1)}} = 0 \tag{B.21}$$

IC2-Torque

$$GJ\,\frac{\partial}{\partial z}\left(\theta_{1_{(z)}} - \theta_{2_{(z)}}\right)\Big|_{z=L_1} = 0 \tag{B.22}$$

By substituting the governing equation to the boundary and interface conditions, we can put these eight equation in the matrix form:

$$\underline{\underline{K_{S_t}}}\;\underline{C_{S_t}} = \underline{F_{S_t}} \tag{B.23}$$

In which K_{S_t} is a matrix which contains all the value in front of the coefficient vector C_{S_t} [A1,B1,C1,A2,B2]. The vector F_{S_t} is the component which does not contain any coefficients in the vector C_{S_t}. The K_{S_t} and F_{S_t} can be seen in the following equation:

$$\underline{\underline{K_{S_t}}} = \begin{bmatrix} -1 & \frac{Kq}{GJ} & 0 & 0 \\ 0 & 0 & -1 & 0 \\ -\frac{L1}{GJ} & -GJ^{-1} & \frac{L1}{GJ} & GJ^{-1} \\ -1 & 0 & 1 & 0 \end{bmatrix} \tag{B.24}$$

$$\underline{F_{S_t}} = \begin{bmatrix} 0 \\ L\tau \\ -\frac{1}{2}\frac{\tau L1^2}{GJ} \\ -L1\tau \end{bmatrix} \qquad \underline{C_S} = \begin{bmatrix} A_1 \\ B_1 \\ A_2 \\ B_2 \end{bmatrix} \tag{B.25}$$

The coefficient vector C_{S_t} can be solved by using matrix operation:

$$\underline{C_S} = \underline{\underline{K_S}}^{-1}\underline{F_S}$$

$$\underline{C_S} = \begin{bmatrix} -(-L1+L)\tau \\ -\frac{GJ(-L1+L)\tau}{Kq} \\ -L\tau \\ -\frac{1}{2}\frac{\tau(-KqL1^2+2GJL-2GJL1)}{Kq} \end{bmatrix} \tag{B.26}$$

Substituting this coefficients to the equation B.1 and B.2, we can obtain the equation for the deformation of the building:

$$\begin{aligned} \theta_{1_{(z)}} &= \frac{1}{GJ}\left((-L1+L)\tau z + \frac{GJ(-L1+L)\tau}{Kq}\right) \\ \theta_{2_{(z)}} &= \frac{1}{GJ}\left(-1/2\tau z^2 + L\tau z + 1/2\frac{\tau\left(-KqL1^2+2GJL-2GJL1\right)}{Kq}\right) \end{aligned} \tag{B.27}$$

B.3. SLENDER HIGH-RISE

The building stiffness is obtained through the static calculation. The model for this calculation is a bending beam which can be seen in FigureB.3.

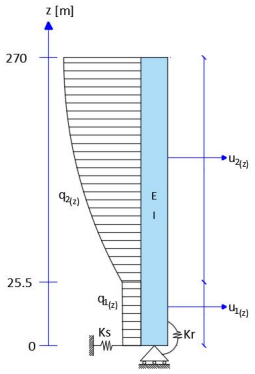

Figure B.3: Bending Beam Model

There are two equations of motion which is separate after L1 = 25.5 m. The first equation which represent the

motion of the beam on the bottom can be derived as:

$$\begin{aligned}
\text{For } 0 \leqslant z \leqslant L1: \quad EI\frac{\partial^4 u_{1_{(z)}}}{\partial z^4} &= q_1 \\
EI\frac{\partial^3 u_{1_{(z)}}}{\partial z^3} &= q_1 z + A_1 \\
EI\frac{\partial^2 u_{1_{(z)}}}{\partial z^2} &= \frac{1}{2}q_1 z^2 + A_1 z + B_1 \\
EI\frac{\partial u_{1_{(z)}}}{\partial z} &= \frac{1}{6}q_1 z^3 + \frac{1}{2}A_1 z^2 + B_1 z + C_1 \\
EI\, u_{1_{(z)}} &= \frac{1}{24}q_1 z^4 + \frac{1}{6}A_1 z^3 + \frac{1}{2}B_1 z^2 + C_1 z + D_1
\end{aligned} \tag{B.28}$$

The second equation which represent the motion of the beam on the top can be derived as:

$$\begin{aligned}
\text{For } L1 \leqslant z \leqslant L: \quad EI\frac{\partial^4 u_{2_{(z)}}}{\partial z^4} &= q_2 \\
EI\frac{\partial^3 u_{2_{(z)}}}{\partial z^3} &= \int q_2 + A_2 \\
EI\frac{\partial^2 u_{2_{(z)}}}{\partial z^2} &= \int\int q_2 + A_2 z + B_2 \\
EI\frac{\partial u_{2_{(z)}}}{\partial z} &= \int\int\int q_2 + \frac{1}{2}A_2 z^2 + B_2 z + C_2 \\
EI\, u_{2_{(z)}} &= \int\int\int\int q_2 + \frac{1}{6}A_2 z^3 + \frac{1}{2}B_2 z^2 + C_2 z + D_2
\end{aligned} \tag{B.29}$$

in which:

$$\begin{gathered}
q_{2_{(z)}} = a\, z^6 + b\, z^5 + c\, z^4 + d\, z^3 + e\, z^2 + f\, z + g \\
\begin{bmatrix} a \\ b \\ c \\ d \\ e \\ f \\ g \end{bmatrix} = \begin{bmatrix} -2.415 \times 10^{-12} \\ 2.33 \times 10^{-9} \\ -8.99 \times 10^{-7} \\ 1.79 \times 10^{-4} \\ -2.05 \times 10^{-2} \\ 1.568 \\ 23.803 \end{bmatrix}
\end{gathered} \tag{B.30}$$

The boundary conditions of the static can be seen in the equations below:

BC1-Deformation:

$$EI\frac{\partial^3 u_{1_{(0)}}}{\partial z^3}\bigg|_{z=0} + K_s\, u_{1(0)} = 0 \tag{B.31}$$

BC2-Bending Moment:

$$EI\frac{\partial^2 u_{1_{(0)}}}{\partial z^2}\bigg|_{z=0} - K_r\frac{\partial u_{1_{(0)}}}{\partial z}\bigg|_{z=0} = 0 \tag{B.32}$$

BC3-Shear Force:

$$EI\frac{\partial^3 u_{2_{(z)}}}{\partial z^3}\bigg|_{z=L} = 0 \tag{B.33}$$

BC4-Rotation:

$$EI\frac{\partial^2 u_{2_{(z)}}}{\partial z^2}\bigg|_{z=L} = 0 \tag{B.34}$$

The interface conditions of the system can be seen in the equation below:
IC1-Deformation:

$$u_{1_{(L_1)}} - u_{2_{(L_1)}} = 0 \tag{B.35}$$

IC2-Rotation:

$$\left.\frac{\partial u_{1_{(z)}}}{\partial z}\right|_{z=L_1} - \left.\frac{\partial u_{2_{(z)}}}{\partial z}\right|_{z=L_1} = 0 \tag{B.36}$$

IC3-Bending Moment:

$$\left.EI\frac{\partial^2 u_{1_{(z)}}}{\partial z^2}\right|_{z=L_1} - \left.EI\frac{\partial^2 u_{2_{(z)}}}{\partial z^2}\right|_{z=L_1} = 0 \tag{B.37}$$

IC4-Shear Force:

$$\left.EI\frac{\partial^3 u_{1_{(z)}}}{\partial z^3}\right|_{z=L_1} - \left.EI\frac{\partial^3 u_{2_{(z)}}}{\partial z^3}\right|_{z=L_1} = 0 \tag{B.38}$$

By substituting the equation B.28 and B.29 to the boundary and interface conditions, we can put these eight equation in the matrix form:

$$\underline{\underline{K_S}}\,\underline{C_S} = \underline{F_S} \tag{B.39}$$

In which K_S is a matrix which contains all the value in front of the coefficient vector C_S [A1,B1,C1,D1,A2,B2,C2,D2]. The vector F_S is the component which does not contain any coefficients in the vector C_S. The K_S and F_S can be seen in the following equation:

$$\underline{\underline{K_S}} = \begin{bmatrix} 1 & 0 & 0 & \frac{K_s}{EI} & 0 & 0 & 0 & 0 \\ 0 & 1 & -\frac{K_r}{EI} & 0 & 0 & 0 & 0 & 0 \\ 0 & 0 & 0 & 0 & L & 1 & 0 & 0 \\ 0 & 0 & 0 & 0 & 1 & 0 & 0 & 0 \\ 1/6\,\frac{L1^3}{EI} & 1/2\,\frac{L1^2}{EI} & \frac{L1}{EI} & EI^{-1} & -1/6\,\frac{L1^3}{EI} & -1/2\,\frac{L1^2}{EI} & -\frac{L1}{EI} & -EI^{-1} \\ 1/2\,\frac{L1^2}{EI} & \frac{L1}{EI} & EI^{-1} & 0 & -1/2\,\frac{L1^2}{EI} & -\frac{L1}{EI} & -EI^{-1} & 0 \\ L1 & 1 & 0 & 0 & -L1 & -1 & 0 & 0 \\ 1 & 0 & 0 & 0 & -1 & 0 & 0 & 0 \end{bmatrix} \tag{B.40}$$

$$\underline{F_S} = \begin{bmatrix} 0 \\ 0 \\ -\frac{aL^8}{56} - 1/42\,bL^7 - 1/30\,cL^6 - 1/20\,dL^5 - 1/12\,eL^4 - 1/6\,fL^3 - 1/2\,gL^2 \\ -1/7\,aL^7 - 1/6\,bL^6 - 1/5\,cL^5 - 1/4\,dL^4 - 1/3\,eL^3 - 1/2\,fL^2 - gL \\ -1/24\,\frac{q1\,L1^4}{EI} + \frac{aL1^{10}}{5040\,EI} + \frac{bL1^9}{3024\,EI} + \frac{cL1^8}{1680\,EI} + \frac{dL1^7}{840\,EI} + \frac{eL1^6}{360\,EI} + \frac{fL1^5}{120\,EI} + 1/24\,\frac{gL1^4}{EI} \\ -1/6\,\frac{q1\,L1^3}{EI} + \frac{aL1^9}{504\,EI} + \frac{bL1^8}{336\,EI} + \frac{cL1^7}{210\,EI} + \frac{dL1^6}{120\,EI} + \frac{eL1^5}{60\,EI} + 1/24\,\frac{fL1^4}{EI} + 1/6\,\frac{gL1^3}{EI} \\ -1/2\,q1\,L1^2 + \frac{aL1^8}{56} + 1/42\,bL1^7 + 1/30\,cL1^6 + 1/20\,dL1^5 + 1/12\,eL1^4 + 1/6\,fL1^3 + 1/2\,gL1^2 \\ -q1\,L1 + 1/7\,aL1^7 + 1/6\,bL1^6 + 1/5\,cL1^5 + 1/4\,dL1^4 + 1/3\,eL1^3 + 1/2\,fL1^2 + gL1 \end{bmatrix} \tag{B.41}$$

The coefficient vector C_S can be solved by using matrix operation:

$$\underline{C_S} = \underline{\underline{K_S}}^{-1}\,\underline{F_S} \tag{B.42}$$

By substituting this coefficients to the equation B.28 and B.29, we can obtain the equation for the deformation of the building.

$$
\begin{aligned}
u_{2_{(z)}} = \frac{1}{EI}\Bigg(&\frac{az^{10}}{5040}+\frac{bz^9}{3024}+\frac{cz^8}{1680}+\frac{dz^7}{840}+\frac{ez^6}{360}+\frac{fz^5}{120}+\frac{1}{24}gz^4-\frac{L}{2520}\Big(60\,aL^6+70\,bL^5+84\\
&cL^4+105\,dL^3+140\,eL^2+210\,fL+420\,g\Big)z^3+\frac{L^2}{1680}\Big(105\,aL^6+120\,bL^5+140\,cL^4+\\
&168\,dL^3+210\,eL^2+280\,fL+420\,g\Big)z^2+\frac{1}{5040\,K_r}\Big(-280\,K_r\,L1^9\,a+630EI\,L^8\,a-630\\
&EI\,L1^8\,a-315\,K_r\,L1^8\,b+720\,EI\,L^7\,b-720\,EI\,L1^7\,b-360\,K_r\,L1^7\,c+840\,EI\,L^6\,c-840\,EI\\
&L1^6\,c-420\,K_r\,L1^6\,d+1008\,EI\,L^5\,d-1008\,EI\,L1^5\,d-504\,K_r\,L1^5\,e+1260\,EI\,L^4\,e-1260\\
&EI\,L1^4\,e-630\,K_r\,L1^4\,f+1680\,EI\,L^3\,f-1680\,EI\,L1^3\,f-840\,K_r\,L1^3\,g+840\,K_r\,L1^3\,q1+\\
&2520\,EI\,L^2\,g-2520\,EI\,L1^2\,g+2520\,EI\,L1^2\,q1\Big)z+\frac{1}{15120\,K_s}\Big(252\,K_s\,L1^{10}\,a+280\,K_s\,L1^9\,b\\
&+315\,K_s\,L1^8\,c+2160\,EI\,L^7\,a-2160\,EI\,L1^7\,a+360\,K_s\,L1^7\,d+2520\,EI\,L^6\,b-2520\,EI\,L1^6\\
&b+420\,K_s\,L1^6\,e+3024\,EI\,L^5\,c-3024\,EI\,L1^5\,c+504\,K_s\,L1^5\,f+3780\,EI\,L^4\,d-3780\,EI\,L1^4\\
&d+630\,K_s\,L1^4\,g-630\,K_s\,L1^4\,q1+5040\,EI\,L^3\,e-5040\,EI\,L1^3\,e+7560\,EI\,L^2\,f-7560\\
&EI\,L1^2\,f+15120\,EI\,Lg-15120\,EI\,L1\,g+15120\,EI\,L1\,q1\Big)\Bigg)
\end{aligned}
\tag{B.43}
$$

BIBLIOGRAPHY

[1] Sondipon Adhikari. Damping models for structural vibration. *Engineering Department*, page 228, 2000.

[2] Atsuo Konishi. Structural Design of Tokyo Sky Tree Atsuo Konishi , Senior Structural Engineer , NIKKEN SEKKEI Wind Engineering CTBUH 2011 Seoul Conference Conference proceeding Unpublished conference paper Magazine article Unpublished Keyword. 2011.

[3] Prabodh V. Banavalkar. Structural systems to improve wind induced dynamic performance of high rise buildings. *Journal of Wind Engineering and Industrial Aerodynamics*, 36:213–224, 1990.

[4] Rachel Bashor, Sarah Bobby, Tracy Kijewski-Correa, and Ahsan Kareem. Full-scale performance evaluation of tall buildings under wind. *Journal of Wind Engineering and Industrial Aerodynamics*, 104-106:88–97, 2012.

[5] C W Bert. Material damping. An introductory review of mathematic measures and experimental technique. *Journal of Sound and Vibration*, 29(2):129–153, 1973.

[6] Daryl Boggs. Acceleration Indexes for Human comfort in Tall Buildings—Peak or RMS? *Preprint*, page 21, 1995.

[7] DJ Cerda and J van der Tempel. Aerodynamic damping in the design of support structures for offshore wind turbines. 2005.

[8] R.L.J.van den Berg. Investigation to damping in high-rise buildings. pages 1–128, 2012.

[9] F.Y.Cheng and K.Lou H.Jiang. Smart Structures: Innovative Systems for Seismic Response Control.

[10] J. D. Hartog. Mechanical Vibration, 1956.

[11] J C D Hoenderkamp. *High-rise Structures: Preliminary Design for Lateral Load*. Technische Universiteit Eindhoven. Department of Architecture, Building and Planning, Structural Design, 2005.

[12] A.sasaki H.Tsukagoshi, Y.Tamura. R e s p o n s e analyses on along-wind and across-wind vibrations of tall buildings in time domain. 47:497–506, 1993.

[13] a Kawaguchi, a Teramura, and Y Omote. Abstract Under these circumstances , the prediction of wind-induced vibration of a building has become an important problem in ensuring the structural safety of a building and the comfort of occupants in the building . [VelocityJ JGeneraliTedl " lWind Fo. 44:1949–1960, 1992.

[14] Ming Yi Liu, Wei Ling Chiang, Jin Hung Hwang, and Chia Ren Chu. Wind-induced vibration of high-rise building with tuned mass damper including soil-structure interaction. *Journal of Wind Engineering and Industrial Aerodynamics*, 96(6-7):1092–1102, 2008.

[15] A V Metrikine. Dynamics, Slender Structures and an Introduction to Continuum Mechanics. page 124.

[16] I Nishimura, T Kobori, M Sakamoto, N Koshika, K Sasaki, and S Ohrui. Active tuned mass damper. *Smart Materials and Structures*, 1(4):306–311, 1999.

[17] Milos Novakt. Effect of Soil on Structural Response To Wind and Earthquake. *ASCE National Structural Engineering meeting, Sans Fransisco*, 3(February):79–96, 1974.

[18] D.J.C. Salzmann and Jan van der Tempel. Aerodynamic damping in the design of support structures for offshore wind turbines. *Proceedings of the Offshore Wind Energy Conference*, pages 1–9, 2005.

[19] S.Y.Chu, T.T.Soong, and A.M.Reinhorn. Active, Hybrid, and Semi-active Structural Control: A Design and Implementation Handbook. page 294, 2005.

[20] TNO Diana. Additional dynamic analysis to EPO building in Rijswijk with DIANA. 2014.

[21] B J Vickery, N Isyumov, and A G Davenport. The Role of Damping, Mass, and Stiffness in the Reduction of Wind Effects on Structures. 11:285–294, 1983.

[22] G B Warburton. Reduction of vibration by control forces. 18(May):1179–1187, 1989.

[23] G B Warburton and E O Ayorinde. Optimum absorber parameters for simple systems. *Earthquake Engineering & Structural Dynamics*, 8(3):197–217, 1980.

[24] Y L Xu, K C S Kwok, and B Samali. Control of wind-induced tall building vibration by tuned mass dampers. *Journal of Wind Engineering and Industrial Aerodynamics*, 40(1):1–32, 1992.

[25] Zonneveld Ingenieurs. EPO Building. 2014.

Dynamic Stiffness and Force - Bending Beam

Matlab file: Model_Bending_Beam_Symbolic.m

```
%% TRANSFER FUNCTION / MECHANICAL ADMITTANCE
% First Model: Ordinary  mass spring dashpot system
% This program is for a single TMD on top of the building
clear;clc;warning('off','all')
syms x omega;
%
```

```
% A.    SELECT CASE
% !     Parameter that are loaded:
%       Soil: Kr Ks Cr Cs
%       Building: EI_star; mass; beta; L;
%       Particular Solution: a b c
        syms Kr Ks Cr Cs EI_star mass beta L
% A.1. DATA:
% A.4. TMD TRANSLATION:
        syms mt Ct Kt
% A.5. WIND LOAD:
%   a. Wind load on building f(omega):
        syms a b c d e f g
%
```

```
% B.    EQUATION OF MOTION (EOM)
% B.1. Particular Solution:
        Ap = -a/(EI_star*beta^4);
        Bp = -b/(EI_star*beta^4);
        Cp = -c/(EI_star*beta^4);
        Dp = -d/(EI_star*beta^4);
        Ep = (360*EI_star*Ap-e)/(EI_star*beta^4);
        Fp = (120*EI_star*Bp-f)/(EI_star*beta^4);
        Gp = (24*EI_star*Cp-g)/(EI_star*beta^4);
        upart = Ap*x^6+Bp*x^5+Cp*x^4+Dp*x^3+Ep*x^2+Fp*x+Gp
            ;
%       upart = Ap*x^4+Bp*x^3+Cp*x^2+Dp*x+Ep;
% B.2. EOM of building - total solution (homogeneous &
    particular):
        u = [cosh(beta*x) sinh(beta*x) cos(beta*x) sin(
            beta*x) upart];
% B.3. EOM of TMD (at z = L):
```

```
34          ut = (Kt+1i*omega*Ct)*subs(u,x,L)/(1i*omega*Ct-
                omega^2*mt+Kt);
35  %
```

```
36  % C.   BOUNDARY CONDITION
37  % C.1. At the bottom of building (at z = 0)
38  %   a. Shear force - translational stiffness:
39          BC1 = (subs(EI_star*diff(u,x,x,x)+(1i*omega*Cs+Ks)
                *u,x,0));
40  %   b. Bending moment - rotational stiffness:
41          BC2 = (subs(EI_star*diff(u,x,x)-(1i*omega*Cr+Kr)*
                diff(u,x),x,0));
42  % C.2. At the top of building (at z = L)
43  %   a. Shear Force - TMD:
44          BC3 = (subs(EI_star*diff(u,x,x,x)-(1i*omega*Ct+Kt)
                *(u-ut),x,L));
45  %   b. Bending moment:
46          BC4 = (subs(diff(u,x,x),x,L));
47  %
```

```
48  % D.   MATRIX & OUTPUT
49          M = [BC1;BC2;BC3;BC4];
50          noc = length(M); %matrix length
51  % D.1. Dynamic stiffness matrix:
52          K_Dyn = M((1:(noc-1)),(1:(noc-1)));
53  % D.2. Force matrix:
54          F = -M((1:(noc-1)),noc);
55          Frequency_Equation = det(K_Dyn)
```

Dynamic Stiffness and Force - Torsion Bar

Matlab file: Model_Torsional_Bar_Symbolic.m

```
1   %% TRANSFER FUNCTION / MECHANICAL ADMITTANCE
2   % This program is for a single TMD on top of the building
3   clear; clc; warning('off','all');
4   syms x omega;
5   %
```

```
6   % A.   SELECT CASE
7   % !    Parameter that are loaded:
```

```
8           syms Kq Cq
9           syms GJ_star rhoJ
10          syms J_tetha K_tetha C_tetha
11          syms a b c d e f g
12          syms L
13  %
    ------------------------------------------------------------------------

14  % B.    EQUATION OF MOTION (EOM)
15  % B.1. Particular Solution:
16          Ap = a/(-omega^2*rhoJ);
17          Bp = b/(-omega^2*rhoJ);
18          Cp = (c+30*GJ_star*Ap)/(-omega^2*rhoJ);
19          Dp = (d+20*GJ_star*Bp)/(-omega^2*rhoJ);
20          Ep = (e+12*GJ_star*Cp)/(-omega^2*rhoJ);
21          Fp = (f+6*GJ_star*Dp)/(-omega^2*rhoJ);
22          Gp = (g+2*GJ_star*Ep)/(-omega^2*rhoJ);
23          tetha_part = (Ap*x^6+Bp*x^5+Cp*x^4+Dp*x^3+Ep*x^2+
                Fp*x+Gp);
24  % B.2. EOM of building - total solution (homogeneous &
        particular):
25          alpha = sqrt(omega^2*rhoJ/GJ_star);
26          tetha = [cos(alpha*x) sin(alpha*x) tetha_part];
27  % B.3. EOM of TMD (at z = L):
28          tetha_t = (K_tetha+1i*omega*C_tetha)*subs(tetha,x,
                L)/(-omega^2*J_tetha+1i*omega*C_tetha+K_tetha);
29  %
    ------------------------------------------------------------------------

30  % C.    BOUNDARY CONDITION
31  % C.1. Torsional Force at the bottom (x = 0):
32          BC1 = subs(GJ_star*diff(tetha,x)-(1i*omega*Cq+Kq)*
                tetha,x,0);
33  %         BC1 = subs((tetha),x,0); %Clamped
34  % C.1. Torsional Force at the top (x = L):
35          BC2 = subs(GJ_star*diff(tetha,x)+(1i*omega*C_tetha
                +K_tetha)*(tetha-tetha_t),x,L);
36  %         BC2 = subs((tetha),x,L); %Clamped
37  %
    ------------------------------------------------------------------------

38  % D.    MATRIX & OUTPUT
39          M = [BC1;BC2];
40          noc = length(M); %matrix length
41  % D.1. Dynamic stiffness matrix:
42          K_Dyn = M((1:(noc-1)),(1:(noc-1)))
```

```
% D.2. Force matrix:
        F = -M((1:(noc-1)),noc)
%
```

Response - Acceleration

Matlab file: V_Response_Spectra.m

```
%% WIND:RESPONSE SPECTRUM
clear;close all;warning('off','all')
% Define the Time axis: Max value and Steps:
time = linspace(0,3600,10000);
u_time = zeros(length(time),2); %Output
global lower_bound upper_bound n_steps;
%
```

```
% A.    FREQUENCY STEP: [rad/s]
        lower_bound = 0.085;
        upper_bound = 11.904442545394877;
        n_steps     = 15000;
%
```

```
% !     Random Phase:
        phase = 2*pi*rand(1,n_steps);
% B.    LOAD PROGRAM:
% B.1. Select Case: Data Properties
        II_DATA_EPO_TNO_DIANA
for comb = 1:2
% B.2. Mechanical Admittance:
%   a. Status: 1.no TMD / 2.with TMD
        status = 1;
%   b. Output: 1.displacement / 2.velocity / 3.
    acceleration
        output = 3;
   if   comb == 1
        III_Model_Bending_Beam
   else
        III_Model_Torsion_Bar
   end
%% B.3. Load Spectrum:
```

```
30          IV_Wind_Spectrum
31  %
    ------------------------------------------------------------------------

32  % C.    RESPONSE SPECTRUM:
33          S_uu = psd.*S_FF';
34  % C.1.  Standard Deviation
35          sd = sqrt(trapz(omega_k,S_uu));
36  %%
    ------------------------------------------------------------------------

37  % D.    RESPONSE IN TIME DOMAIN:
38  % D.1.  Amplitude:
39          frequency_step = omega_k(2)-omega_k(1);
40          ak = sqrt(2*S_uu'*frequency_step);
41  % D.2.  Response:
42          u_time_n = ak.*sin(omega_k.*time'+phase);
43          u_time(:,comb) = u_time_n*ones(n_steps,1);
44  %
    ------------------------------------------------------------------------

45  % E.    PLOTTING:
46  % E.1.  Response Spectrum:
47          figure;plot(omega_k'/2/pi,S_uu)
48          title('Response Spectrum'); ylabel('S_u_u');
                xlabel('frequency [Hz]');
49  % E.2.  Response in time domain:
50          figure;subplot(1,3,[1,2]);plot(time,u_time(:,comb)
                );
51          title('Response'); ylabel('acceleration [m/s^2]');
                 xlabel('time [s]');ylim([-0.07 0.07]);
52  % E.3.  Probability Density Function:
53          x_psd_range = 0.07;
54          x_psd = linspace(-x_psd_range,x_psd_range,1000);
55          f = 1/sqrt(2*pi*sd^2)*exp(-x_psd.^2/(2*sd^2));
56          subplot(1,3,3);plot(f,x_psd);ylim([-0.07 0.07]);
57  end
58  % E.4.  Total Response for Bending and Torsion
59          total_response = sum(u_time,2);
60          bending_acc(para) = max(abs(u_time(:,1)));
61          max(abs(u_time(:,2)));
62          rmtasdf = max(abs(total_response));
```

Data Properties

Matlab file: II_DATA_EPO_TNO_DIANA.m

```
%% EPO BUILDING DATA PARAMETER:
% A.    SOIL PROPERTIES:
% A.1. BENDING PROPERTIES:
%   a. Clamped Base:
        Kr=1e100; Ks=1e100; Cs=0; Cr=0;
%   b. Data from TNO Diana:
        Kr=7.65e12; Ks=3.62e10; Cs=3.90e8; Cr=1.43e11;
%   c. Data from Sergio:
        Kr=2.33e13; Ks=1.56e10; Cs=8.05e8; Cr=5.79e11;
% A.1. TORSION PROPERTIES:
        Kq=6.74e13;Cq=7.24e11;
%
```

```
% FREQUENCY DEPENDENT SSI:
  load('Stiffness_data.mat');
  freq2 = freq*2*pi;
% Srpings and dashpots
  K_horizontal = real(Kh);  % Horizontal stiffness spring N/m
  K_rotational= real(Kr);   % Rotational stiffness spring Nm/rad
  C_horizontal = imag(Kh)./(2*pi*freq'); % Horizontal dashpot Ns/m
  C_rotational = imag(Kr)./(2*pi*freq'); % Rotational dashpot Nsrad/m
% Fitting
  [Ks_omega,gof] = fit(freq2',K_horizontal,'cubicinterp');
  [Kr_omega,gof] = fit(freq2',K_rotational,'cubicinterp');
  [Cs_omega,gof] = fit(freq2(2:41)',C_horizontal(2:41),'cubicinterp');
  [Cr_omega,gof] = fit(freq2(2:41)',C_rotational(2:41),'cubicinterp');
%
```

```
% B.    EPO BUILDING SLENDERNESS 1:5
% !     EI[Nm2]; rho*area[kg/m]; C_star[s]
% B.1. Building Bending:
```

```
30          L = 105; %[m] Building Height
31          EI = 4.7E+13; %Building Stiffness
32          Cstar = 8.5e-3; %Material Damping
33          mass = 8.7e5; %Building mass/length
34  % B.2. TMD Bending:
35  % !     Kt/Ct_parameter = [1.noTMD;    2.Optimum    3.Ct=0;
        4.Ct=infty];
36          mt = 4.4e5; %[kg] TMD Mass
37  %    a. Original TNO Diana Value:
38          Kt_parameter=[0;   1.694e6*ones(3,1)]; %[N/m] TMD
              spring stiffness
39          Ct_parameter=[0;   1.394e5;         0;      1e15]; %[Ns
              /m] TMD damping
40  %    b. With Formula:
41          mass_ratio = mt/mass/L;
42          Kt_parameter=[0;   (1/(1+mass_ratio)*2.0226)^2*mt*
              ones(3,1)]; %[N/m] TMD spring stiffness
43  % B.3. Building Torsion:
44          Rad = 61.5;
45  %    a. Normal Building:
46          GJ = 1.9e13;
47          Cstar_tetha = 1.12e-2;%[m]
48          rhoJ = GJ/(1.7907*2*L/pi)^2;
49  % B.4. TMD Torsion:
50          J_tetha = 4.4e5*Rad^2; %[kg*m^2]
51          K_tetha_parameter = Kt_parameter*Rad^2; %[N/m2]
52          C_tetha_parameter = Ct_parameter*Rad^2; %[Ns/m2]
53  %
```

Mechanical Admittance - Bending Beam

Matlab file: III_Model_Bending_Beam.m

```
1  %% TRANSFER FUNCTION / MECHANICAL ADMITTANCE
2  % First Model: Ordinary  mass spring dashpot system
3   global lower_bound upper_bound n_steps;
4  % Set the Looping variable for plotting (Variables are
       determined in
5  % Response Spectra file)
6   a_frf = linspace(lower_bound,upper_bound,n_steps); n_frf
       = length(a_frf);
```

```
%
-------------------------------------------------------------------------

% A.1. FORCE COEFFICIENTS: f(x) = ax^6+bx^5+cx^4+dx^3+ex
    ^2+fx+g
        load('coeff')
        a=coeff(1);b=coeff(2);c=coeff(3);d=coeff(4);e=
            coeff(5);f=coeff(6);g=coeff(7);
%   a  Set the Location Point for the Output:
        x = L;
        n_Ct = length(Ct_parameter);
        FRF = zeros(n_frf,n_Ct); %Output: Frequency
            Response Function
        FE = zeros(n_frf,1); %Output: Frequency Equation
%   b. Loop for Ct Parameter:
  for   i = status:status
%   c. Set TMD parameter:
        Kt=Kt_parameter(i);Ct=Ct_parameter(i);
%   d. Loop for FRF:
  for   j = 1:n_frf
        omega = a_frf(j);
% A.2. Building Parameter:
        Ks=Ks_omega(j);Cs=Cs_omega(j);
        Kr=Kr_omega(j);Cr=Cr_omega(j);
        EI_star = EI*(1+1i*omega*Cstar);
        beta = (mass*omega^2/EI_star)^(1/4);
%
-------------------------------------------------------------------------

% D.   MATRIX & OUTPUT
% D.1. Dynamic stiffness matrix:
%      This value obtain from Model_Bending_Beam_Symbolic
    .m file
        K_Dyn;
        F;
        FE(j) = Frequency_Equation;
%
-------------------------------------------------------------------------

% E.   LOOPING
% a.   Coefficient matris:
        u = [ cosh(beta*x), sinh(beta*x), cos(beta*x), sin
            (beta*x), - (g + (24*c)/beta^4)/(EI_star*beta
            ^4) - (c*x^4)/(EI_star*beta^4) - (d*x^3)/(
            EI_star*beta^4) - (x*(f + (120*b)/beta^4))/(
            EI_star*beta^4) - (x^2*(e + (360*a)/beta^4))/(
```

```
            EI_star*beta^4) - (a*x^6)/(EI_star*beta^4) - (b
            *x^5)/(EI_star*beta^4)];
% b.   Coefficient matris:
        U = (K_Dyn)\(F);
        A = (U(1)); B = (U(2)); C = (U(3)); D = (U(4));
        Coeff = [A;B;C;D;1];
        if output == 1
% c.   Output displacement:
        FRF(j,i) = (abs(u*Coeff));
        elseif output == 2
% d.   Output velocity:
        FRF(j,i) = (abs(1i*omega*(u*Coeff)));
        elseif output == 3
% e.   Output acceleration:
        FRF(j,i) = (abs(-omega^2*(u*Coeff)));
        end
% f.   Output TMD displacement:
        FRF(j,i) = (abs(ut*Coeff));
    end
%
```

```
% F.   OUTPUT
% F.1. Frequency Response Function:
        u_frf = FRF(:,i);
% F.2. Power Spectral Density:
% !    Transfer Function |FRF|^2:
        psd = FRF(:,i).^2;
%
```

```
% G.   Plotting:
% G.2. Frequency Equation
        figure;subplot(1,2,1);hold on;
        findpeaks(-abs(real(FE)),a_frf/2/pi);refline(0,0);
        xlabel('frequency [Hz]');ylabel('Re(FE)');title('
            Real Part Frequency Equation');
        [pks,nfre]=findpeaks(-abs(real(FE)),a_frf/2/pi);
        subplot(1,2,2);hold on;
        findpeaks(-abs(imag(FE)),a_frf/2/pi);refline(0,0);
        xlabel('frequency [Hz]');ylabel('Im(FE)');title('
            Imaginary Part Frequency Equation');
        [pks,nfim]=findpeaks(-abs(imag(FE)),a_frf/2/pi);
        figure;
        plot(a_frf/2/pi,abs(FE));refline(0,0);
```

```
76          xlabel('frequency [Hz]');ylabel('Frequency
                Equation');title('Frequency Equation');
77  % G.2. FRF
78          figure;subplot(1,2,1);
79  %       findpeaks(u_frf,(a_frf/2/pi));
80          plot((a_frf/2/pi),u_frf);
81          xlabel('frequency [Hz]');ylabel('|u(omega,L)|');
                title('FRF');
82  % G.3. PSD
83          subplot(1,2,2);
84          findpeaks(psd,a_frf/2/pi,'Annotate','extents','
                WidthReference','halfheight');
85          xlabel('frequency [Hz]');ylabel('|H_s|^2 [(m^2/N)
                ^2]');title('Mechanical Admittance');
86          [pks,locs,widths,proms]=findpeaks(psd,(a_frf/2/pi)
                ,'WidthReference','halfheight');
87          zeta = widths./locs/2 %damping ratio
88          locs
89    end
```

Mechanical Admittance - Torsional Bar

Matlab file: III_Model_Torsion_Bar.m

```
1   %% TRANSFER FUNCTION / MECHANICAL ADMITTANCE
2   % This program is for a single TMD on top of the building
3   global lower_bound upper_bound n_steps;
4   %
        ------------------------------------------------------------------------------------------

5   % B     Particular Solution:
6           coeff = [1.99446534884015e-08,-6.73641900229052e
                -06,0.000760218918796258,-0.0325190735908715,0.432176621836927,-0.175

7           a=coeff(1);b=coeff(2);c=coeff(3);d=coeff(4);e=
                coeff(5);f=coeff(6);g=coeff(7);
8   %
        ------------------------------------------------------------------------------------------

9   % E.    LOOPING
10          x = L;
11  % !     Set the Looping variable for plotting (Variables
        are determined in Response Spectra file)
12          a_frf = linspace(lower_bound,upper_bound,n_steps);
```

```
% E.1. SOLUTION OF THE RESPONSE:
        n_Ct = length(C_tetha_parameter);
        FRF = zeros(n_steps,n_Ct);
        FE = zeros(n_steps,n_Ct);
%   a. Loop for Ct Parameter (All Ct values:[1:n_Ct];
    noTMD only:[1:1]):
   for  i = status:status
%   b. Set TMD parameter:
%       1.noTMD;    2.Optimum    3.Ct=0;    4.Ct=infty;
        K_tetha = K_tetha_parameter(i);C_tetha =
            C_tetha_parameter(i);
%   c. Loop for FRF:
   for  j = 1:n_steps
        omega = a_frf(j);
        GJ_star = GJ*(1+1i*omega*Cstar_tetha);
%   d. Stiffness and Force Matrix:
%       This value obtain from Model_Torsion_Bar_Symbolic.
    m file
        K_Dyn;
        F;
%   e. Coefficient matrix for the response:
        U = (K_Dyn)\(F);
        A = (U(1)); B = (U(2));
        Coeff = [A;B;1];
%   f. Response:
        tetha = [ cos(x*((omega^2*rhoJ)/GJ_star)^(1/2)),
            sin(x*((omega^2*rhoJ)/GJ_star)^(1/2)), - (g -
            (2*GJ_star*(e - (12*GJ_star*(c - (30*GJ_star*a)
            /(omega^2*rhoJ)))/(omega^2*rhoJ)))/(omega^2*
            rhoJ))/(omega^2*rhoJ) - (a*x^6)/(omega^2*rhoJ)
            - (b*x^5)/(omega^2*rhoJ) - (x^4*(c - (30*
            GJ_star*a)/(omega^2*rhoJ)))/(omega^2*rhoJ) - (x
            ^3*(d - (20*GJ_star*b)/(omega^2*rhoJ)))/(omega
            ^2*rhoJ) - (x^2*(e - (12*GJ_star*(c - (30*
            GJ_star*a)/(omega^2*rhoJ)))/(omega^2*rhoJ)))/(
            omega^2*rhoJ) - (x*(f - (6*GJ_star*(d - (20*
            GJ_star*b)/(omega^2*rhoJ)))/(omega^2*rhoJ)))/(
            omega^2*rhoJ)];
% E.2. OUTPUT:
        if output == 1
%   a. Output displacement:
        FRF(j,i) = 78*(abs(tetha*Coeff));
        elseif output == 2
%   b. Output velocity:
        FRF(j,i) = 78*(abs(1i*omega*(tetha*Coeff)));
        elseif output == 3
```

```
%    c. Output acceleration:
        FRF(j,i) = 78*(abs(-omega^2*(tetha*Coeff)));
        end
%    d. Output TMD displacement:
%        FRF(j,i) = eval(abs(tetha_t*Coeff));
% E.3. Frequency Equation
        FE(j,i) = abs(det(K_Dyn));
   end
   end
%
```

```
% F.    OUTPUT
% F.1. Frequency Response Function:
        u_frf = FRF(:,i);
% F.2. Power Spectral Density:
% !     Transfer Function |FRF|^2:
        psd = FRF(:,i).^2;
%
```

```
% G.    Plotting:
% G.1. FE
        figure; plot((a_frf/2/pi),(FE(:,i)));
        xlabel('frequency [Hz]');ylabel('Frequency
            Equation');title('FE');
% G.2. FRF
        figure; subplot(1,2,1);
        plot((a_frf/2/pi),u_frf);
        xlabel('frequency [Hz]');ylabel('|u(omega,L)|');
            title('FRF');
% G.3. PSD
        subplot(1,2,2)
        findpeaks(psd,a_frf/2/pi,'Annotate','extents','
            WidthReference','halfheight');
        xlabel('frequency [Hz]');ylabel('|H_s|^2 [(m^2/N)
            ^2]');title('Mechanical Admittance');
        [pks,locs,w] = findpeaks(psd,a_frf/2/pi,'
            WidthReference','halfheight');
        zeta = w./locs/2 %damping ratio
        locs
%
```

Dynamic Wind Load

Matlab file: IV_Wind_Spectrum.m

```
%% WIND: LOAD SPECTRUM
%    !  fL = dimensionless frequency
%    !  n = frequency in Hz
%    !  omega = frequency in rad/s
%
```

```
% A.    INPUT PARAMETER
% A.1.  Refference Height:
%    a. Building height and width:
        H_height = L; B_width = 156; %[m]
        z = H_height;
% A.2.  Basic velocity [m/s]:
        vb_1 = 20.5; %(1year) - RMS
        vb_50 = 27; %(50years) - Peak
        vb = vb_50;
% A.3.  Roughness length [m]:
        zo = 1;
        zo_II = 0.05;
        kr = 0.19*(zo/zo_II)^0.07;
% A.4.  Minimum & Maximum Height [m]:
        z_min = 10;
        z_max = 200;
% A.5.  Factor - Turbulence Length(L(z)):
        kl = 1;
        Lt = 300;
%    a. Refference height for L(z):
        zt = 200;
% A.6.  Pressure Coefficient:
        Cp = 1.5;
% A.7.  Alpha:
        alpha = 0.67+0.05*log(zo);
%
```

```
% B.    LOAD SPECTRUM
% B.1.  Variance Spectrum (Solari):
%    a. Standard deviation:
        sigma_v = kr*vb*kl;
%    b. Mean wind speed [m/s]:
        vm = vb*kr*log(z/zo);
```

```
38          vm2 = vb*kr*log(H_height/zo);
39  %   c. Turbulence length:
40          L_turbulence = Lt*(z/zt)^alpha;
41  %   d. Frequency:
42          omega_k = linspace(lower_bound,upper_bound,n_steps
                );
43          n = omega_k/(2*pi);
44          fL = n*L_turbulence/vm;
45  %   e. Variance spectrum:
46          SL = 6.8*fL./(1+10.2*fL).^(5/3);
47  % B.2. Wind Spectrum(Svv)[rad/s]:
48          Svv = SL*sigma_v^2./omega_k;
49  %
```

```
50  % B.3. Aerodynamic Admittance [dimensionless]:
51  %   a. Height:
52          eta_h = 4.6*H_height*fL/L_turbulence;
53          Rh = 1./eta_h-(1-exp(-2*eta_h))./(2*eta_h.^2);
54  %   b. Width:
55          eta_b = 4.6*B_width*fL/L_turbulence;
56          Rb = 1./eta_b-(1-exp(-2*eta_b))./(2*eta_b.^2);
57  %   c. Admittance:
58          xi2 = Rh.*Rb; %xi2 = addimitance^2
59  %
```

```
60  % B.4. Load Spectrum:
61  %   a. Load coefficient:
62          rho_air = 1.25; %[kg/m^3]
63          Cw = (Cp*rho_air*vm2)^2;
64          S_FF = Cw*Svv.*xi2;
65  %
```

```
66  % C.   PLOTTING
67  % C.1. Variance Spectrum
68            figure;plot(fL,SL)
69            title('Variance Spectrum'); ylabel('S_v_v [(-)]'
                  ); xlabel('dimensionless frequency');
70  % C.2. Wind Spectrum
71            figure;plot(omega_k,Svv)
72            title('Wind Spectrum'); ylabel('S_v_v [(m/s)^2/(
                  rad/s)]'); xlabel('frequency [rad/s]');
73  % C.3. Aerodynamic Admittance
74            figure;plot(omega_k,xi2)
```

```
75          title('Aerodynamic Admittance'); ylabel('xi^2');
                xlabel('frequency [rad/s]');
76  % C.4. Load Spectrum
77          figure;plot(omega_k,S_FF)
78          title('Load Spectrum'); ylabel('S_F_F [N^2/(rad/
                s)'); xlabel('frequency [rad/s]');
```